

AD-A270 437 NON PAGE .

Form Approved  
GSA No. 0704-0188Public  
gathering  
collected  
data

Page 1 hour per response, including the time for reviewing instructions, searching existing data sources, gathering of information, and completion of this form. Send comments regarding this burden estimate or any other aspect of this Washington Headquarters Services, Directorate for Information Operations and Reports, 1215 Jefferson Avenue, Washington, DC 20583.

1. A

E

3. REPORT TYPE AND DATES COVERED  
Final Technical Report: 6/

## 4. TITLE AND SUBTITLE

"Mesoepitaxy: A 'Universal' Route to Oriented Materials"

## 5. FUNDING NUMBERS

AFOSR 90-0283

## 6. AUTHOR(S)

Professor Paul Smith SSN 222-64-5904  
Professor Alan J. Heeger SSN 508-34-6588

## 7. PERFORMING ORGANIZATION NAME(S) AND ADDRESS(ES)

Institute for Polymers and Organic Solids  
University of California, Santa Barbara  
Santa Barbara, California, Santa Barbara 93106-50908. PERFORMING ORGANIZATION  
REPORT NUMBER

T2/0283

AEOSR-TR- 93 07 46

## 9. SPONSORING/MONITORING AGENCY NAME(S) AND ADDRESS(ES)

Dept. of the Air Force  
Air Force Office of Scientific Research  
Bolling Air Force Base, DC 20332-644810. SPONSORING/MONITORING  
AGENCY REPORT NUMBER

2305/C

## 11. SUPPLEMENTARY NOTES

## 12a. DISTRIBUTION/AVAILABILITY STATEMENT

Unclassified/Distribution Unlimited

This document has been approved  
for public release and sale; its  
distribution is unlimited.

12b. DISTRIBUTION STATEMENT

DTIC  
ELECTE  
S A D  
88107 1993

## 13. ABSTRACT (Maximum 200 words)

The friction-deposited PTFE layers and their ability to act as orientation inducing substrates were fully characterized. The PTFE layers were studied by optical microscopy, scanning electron microscopy, atomic force microscopy, and by electron diffraction. Both the topology and the molecular structure were determined. The mechanism of mesoepitaxy was explored and clarified in detail through the use of overlayers. The mesoepitaxy technique was expanded from planar surfaces to the internal surfaces of polyethylene oriented by gel processing. There is serious interest by industry in using the PTFE layers for orientation. Areas of specific interest include polarizers for liquid crystal displays, and thin film transistors fabricated from oriented organic semiconductors. UNLAX Corp. (Santa Barbara) has taken an option on exclusive license on the technology and is working with several companies toward development of the technology.

93-23511



93 10 6 03 5

## 14. SUBJECT TERM

mesoepitaxy, gel-processing, oriented polymers

## 15. NUMBER OF PAGES

## 16. PRICE CODE

17. SECURITY CLASSIFICATION  
OF REPORT

Unclassified

18. SECURITY CLASSIFICATION  
OF THIS PAGE

Unclassified

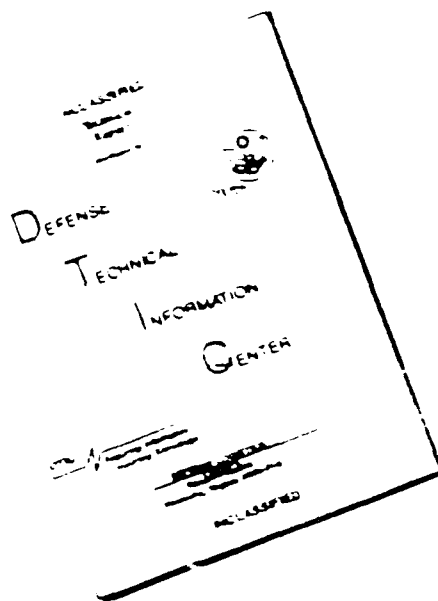
19. SECURITY CLASSIFICATION  
OF ABSTRACT

Unclassified

## 20. LIMITATION OF ABSTRACT

none

# DISCLAIMER NOTICE



THIS DOCUMENT IS BEST  
QUALITY AVAILABLE. THE COPY  
FURNISHED TO DTIC CONTAINED  
A SIGNIFICANT NUMBER OF  
PAGES WHICH DO NOT  
REPRODUCE LEGIBLY.

**Final Technical Report**  
to  
**Air Force Office of Scientific Research**

**Mesoepitaxy: A 'Universal' Route  
to  
Oriented Materials**

Agency Award Number: AFOSR-90-0283  
Period of Performance: June 15, 1990 - June 14, 1993

Institute for Polymers and Organic Solids  
University of California at Santa Barbara  
Santa Barbara, CA 93106

**Principal Investigators:**

Alan J. Heeger, Professor of Physics  
and Professor of Materials (joint)

Paul Smith, Professor of Materials  
and Professor of Chemical Engineering (joint)

Accession For	
NTIS	CRA&I <input checked="" type="checkbox"/>
DTIC	TAB <input type="checkbox"/>
Unpublished	<input type="checkbox"/>
Justification	
By	
Distribution/	
Availability Codes	
Dist	Avail and/or Special
A-1	

**DTIC QUALITY INSPECTED 2**

I. Publications resulting from AFOSR-90-0283:

- "Characterization of Friction-Deposited Poly(tetrafluoroethylene) Transfer Films"  
D. Fenwick, K.J. Ihn, F. Motamedi, J.-C. Wittmann and P. Smith, J. Appl. Polym. Science (in press).
- "Polymer Friction-Transfer Layers as Orienting Substrates"  
F. Motamedi, K.J. Ihn, D. Fenwick, J.-C. Wittmann and P. Smith, J. Polym. Sci. Polym. Phys. Ed. (in press).
- "Molecular Structure and Thickness of Highly Oriented Poly(tetrafluoroethylene) Films Measured by Atomic Force Microscopy"  
P. Dietz, P.K. Hansma, K.J. Ihn, F. Motamedi, and P. Smith, J. Mater. Sci., **28**, 1372 (1993).
- Elastic Properties of Thin Ultra-Oriented Poly( $\epsilon$ -caprolactone) Films Grown on PTFE Substrates as Revealed by Brillouin Spectroscopy"  
J.K. Kruger, M. Precht, P. Smith, S. Meyer, and J.-C. Wittmann, J. Polym. Sci. Polym. Phys. Ed. **30**, 1173 (1992).
- "Molecular Resolution of Thin, Highly Oriented Poly(tetrafluoroethylene) Films Measured with the Atomic Force Microscope"  
H. Hansma, F. Motamedi, P. Smith, P. Hansma, and J.-C. Wittmann, Polymer Commun. **33**, 647 (1992).
- "Highly Ordered Conjugated Polymers in Polyethylene: Orientation by Mesoepitaxy"  
T.W. Hagler, K. Pakbaz, J. Moulton, F. Wudl, P. Smith and A.J. Heeger, Polymer. Commun., **32**, 339 (1991).
- "Enhanced Order and Electronic Delocalization in Conjugated Polymers Oriented by Gel Processing in Polyethylene"  
T.W. Hagler, K. Pakbaz, K.F. Voss and A.J. Heeger, Phys. Rev. B **44**, 8652 (1991).
- "Highly Oriented, Thin Layers of Poly(tetrafluoroethylene): A Versatile Substrate for Oriented Growth of Materials"  
J.-C. Wittmann, and P. Smith, Nature, **352**, 414 (1991).

Copies of each of the above (preprints or reprints) are enclosed.

## II. Potential for Impact on Technology

The University of California filed for a patent (United States and foreign) on this technology based on the early work which subsequently resulted in the awarding of the AFOSR contract. The patent was granted by the United States Office of Patents and Trademarks (U.S. Patent Number 5,180,470).

UNIAX Technology (Santa Barbara, CA) has taken an option from the University of California for exclusive license to the technology. UNIAX is currently working with a number of companies toward applications of technology:

Gore & Associates (Delaware USA)

Rockwell Science Center (Thousand Oaks, CA, USA)

Sumitomo Chemical (JAPAN)

Application areas of current specific activity include the following:

Thin film transistors (FETs) where the orientation of the organic layer by the PTFE will lead to higher mobilities and thus to faster device performance;

Polarizing thin films for use in liquid crystal displays

**Characterization of**  
**Friction-Deposited Poly(tetrafluoroethylene) Transfer Films**

David Fenwick, Kyo Jin Ihn, Farshad Motamedi  
Jean-Claude Wittmann\* and Paul Smith\*\*

Materials Department,  
University of California at Santa Barbara  
Santa Barbara, Calif. 93106

[Key words: poly(tetrafluoroethylene), oriented films, X-ray diffraction,  
transmission electron microscopy]

\*Institut Charles Sadron (CRM-EAHP), 6 rue Boussingault, 67083 Strasbourg,  
France

\*\*and Department of Chemical & Nuclear Engineering

## Abstract

The structure of oriented transfer films of poly(tetrafluoroethylene) (PTFE), previously used as orientation inducing layers for a variety of materials, was studied. Transmission electron microscopy and X-ray diffractometry were employed to determine the continuity and relative volume of the PTFE films, which were deposited onto glass substrates by friction transfer at controlled temperatures, pressures, and sliding rates. The thickness and continuity of the films were found to increase with increasing temperature and applied pressure. In the range of sliding rates used (0.1 to 10 mm/s), no significant correlation between this processing variable and the thickness or continuity was apparent. Transmission electron microscope investigations showed that, generally, the (100) plane of the PTFE crystalline unit cell was parallel to the glass surface.

## Introduction

It is well established that when poly(tetrafluoroethylene) (PTFE) is rubbed against a clean surface, under appropriate conditions, a highly oriented thin film is deposited onto the surface [1 - 3]. The PTFE chain axes in these so-called "transfer films" are oriented parallel to the surface and along the sliding direction. Recently, these films were shown to act as very effective substrates for promoting oriented growth of a variety of materials, including polymers, liquid crystals and certain small organic and inorganic molecules, deposited onto them from solution, the melt or vapor phase [4].

The effectiveness of these friction-deposited PTFE transfer films as orienting substrates is expected to significantly depend on the degree of chain orientation within the film, its surface topography and continuity. The absolute thickness and its fluctuations across the film are also likely to be important features for certain applications of oriented materials grown onto the PTFE layers, e.g. in optical components. Thus, it is important to determine the effects of the various deposition parameters on the characteristics of the films and establish procedures for optimal transfer-film formation.

Numerous previous studies, particularly in the field of wear, have dealt with PTFE transfer layers, unfortunately, not always yielding a simple and consistent documentation of the effects of temperature, pressure and sliding rate on their thickness [1 - 3, 5 - 12]. Films deposited at temperatures  $\geq 20$  °C and sliding rates  $< 100$  mm/s reportedly have thicknesses that range from a few atomic layers [5 - 7] to 10 - 40 nm [1]. In studies in which spectroscopic techniques were used to measure the film "thickness", the actual measured parameter was the amount of deposited PTFE, and the continuity of the film was not considered in the calculations [5 - 7]. Clearly, the amount of PTFE deposited is, in fact, a function of both film thickness and continuity. Yang et



*al.* [8] found that the amount of PTFE deposited on stainless steel increased with increasing temperature and pressure, but Jain and Bahadur [9] reported that for PTFE deposited on polyethylene, the amount actually decreased with increasing pressure. Both Jain and Bahadur [9] and Wheeler [7] claimed that the amount deposited increased with increasing sliding rate within the range of 10 mm/s to 100 mm/s.

Relatively thick PTFE layers have been deposited under more extreme conditions. Makinson and Tabor [1] found that the thickness of PTFE layers deposited at a relatively low temperature of  $-3^{\circ}\text{C}$  and a sliding rate of 10 mm/s was 0.5 - 5  $\mu\text{m}$ . Briscoe *et al.* [2] observed that at room temperature and sliding rates  $>100$  mm/s the deposited film contained relatively thick, irregular fragments. However, Tanaka *et al.* [10] reported that the thickness of films formed at room temperature and sliding rates of 300 mm/s was only 30 nm, and argued that the thickness was relatively independent of the sliding rate or temperature except under extreme conditions. For PTFE deposited at very high sliding rates ( $>500$  mm/s), the reported values of thickness range from  $\sim 0.1$   $\mu\text{m}$  [1] to  $\sim 1$   $\mu\text{m}$  [11 - 13].

The effect of sliding rate and temperature on the degree of orientation of the deposited PTFE macromolecules has not been studied in detail. Makinson and Tabor [1] found that PTFE chains deposited at room temperature and a sliding rate of 10 mm/s are highly oriented in the sliding direction. PTFE deposited at a temperature of  $-3^{\circ}\text{C}$  and the same sliding rate was isotropic, as indicated by birefringence measurements. Pooley and Tabor [3] observed that highly oriented films were formed at sliding rates of  $\sim 1$  mm/s and temperatures of  $30^{\circ}\text{C}$  to  $150^{\circ}\text{C}$ . Tanaka *et al.* [10] claimed that the PTFE chains were oriented in the sliding direction for films deposited at room temperature and sliding rates of 300 mm/s. However, critical examination of their published

electron diffraction pattern reveals that the degree of orientation in the films was relatively poor.

In the current work we re-examined the effect of temperature, pressure, and sliding rate on the thickness and continuity of PTFE films that were friction-deposited on cleaned glass slides. X-ray diffractometry was used to measure the relative volume of the films, and the continuity or glass-substrate coverage of the films was derived from transmission electron microscopy (TEM) images.

## Experimental

### *Friction Deposition*

The deposition method involved sliding one end of a 9 mm diameter PTFE rod on a glass slide at controlled temperatures, pressures, and sliding rates. Common commercial grade, melt-crystallized PTFE rods, machined to the appropriate size, were used. Silica glass slides were cleaned in a ~ 1% KOH/ 10 % water/ 90 % ethanol solution for at least 1 hour, rinsed with distilled water and blow dried with pressurized air prior to use.

Figure 1 is a schematic drawing of the apparatus used in this study. Details of its design are discussed in a separate publication [14]. The PTFE rod and the glass substrate were heated to the same\* desired temperature and brought into contact. An appropriate contact load was applied and the glass substrate traversed at a controlled speed. The PTFE coated glass was subsequently cooled in air.

---

\* It was found that heating only the PTFE rod or the glass slide, generally, yielded inferior layers, and less reproducible results.

PTFE films were deposited at temperatures of 30, 200, 250 and 300 °C, contact pressures of 0.05, 0.3, 0.8 and 1 MPa, and sliding rates of 0.1, 1 and 10 mm/s. Only one deposition parameter (e.g., temperature) was varied at any time. In each set of experiments, films were produced consecutively with the PTFE rod at a fixed orientation relative to the sliding direction, unless indicated otherwise.

#### *X-ray Diffraction*

Relative volumes of deposited PTFE films were obtained from the relative intensities of the 010 reflection of the PTFE crystal lattice, as measured by X-ray diffractometry (Scintag diffractometer model 2000). This measurement was performed at 25 °C where PTFE is in its crystalline phase IV [15]. The integrated intensity was calculated by counting at regular angular increments across the peak. The scheme of the analysis is detailed below.

#### *Transmission Electron Microscopy*

The degree of film continuity was determined by transmission electron microscopy (TEM). For this purpose PTFE transfer films were decorated with low molecular weight polyethylene by vapor deposition in vacuum [16]. This technique is known to be very effective in revealing the oriented structure of surfaces. The samples were subsequently shadowed with Pt and coated with carbon in vacuum. Several drops of poly(acrylic acid) (50% aq. solution) were applied to the coated PTFE films. After drying, the poly(acrylic acid) was peeled off together with the PTFE and the carbon coating. The samples were allowed to float on the surface of distilled water until the poly(acrylic acid) dissolved, and the PTFE films were placed on Cu grids for examination in the electron microscope.

Images and diffraction patterns were recorded with a JEOL 100CX instrument operated at 80 kV. The overall continuity, or degree of coverage, of PTFE was calculated after measuring the continuity in TEM images of many representative areas of the sample. The PTFE films, which were observed at a magnification of 5000 times, were scanned in a direction perpendicular to the sliding direction.

### Results and Discussion

Electron diffraction studies revealed that highly oriented films of PTFE in its hexagonal crystal structure were formed over the entire range of deposition conditions employed in this work, i.e. at temperatures of 30 to 300 °C, pressures of 0.05 to 1.0 MPa, and sliding rates of 0.1 to 10.0 mm/s (see Experimental). Figure 2 shows a typical diffraction pattern, displaying the superb chain orientation in the transfer films. Importantly, the nature and quality of the diffraction pattern, and hence the degree of molecular orientation, were not noticeably affected by the deposition conditions; although, of course, the intensity of the diffraction spots were dependent upon the film thickness.

When the PTFE samples were rotated around the chain axis in the electron microscope, strong structure factors of the 100 or  $1\bar{1}0$  reflections appeared at angles of  $\pm 30^\circ$ . This observation revealed that the (010), or close-packed, plane of PTFE was parallel to the substrate surface, as shown in Figure 3(a). In this orientation, the  $b^*$ -axis is normal to the substrate surface (Figure 3(b)).

### *X-ray Measurements*

The thickness of the PTFE films formed by the friction-deposition method onto glass slides was generally less than 50 nm, which was not sufficient for

detection in a conventional X-ray Laue camera in the transmission mode. However, we succeeded in measuring the intensity of the 010 reflection using the following method.

In the X-ray diffractometer used, the source and the counter were set to rotate at the same angle  $\theta$  from the horizontal as shown in Figure 4, while the sample was located in the horizontal plane with the PTFE chain axis in the plane of the incident and diffracted beams. The Ewald construction, shown in Figure 4, illustrates that the X-ray counter records the intensity profile along the direction normal to the sample surface, i.e. parallel to the  $b^*$ -axis. The intensity profile of the 010 reflection was recorded. This reflection, which is equivalent to the 100 and  $1\bar{1}0$  reflections, is the most intensive of the hexagonal phase IV of PTFE. Figure 5 shows a typical intensity profile of the 010 reflection at the  $18^\circ$  diffraction angle  $2\theta$ .

For very thin materials, in which there is little absorption of X-rays, the integrated intensity of a diffraction peak is proportional to the volume of irradiated material according to the following equation [17]:

$$I \propto I_0 F_{hkl}^2 V \quad (1)$$

where  $V$  is the volume of the sample,  $F_{hkl}$  is the structure factor, and  $I_0$  is the intensity of the incident beam. The latter was approximately constant during the period of the measurements, typically ~90 min; the measured intensity of the 010 reflection for a given sample did not change significantly during this period. Accordingly, the integrated intensity of the 010 reflection peak was taken to be proportional to the irradiated film volume, which was near the center of the sample.

Figures 6 and 7 show the results of measured relative volumes and continuity of the deposited films. "Continuity" here is defined as the fraction of a given glass substrate area covered with PTFE. Both the volume and the continuity increased with increasing deposition temperature and applied pressure. These results are consistent with some of the earlier studies which revealed that the amount of PTFE deposited on a steel surface increases with increasing temperature [8] and applied pressure [8, 18].

Different regions of a relatively discontinuous film, which was "decorated" with vaporized polyethylene, are shown in Figures 8(a) and 8(b). Polyethylene lamellae formed by this method were aligned on the PTFE layers and randomly oriented on the uncoated glass surfaces between these layers. Clearly, the PTFE continuity, or degree of coverage, was greater in the region shown in Figure 8(a). These PTFE layers were essentially uninterrupted and their widths approximately constant, along the sliding direction. Perpendicular to this direction, however, the degree of PTFE coverage generally varied from site to site. Because of this feature, the overall continuity was calculated only after measuring the continuity of many such areas of a film. The continuity values shown in Figures 6 and 7 are those of films with an intermediate value of relative volume (or X-ray signal intensity) compared to that of other films produced under the same conditions.

Figure 6 shows that the thickness and continuity of friction-deposited films increased significantly with increasing temperature. The volume of deposited PTFE changed by a factor of about 15 over the temperature range of 200 °C to 300 °C, while the continuity changed by a factor of only about 2.6 (from ~30 % to ~80 %). This implies that the PTFE thickness changed by a factor of ~6 over this temperature range.

The X-ray signal from films produced at temperatures well below 200 °C and the aforementioned pressure and sliding rates was undetectable, and thus the relative volume of deposited PTFE could not be determined at these temperatures. The continuity of films produced at room temperature was very low ( $\sim 5\%$ ), although parts of the PTFE film may have been too thin to be detected in the electron microscope at the magnification used (i.e., 5000 times), despite the polyethylene decoration and Pt shadowing.

The thickness and continuity increased significantly with increasing applied pressure for films produced at a temperature of 300 °C and a sliding rate of 1 mm/s (Figure 7). Films produced at the highest pressure (1.0 MPa) were  $\sim 50\%$  continuous, while those produced at the lowest pressure (0.05 MPa) covered only  $\sim 10\%$  of the glass surface. The volume of deposited films changed by a factor of  $\sim 8$  over the pressure range studied, compared to approximately a 5-fold change in the continuity and a 1.5-fold change in thickness.

No significant correlation was found between the sliding rate, in the range studied, and the thickness and continuity of the films. For films produced at the same pressure and temperature, the volume decreased with increasing sliding rate in some series of runs—at most by a factor of  $\sim 2.5$  over the range of 0.1 to 10 mm/s—while in other cases there was no significant effect of the rate on the deposited volume. These results are in accord with another published study, which also reported little effect of the sliding rate on the amount of deposited PTFE, within the range of 1 mm/s to 10 mm/s [7].

Previous atomic force microscopy measurements indicated that the average thickness of films produced at a temperature of 300 °C, a pressure of 0.3 MPa, and a sliding rate of 1 mm/s was  $\sim 15$  to 40 nm [19]. The uncertainty in this measurement was due to fluctuations in the thickness across the film and

to the fact that AFM measurements were confined to small areas. Large-scale fluctuations in the thickness were often visible to the naked eye, some portions of a film being more prominent than others. This most likely resulted from variations in the local contact pressures at the PTFE/glass interface.

Interestingly and importantly, similar overall film volume and continuity were obtained when the films were produced consecutively while maintaining the same polymer rod orientation, in addition to keeping other parameters the same. Differences in the volume and continuity, on the other hand, were observed when the rod orientation was not maintained in consecutive runs. This implies that variations in the topography of the rod surface relative to the sliding direction directly affect the quality of the deposited films.

The above experimental results of the formation of PTFE transfer films onto glass surfaces are readily understood and explained in terms of its initiation at only the area of the polymer rod surface that is first to contact the glass substrate during sliding, the remainder of the rod surface being elevated above the glass. The continuity and thickness of a film would then be dependent upon the surface roughness of the rod tip and the substrate, and the local contact pressure at this area. The interfacial contact area, of course, increases with increasing temperature and applied pressure due to thermomechanically activated plastic flow of the polymer at the interface, resulting in a greater film continuity and thickness. Thus, the formation of optimum PTFE transfer layers for use as orientation-inducing substrates eventually will be dictated by the "smoothness" of the PTFE-substrate interface; and, naturally, on the absence of impurities and foreign matter both in the PTFE and on the substrate surface.



### **Acknowledgments**

This work as supported by the Air Force Office of Scientific Research AF90-0283. The authors are deeply indebted to David P. Bothman of the Mechanical & Environmental Engineering Department of UCSB for his invaluable contributions to this work and for the design and development of the friction-deposition instrument.

## References

- (1) K. R. Mackinson and D. Tabor, *Proc. Roy. Soc. (London)*, **A281**, 49 (1964)
- (2) B. J. Briscoe, C. M. Pooley, and D. Tabor, *Advances in Polymer Friction and Wear*, Ed. L. H. Lee, **5A**, 191-202 (1975)
- (3) C. M. Pooley and D. Tabor, *Proc. R. Soc. (London)*, **A. 329**, 251 (1972)
- (4) J. C. Wittmann and P. Smith, *Nature*, **352**, 414 (1991)
- (5) S. V. Pepper, *J. Appl. Phys.*, **45**, 2947 (1974)
- (6) J. L. Lauer, B. G. Bunting, and W. R. Jones, *Tribology Transactions*, **31**, 282 (1987)
- (7) D. R. Wheeler, *Wear*, **66**, 355 (1981)
- (8) E. L. Yang, J. P. Hirvonen, and R. O. Tiovanen, *Wear*, **146**, 367 (1991)
- (9) K. V. Jain and S. Bahadur, *Wear*, **46**, 177 (1977)
- (10) K. Tanaka, Y. Uchiyama, and S. Toyooka, *Wear*, **23**, 153 (1973)
- (11) S. K. Biswas and K. Vijayan, *J. Mat. Sci.*, **23**, 1877 (1988)
- (12) V. R. Agarwal, U. T. S. Pillai, and A. Sethuramiah, *Wear of Materials*, **1**, 501 (1989)
- (13) M. K. Kar and S. Bahadur, *Wear*, **63**, 105 (1980)
- (14) F. Motamedi, K. J. Ihn, D. Fenwick, J. C. Wittmann, and P. Smith, submitted to *J. Polym. Sci., Polym. Phys. Ed.*
- (15) G. M. Martin and R. K. Eby, *J. Res. Nat'l. Bur. Standards*, **72A**, 467 (1968)
- (16) J. C. Wittmann and B. Lotz, *J. Polym. Sci., Polym. Phys. Ed.*, **23**, 205 (1985)
- (17) B. E. Warren, *X-ray Diffraction*, Addison-Wesley Publishing Co., 1969
- (18) J. P. Hirvonen and E. L. Yang, *Mat. Lett.*, **8**, 197 (1989)
- (19) H. Hansma, F. Motamedi, P. Smith, P. Hansma, and J. C. Wittmann, *Polymer*, **33**, 647 (1992)

## Figure Captions

Figure 1. Schematic diagram of the friction deposition equipment.

Figure 2. Electron diffraction pattern of a friction-deposited PTFE transfer layer.  
The friction direction is parallel to the meridional in the pattern.

Figure 3. (a) Schematic arrangement of PTFE molecules onto the glass surface. Molecular axes are normal to the figure. (b) Distribution of structure factors in the arrangement of the PTFE molecules in (a). The figure illustrates that the 100 and  $1\bar{1}0$  structure factors exist at  $\pm 30^\circ$  from the horizontal.

Figure 4. Ewald construction of the X-ray diffractometer in the reflection mode. The intensity profile of the reflections normal to the sample surface is detected.

Figure 5. Intensity profile of the 010 reflection of a deposited PTFE layer. The sample was prepared at a temperature of  $300^\circ\text{C}$ , a pressure of 0.8 MPa, and a sliding rate of 1 mm/s.

Figure 6. Relative volume and continuity of PTFE films deposited at a pressure of 0.8 MPa, a sliding rate of 1 mm/s, and various temperatures. The relative volume was deduced from X-ray diffraction measurements, and the continuity from TEM observations.

Figure 7. Relative volume and continuity of PTFE films deposited at a temperature of 300 °C, a sliding rate of 1 mm/s, and various pressures.

Figure 8. TEM images of discontinuous regions of a PTFE transfer film. Polyethylene lamellae formed by vapor deposition are aligned on the PTFE layers and randomly oriented on the non-coated glass surface between these layers. The long axes of the polyethylene lamellar crystals on the PTFE layers are oriented perpendicular to the sliding direction. Note that the degree PTFE coverage is greater in (a) than in (b). Bar = 500 nm.

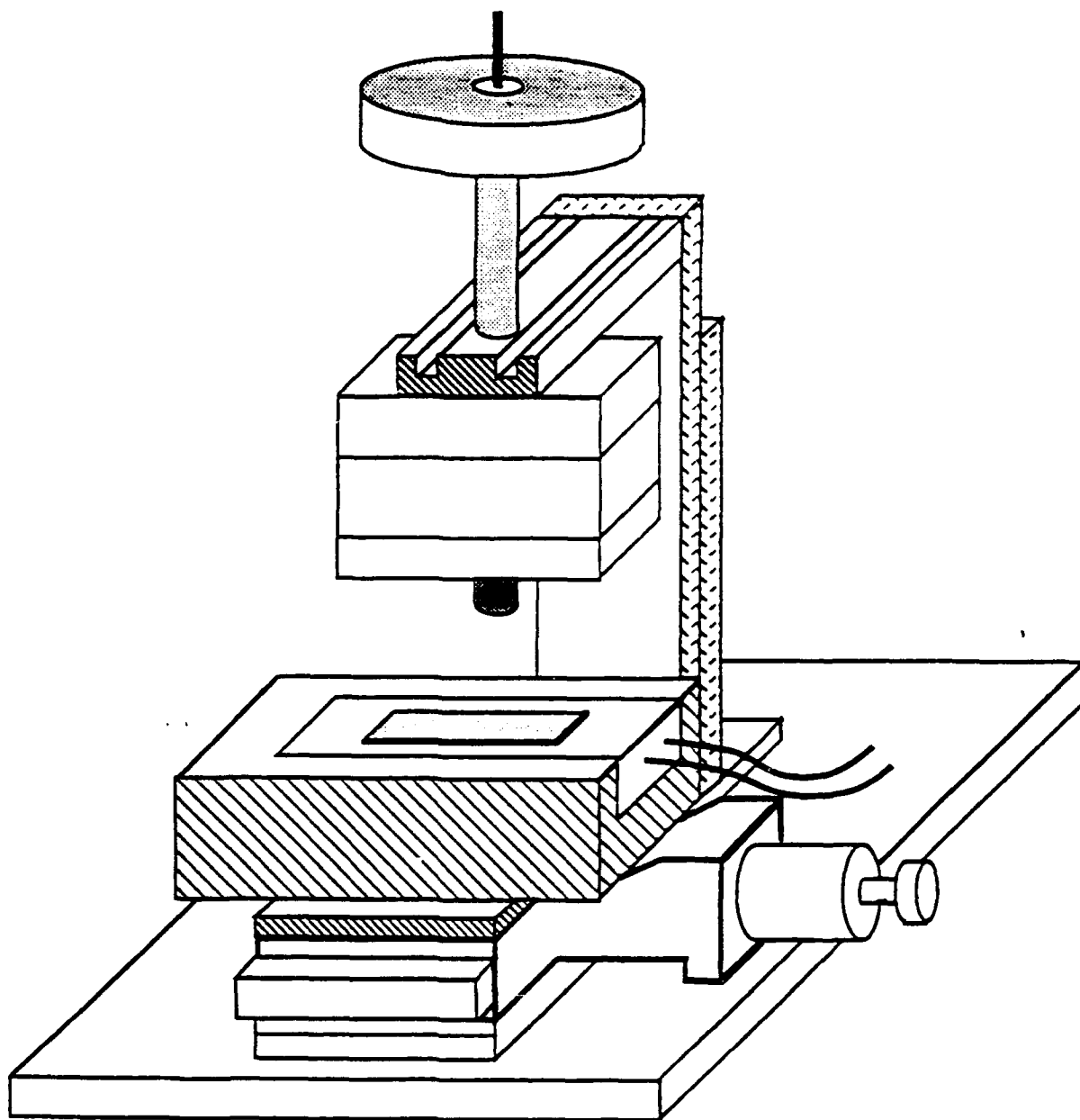


Figure 1. Fenwick *et al.*

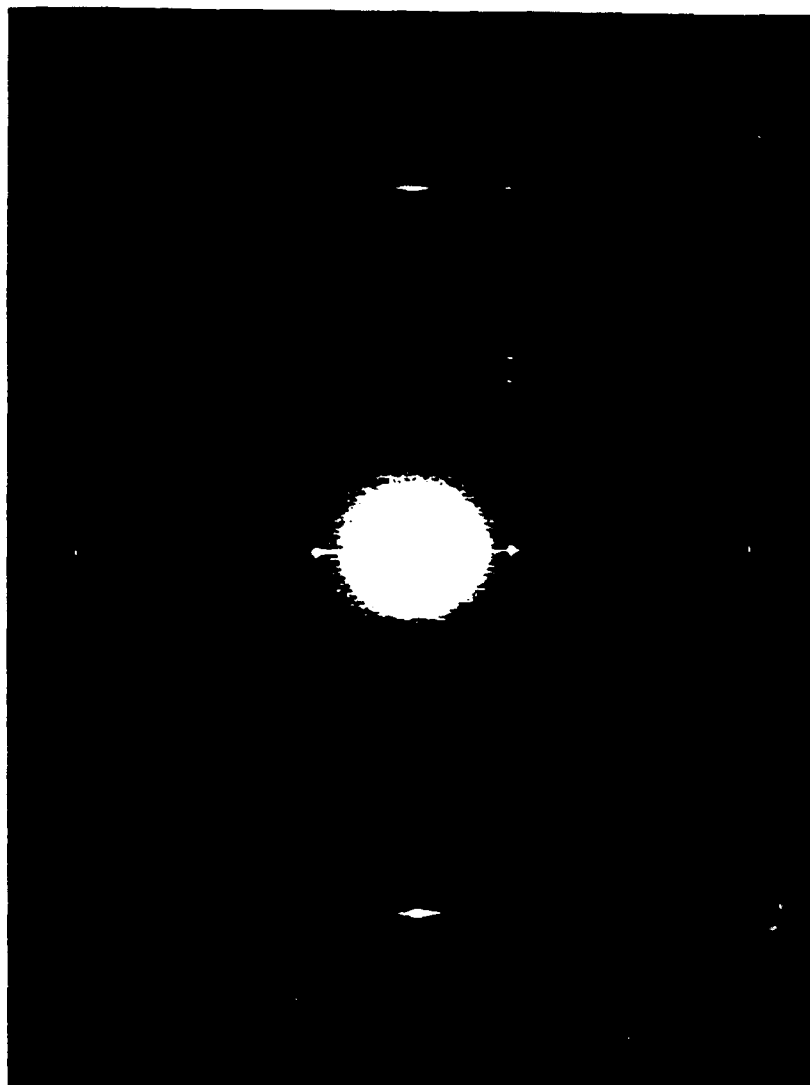
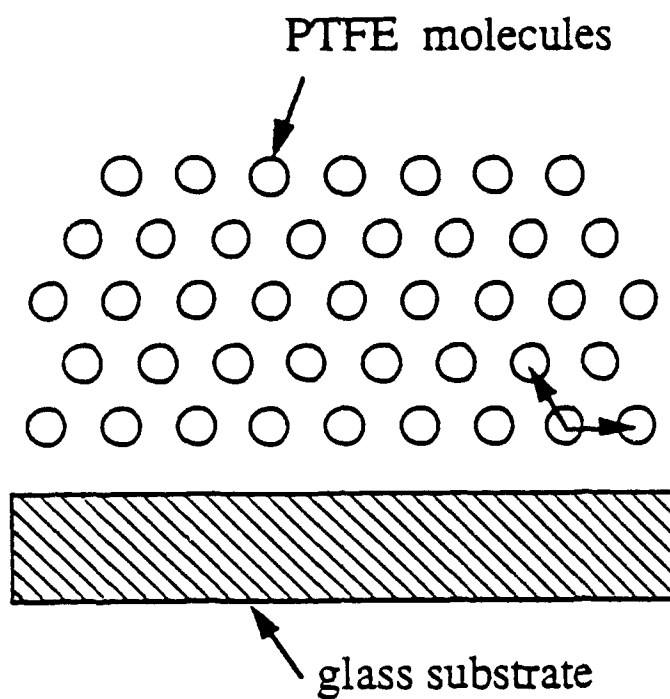


Figure 2. Fenwick *et al.*

**a**



**b**

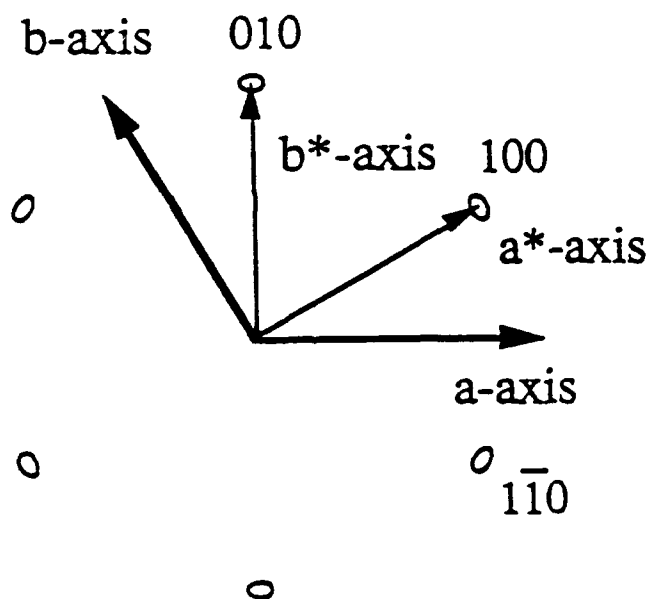


Figure 3. Fenwick *et al.*

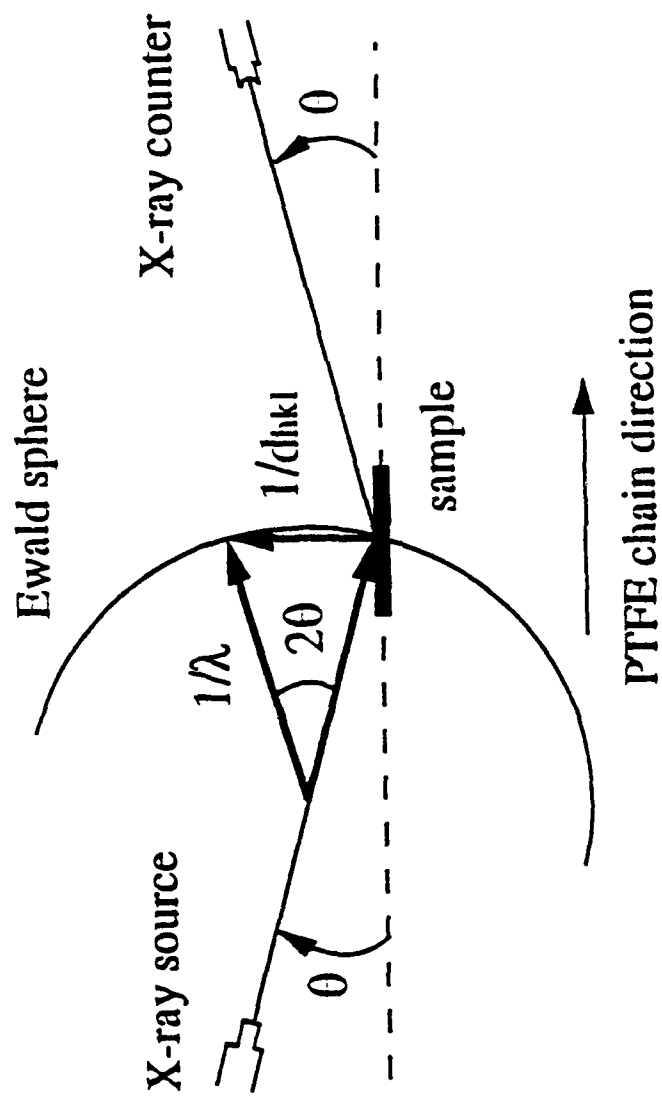


Figure 4. Renwick *et al.*



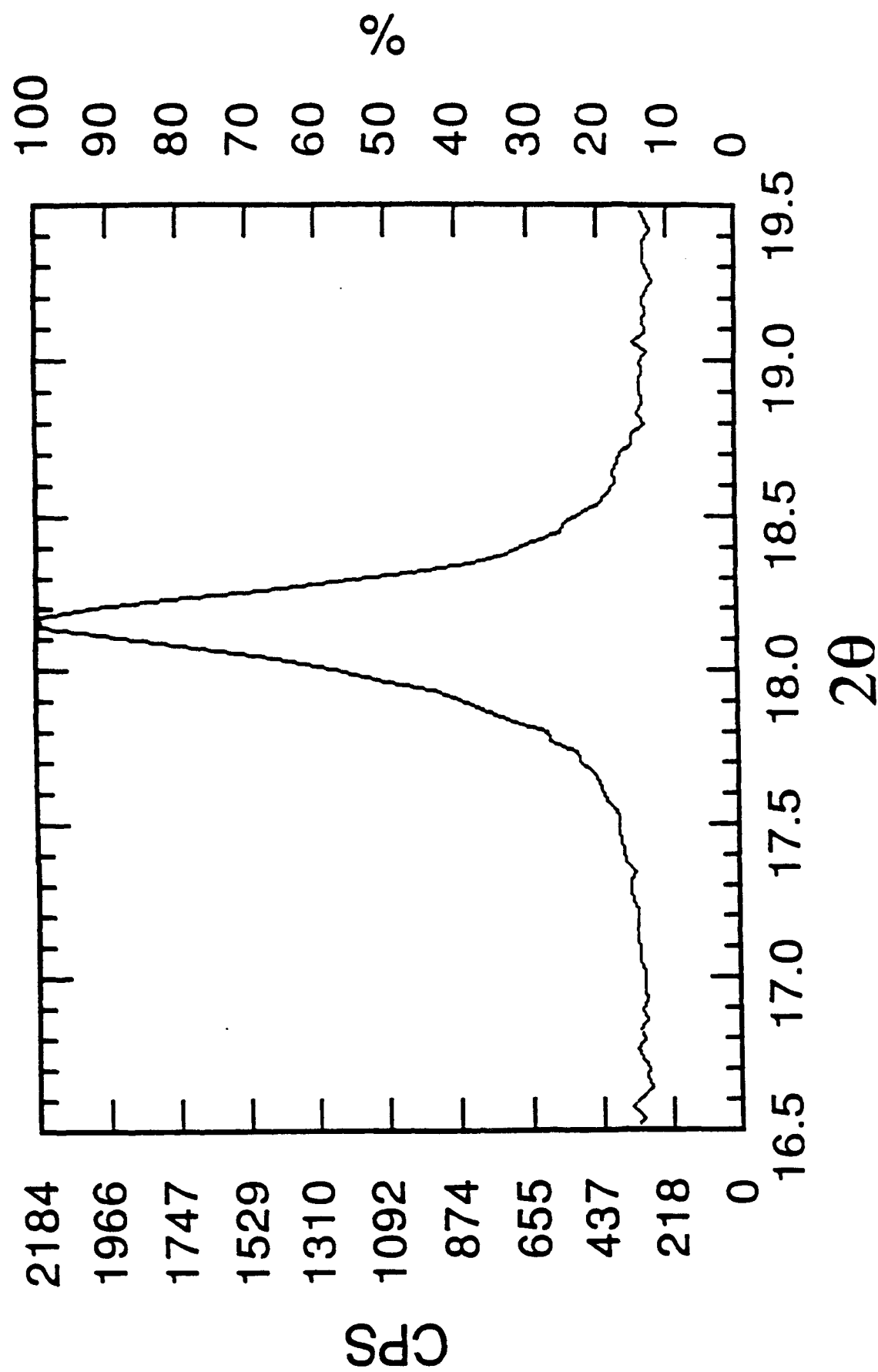


Figure 5. Fenwick *et al.*

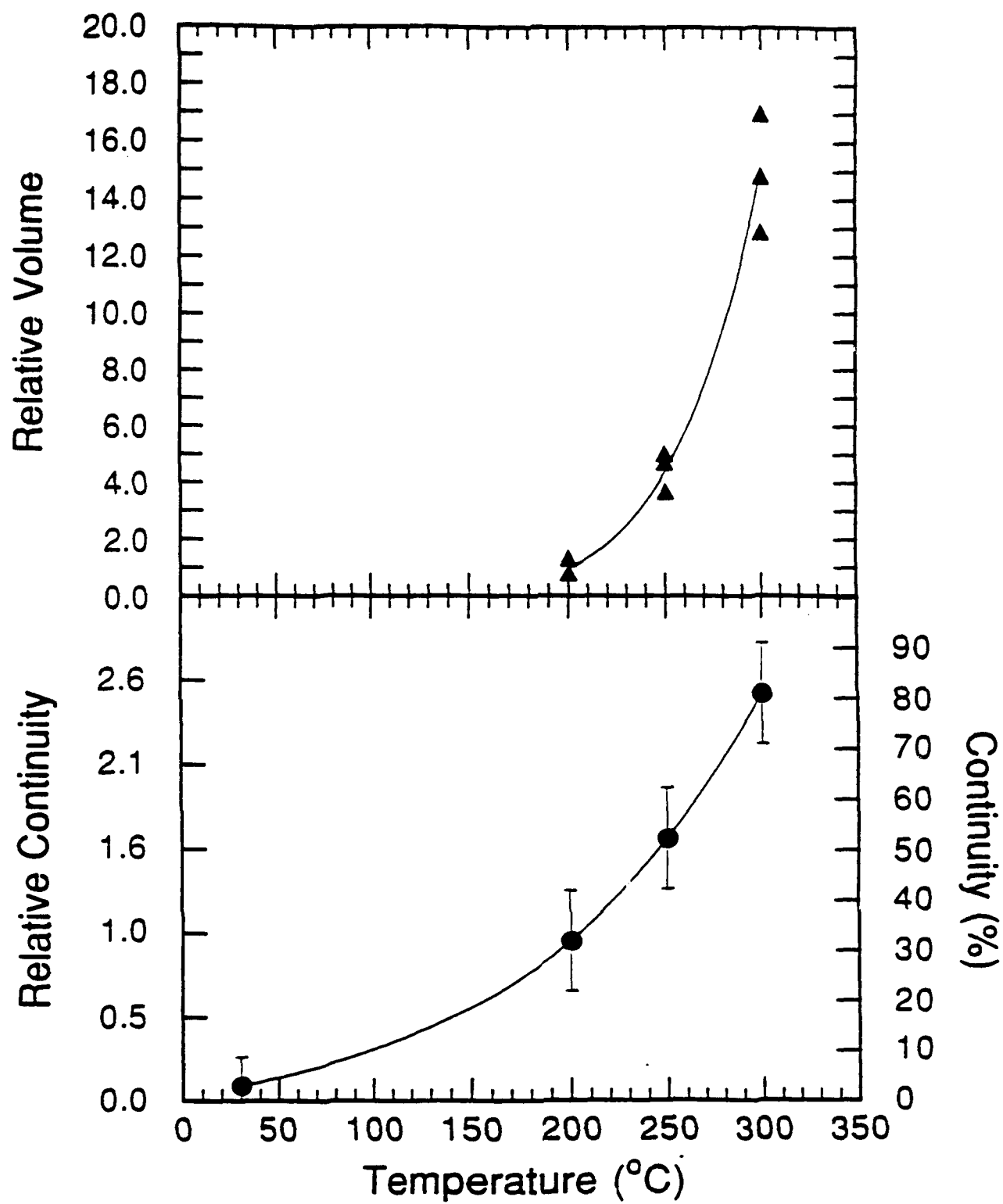


Figure 6. Fenwick *et al.*

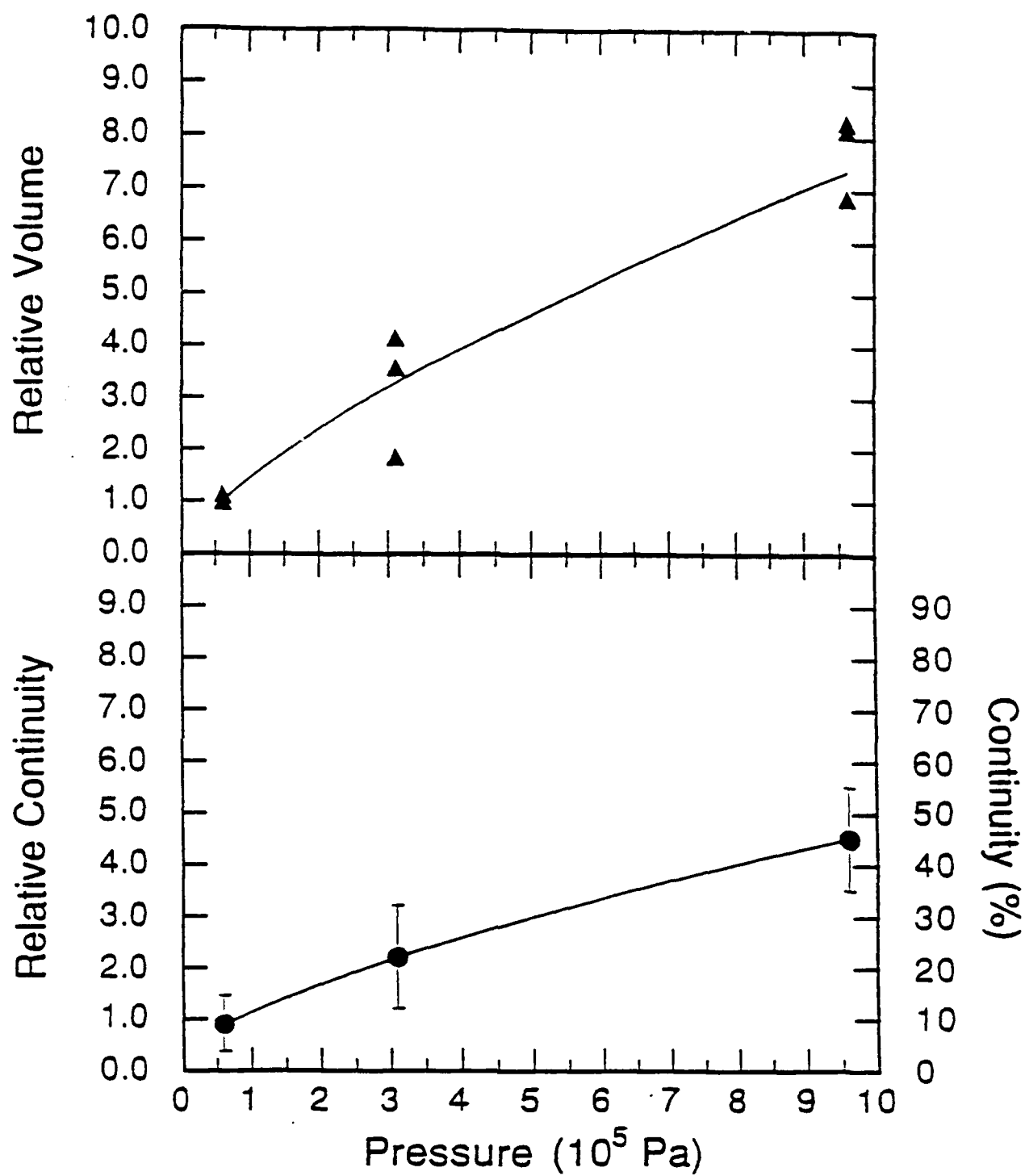


Figure 7. Fenwick *et al.*

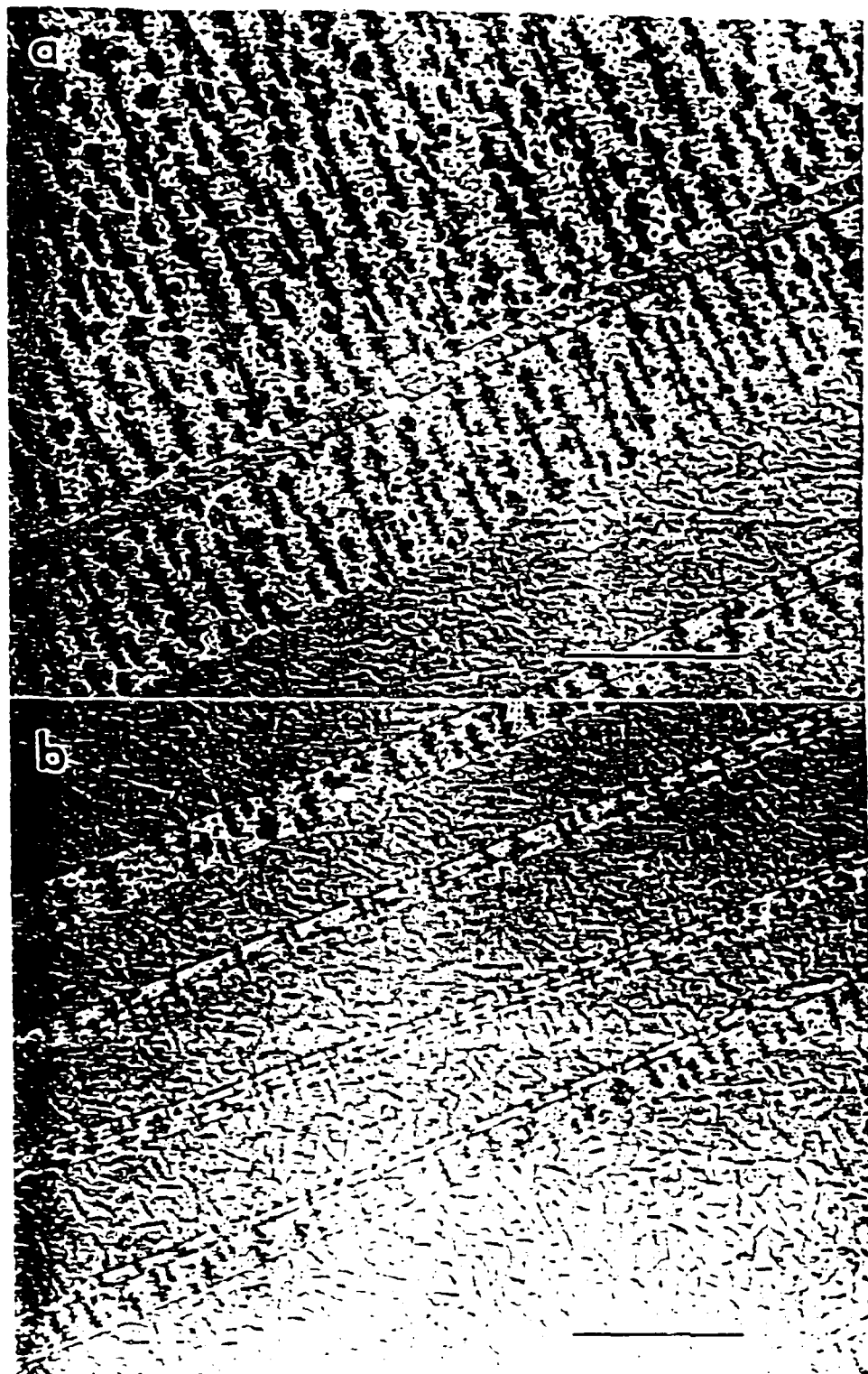


Figure 8 Fenwick *et al.*

# Polymer Friction-Transfer Layers as Orienting Substrates

Farshad Motamedi, Kyo Jin Ihn, David Fenwick,  
Jean-Claude Wittmann\* and Paul Smith\*\*

Materials Department,  
University of California at Santa Barbara  
Santa Barbara, Calif. 93106

- \* Institut Charles Sadron (CRM-EAHP), 6 rue Boussingault, 67083 Strasbourg, France
- \*\* and Department of Chemical & Nuclear Engineering

[Key words: orienting substrates, friction-transfer layers, polyethylene, poly(tetrafluoroethylene)]

## Abstract

A variety of polymers were investigated as candidates for the formation of oriented layers by friction transfer. Only polyethylene, the liquid-crystalline Vectra<sup>®</sup> and fluorinated ethylene-propylene copolymer were found to yield oriented transfer layers. These layers, in turn, were found to induce the oriented growth a variety of species deposited onto them from the melt, solution or vapor phase. The present orientation-inducing friction-transfer layers, however, were found to be inferior to those of poly(tetrafluoroethylene) [PTFE], described previously.

## Introduction

Recently, we reported (1) that oriented, thin layers of poly(tetrafluoroethylene) [PTFE], formed onto various supports by friction transfer (2-7), have the remarkable capacity of inducing oriented growth of a wide variety of materials. It was found that many species, including both flexible and rigid polymers, small molecules, liquid crystals, monomers, as well as some metals and inorganics, form highly ordered structures when grown onto these PTFE layers from the melt, solution or vapor phase (1). This unexpected finding has prompted us to reinvestigate the potential of polymers other than PTFE to form oriented transfer layers, and to examine their orientation-inducing faculty.

The important observation that rubbing solid PTFE against various surfaces, such as glass or steel, under certain experimental conditions, may yield a thin and oriented layer of the polymer onto the support was first made by researchers in the field of polymer tribology in their studies of the friction and wear properties of various polymers [2-5]. These authors also reported that linear polyethylene [PE] may form similar thin oriented films, often referred to as transfer layers. The friction behavior of selected other polymers, such as polyamides, polypropylene, poly(oxymethylene) and poly(ethyleneterephthalate) were also studied [6,7], but was not seen to resemble that of PTFE or PE; both in terms of tribological characteristics and the formation of transfer layers. Accordingly, because of the distinctive low frictional properties of the latter two polymers, these materials were categorized in the tribology literature as a special class of polymers.

As was stated above, the purpose of this study was to reexamine the formation of friction-transfer layers of polymers other than PTFE, and to study their orientation-inducing faculty. In that sense, this work is a supplement to the earlier study [1].

## Experimental details

### Materials

The polymers examined in this work for the formation of friction-transfer layers were high density polyethylene [PE; Alathon 7050,  $M_w = 6 \times 10^4$ ], ultra-high molecular weight polyethylene [UHMW PE; Hostalen GUR 415,  $M_w = 2 \times 10^6$ ], the aromatic liquid-crystalline polyester copoly(p-hydroxybenzoic acid-2-hydroxy-6-naphthoic acid) [Vectra<sup>®</sup>, Hoechst-Celanese], a perfluorinated copolymer of ethylene and propylene [FEP T100, Du Pont], poly(butylene terephthalate) [PBT, Aldrich Chemical Co.], nylon 12 [Polysciences Inc.], isotactic polypropylene [Polysciences Inc.] and poly(oxymethylene) [polyacetal, Aldrich Chemical Co.].

Rods of all of the above materials were made by heating the polymers under moderate pressure to temperatures of about 20 °C above their respective melting or softening temperatures, and subsequent cooling to ambient. In addition, rods of UHMW PE were made both by crystallizing the polymer from the melt and by gelation-crystallization from a 1% w/w solution in xylene [details in ref. 8].

### Equipment

Figure 1 is a photograph of the equipment that was built for the accurate and consistent deposition of oriented thin films through friction transfer. It is comprised of two components; the lower part consists of a movable stage the speed and direction of which is controlled by a stepper motor (Daedal Inc.), and a temperature controlled block which houses the support (usually a glass microscope slide) onto which the layer is deposited. The upper part is a temperature controlled chamber which vertically holds a cylindrical polymer rod (10 mm diameter, 15 mm length). The upper part is vertically adjustable allowing for accurate controlling of the separation between the upper and lower parts. Interfacial pressure between polymer

and support is controlled by applying known weights to the polymer rod while in contact with the support.

Microscope glass slides were used as supports, which were washed with an ethanolic KOH solution prior to use.

### *Methods*

The transfer films were prepared by first heating the support and the polymer rod to the desired deposition temperature and bringing to contact. An appropriate contact pressure was applied and the lower part carrying the support traversed. The latter was subsequently removed and cooled in air.

Typically, the contact pressure applied was  $5 \text{ kg/cm}^2$ ; and the traverse rate was  $1 \text{ mm/s}$ . The deposition temperatures were varied over a wide range and optimized for each polymer material to yield the best possible transfer films. Most often, optimum temperatures were found to be about 0.90 - 0.95 times the respective melting points (in centigrades) of each of the polymer species.

### *Characterization*

The results of the friction-transfer experiments were examined for each polymer both by polarizing optical and transmission electron microscopy, with Nikon Microphot FX and Jeol 100CX instruments, respectively.

In selected cases, the orientation-inducing faculty of polymer coated glass slides were studied by crystallizing various materials onto the polymer transfer layers. For this purpose, poly( $\epsilon$ -caprolactone) [PCL] was grown onto the layers from the melt at  $100^\circ\text{C}$ ; poly(*p*-xylylene) [PPX] was polymerized directly from the pyrolyzed monomer [11]; liquid crystalline mixtures of 4-cyano-4'-*n*-alkylbiphenyls were contacted with the layers at room temperature; polyaniline [PANI,  $M_w \sim 2 \times 10^4$ , UNLAX Corporation] and poly-*p*-(phenylene terephthalamide) [PPTA,  $M_w \sim 4 \times 10^4$



Du Pont] were precipitated from 2 wt % solutions in  $\text{H}_2\text{SO}_4$  at 25 °C by exposure to moist air; and the paraffin tricosane ( $\text{C}_{23}\text{H}_{48}$ ) was crystallized from the melt at 50 °C.

## Results and Discussion

Of the polymers examined in this work, only polyethylene, Vectra® and the fluorinated polymer FEP were found to produce adequate transfer layers. The other macromolecular materials used, when slid against the heated support, either formed highly irregular, discontinuous deposits onto the glass surface without appreciable molecular orientation; or did not interact with the glass support at all, as in the case of poly(oxymethylene). Amongst the various polyethylene samples of different molecular weight and different methods of crystallization [i.e. from solution or melt], the melt-crystallized linear polyethylene of relatively low  $M_w = 60,000$  yielded superior transfer layers with respect to their continuity and degree of orientation. Remarkably, no clear distinction could be made between the layers produced using UHMW PE rods prepared from melt- or solution crystallized polymer. Previously, it was established that solution-crystallized UHMW PE is characterized by a drastically reduced number of entanglements per chain molecule in comparison with melt-crystallized material, which accounts for the remarkable solid-state flow and tensile deformation behavior of the former, solution-precipitated samples [8]. The lack of a difference in the friction transfer behavior between these two UHMW PE specimens of different solidification history seems to indicate that the molecular phenomena that control this process do not include molecular entanglements; and that the friction transfer mechanism indeed is to be distinguished from simple tensile deformation at the glass-polymer interface.

Figures 2a-c show electron diffraction patterns of transfer layers of HDPE, Vectra® and FEP, respectively. As inferred from these diffraction patterns, the layers were oriented in the direction of sliding; however, especially for the latter two

materials only moderate orientation was achieved in comparison with the previous layers of PTFE [1]. Typically, the layer thicknesses were 2-10 nm for HDPE (hence the very weak diffraction pattern in 2a), 50-200 nm for Vectra® and 10-50 nm for FEP; as opposed to 15-40 nm for PTFE [9]. It is interesting to note that the electron diffraction pattern of the HDPE is indicative of a double orientation of the unit cell in the transfer layers, much like that found for ultra-drawn films of gel-crystallized UHMW PE [12]. Also here, the a-axis was oriented perpendicular to the film surface.

The results presented above are in general accord with earlier findings by Tabor, Briscoe and coworkers [3-5], and reconfirm the notion that the formation of oriented layers of polymers by friction transfer requires relatively weak interchain interactions and "smooth" molecular profiles. As a matter of fact, there appears to be a simple, inverse correlation between the strength of secondary bonds and the degree of order and orientation of the macromolecules in the transfer layers.

Figure 3 shows a transmission electron micrograph (TEM) of the polyethylene transfer layer that, for the purpose of contrast enhancement, was decorated with low molecular weight polyethylene by the vapor deposition technique, commonly referred to as polymer decoration [13]. The latter is a relatively simple technique which was found to be useful, among others, for the analysis of orientation layers. Vapor-deposited (low molecular weight) polyethylene molecules tend to align onto the orientation layers, forming lamellae that run perpendicular to the molecular axis of this layer. By contrast, randomly oriented lamellar crystals are formed on the bare glass support surface. Both oriented as well as randomly oriented lamellae are visible in Figure 3, which is indicative of the fact that the average coverage of the glass support with PE transfer layers was poor (typically less than 50%) compared to that observed for PTFE. FEP and Vectra® showed similar coverage to PE. [More quantitative observations of the coverage as a function of deposition parameters for PTFE transfer layers are presented in a separate publication].

Following essentially the same procedures as those described in earlier work on PTFE orientation layers [1], the present friction-transfer layers were examined for their ability to induce oriented growth of various materials. For this purpose, a limited selection of species of significantly different physico-chemical characteristics were employed.

Despite the relatively low level of surface coverage (approximately 50%), the above three polymer friction-transfer layers were found to orient small molecular liquid crystals surprisingly well. Figure 4 displays an optical micrograph, taken with crossed polarizers, of a liquid crystal mixture of 4-cyano-4'-n-alkylbiphenyls that was deposited onto a glass support partially covered with the PE transfer layer. The left-hand side of this micrograph shows the typical nematic texture of the liquid crystalline material, while the right-hand side reveals a highly birefringent, oriented phase which resulted from alignment on the PE orientation layer.

Figure 5 is a electron diffraction pattern of oriented poly(*p*-xylylene) (PPX) film, in its  $\beta$  crystal form, vapor deposited-polymerized directly onto the PE layer. In this process [10,11], the dimer was pyrolyzed at 650 °C, and, under vacuum contacted with the orientation layer, which was kept at ambient temperature, to yield as-polymerized PPX in the  $\alpha$ -form. Subsequently, the as-formed PPX layer was annealed at 300 °C, (which was approximately 170 °C above the melting temperature of the PE orientation layer!) for conversion to the  $\beta$ -crystal modification and to enhance molecular order. The observed high degree of orientation in the annealed specimen clearly indicates that orientation of the PPX was induced during the polymerization process, into the  $\alpha$  form, and is maintained, or even enhanced, during the solid-solid transition to the  $\beta$  form.

Table 1 briefly summarizes the results obtained with some of the polymer materials used as orientation layers and of experiments of other materials deposited onto these layers. The degree of homogeneity, perfection and orientation is

qualitatively ranked based on polarized optical microscopic observations, complemented, where necessary, with TEM studies. In the case of the growth of polyaniline and poly(*p*-phenylene terephthalamide) [Kevlar<sup>®</sup>] by precipitation from concentrated sulfuric acid onto Vectra<sup>®</sup>, the solvent partially dissolved the orientation layer; and, thus, a meaningful observation could not be made. For reference purposes, earlier results obtained with PTFE friction-transfer layers [1] are included in this table, also. In all cases, the PTFE orientation layers invariably were superior to the friction-transfer layers of the other materials studied; with PE next as being moderately satisfactory and efficient. Clearly, this was due wholly or at least in a significant part to the relatively modest orientation of the present friction-transfer layers, and their inhomogeneity and discontinuity.

The origin of the observed orienting faculty of the layers of the present polymers is expected to be similar to that of the PTFE layers, which is tentatively attributed to the specific ("fractal") nanoscale surface topography of these layers [9], often in combination with the more classical epitaxial phenomena that are assisted by matching of specific crystal lattice features of the orientation layers and the material deposited onto them. A detailed discussion regarding this important mechanistic issue will be presented in a separate publication.

## Conclusions

Several polymers were investigated with respect to their ability to yield oriented layers by friction transfer [4]. Among the different materials studied, only polyethylene, the thermotropic liquid-crystalline Vectra<sup>®</sup> and the fluorinated FEP were found to yield oriented transfer layers. These layers were examined with respect to their orienting capacity, and were found to orient a significant variety of species deposited onto them from the melt, solution or vapor phase. In many

respects, however, the present friction-transfer layers and their orientation-inducing faculty were found to be inferior to previously described PTFE layers.

### Acknowledgment

This work as supported by the Air Force Office of Scientific Research AF90-0283. Vectra® and Kevlar® are trade names of Hoechst/Celanese and E. I. du Pont de Nemours & Company, Inc., respectively. Vectra® was kindly supplied by Dr. M. Jaffe of Hoechst/Celanese, and polyaniline by UNLAX Corporation of Santa Barbara, Calif. The authors are deeply indebted to David P. Bothman of the Mechanical & Environmental Engineering Department of UCSB for his invaluable contributions to this work and for the design and development of the friction-deposition instrument.

## References

1. J. C. Wittmann, and P. Smith, *Nature*, 352, 414 (1991).
2. R. C. Bowers, W. C. Clinton, and W. A. Zisman, *Lubrication Eng.*, 9, 204 (1953).
3. K. R. Makinson, and D. Tabor, *Proc. Roy. Soc. (London)*, A281, 49 (1964).
4. B. J. Briscoe, *Am. Chem. Soc. Symp. Ser.*, 287 (ed. Lee, L.H.), 151 (1985).
5. C. M. Pooley, and D. Tabor, *Proc. Roy. Soc. Lond. A*, 329, 251 (1972).
6. K. Tanaka, and T. Miyata, *Wear*, 41, 383 (1977).
7. M. K. Kar, and S. Bahadur, *Wear*, 63, 105 (1980).
8. P. Smith, P. J. Lemstra, and H. C. Booij, *J. Polym. Sci., Polym. Phys. Ed.*, 19, 877 (1981).
9. H. Hansma, F. Motamedi, P. Smith, P. Hansma, and J. C. Wittmann, *Polymer*, 33, 647 (1992).
10. W.F. Gorham, *J. Polym. Sci., Part A1*, 3027 (1966).
11. S. Isoda, *Polymer*, 25, 615 (1984).
12. P. Smith, A. Boudet and H. Chanzy, *J. Mater. Sci. Lett.*, 4, 13 (1985).
13. J. C. Wittmann, and B. Lotz, *J. Polym. Sci., Polym. Phys. Ed.*, 23, 205 (1985).

Table 1

Qualitative Ranking of Efficiency of Friction-Transfer Layers of Different Polymers  
for Inducing Oriented Growth

Friction-Transfer Polymer	PTFE	PE*	Vectra®	FEP
Material Deposited				
PCL	+++	++	+	+
PPX	+++	++	-	-
LC	+++	++	++	+
PANI	+++	++	-	+
PPTA	+++	++	-	-
C <sub>23</sub> H <sub>48</sub>	+++	++	+	-

(+) signs indicate increasing quality of orientation of the crystallizing material onto the friction-transfer layers. (-) refers to no significant orientation observed. *Materials* - PCL: poly-ε(caprolactone) grown from the melt, 100 °C; PPX: poly(*p*-xylylene) by direct polymerization from the monomer [11]; LC: liquid crystalline mixture of 4-cyano-4'-*n*-alkylbiphenyls; PANI: polyaniline from a 2 wt % solution in H<sub>2</sub>SO<sub>4</sub>, at 25 °C; PPTA: poly-*p*-(phenylene terephthalamide), from a 2 wt% solution in H<sub>2</sub>SO<sub>4</sub>, at 25 °C; Tricosane (C<sub>23</sub>H<sub>48</sub>) from the melt at 50 °C.

\*The polyethylene layer was produced using HDPE, M<sub>w</sub> = 60,000.

## Figure Captions

1. Photograph of the equipment used for the preparation of friction-transfer layers showing, from left to right the computer control, the deposition device and the temperature and rate controls, resp.
2. Electron diffraction patterns of friction-transfer layers of: a) polyethylene [HDPE,  $M_w = 6 \times 10^4$ ], b) Vectra<sup>®</sup> and c) fluorinated ethylene-propylene copolymer [FEP]. Deposition direction and chain axes are vertical.
3. Transmission electron micrograph of oriented polyethylene friction-transfer layer decorated with vaporized, low molecular weight polyethylene.
4. Optical micrograph, taken with crossed polarizers, of a mixture of small molecular liquid crystals [4-cyano-4'-n-alkylbiphenyls] deposited onto a glass support that was partially covered with a polyethylene friction-transfer orientation layer.
5. Electron diffraction pattern of an oriented poly(*p*-xylylene) [PPX] film, polymerized from the monomer onto a polyethylene friction-transfer orientation layer. PPX chain axis is vertical.





Page 1

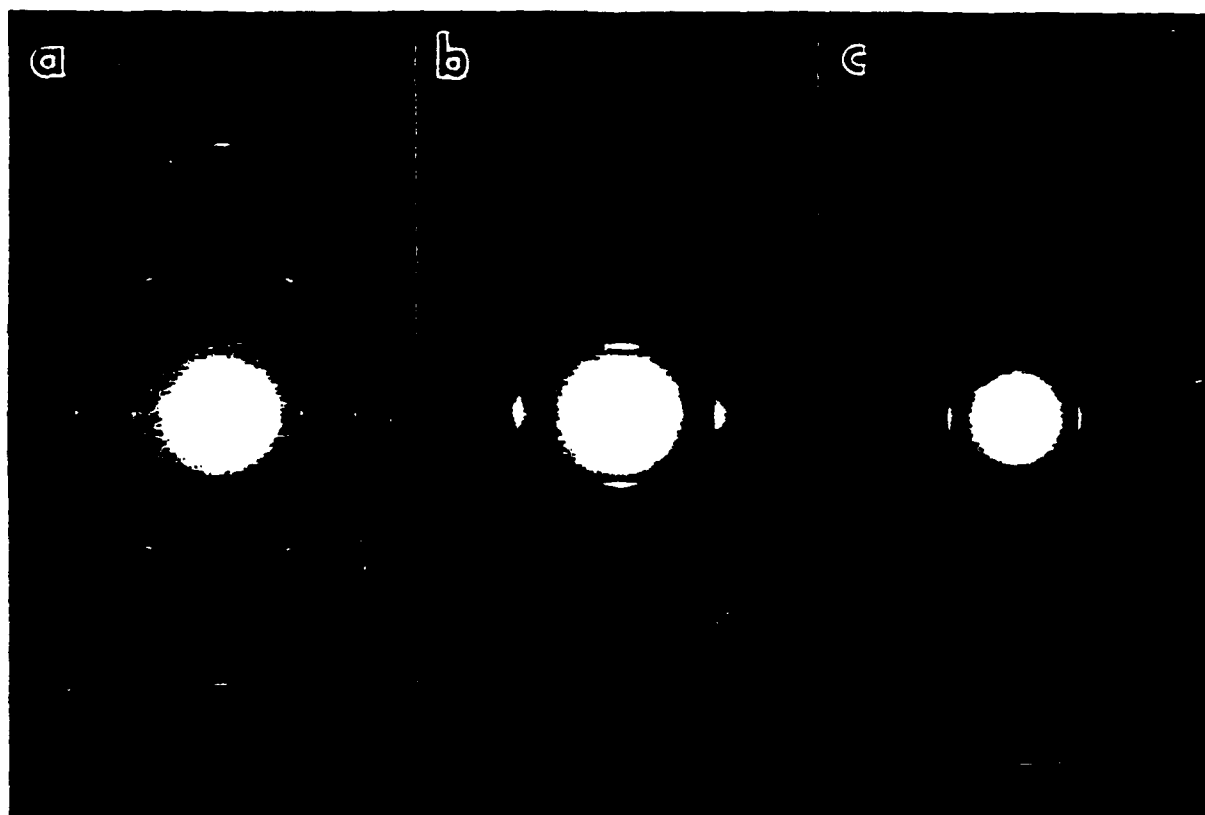


Fig. 2

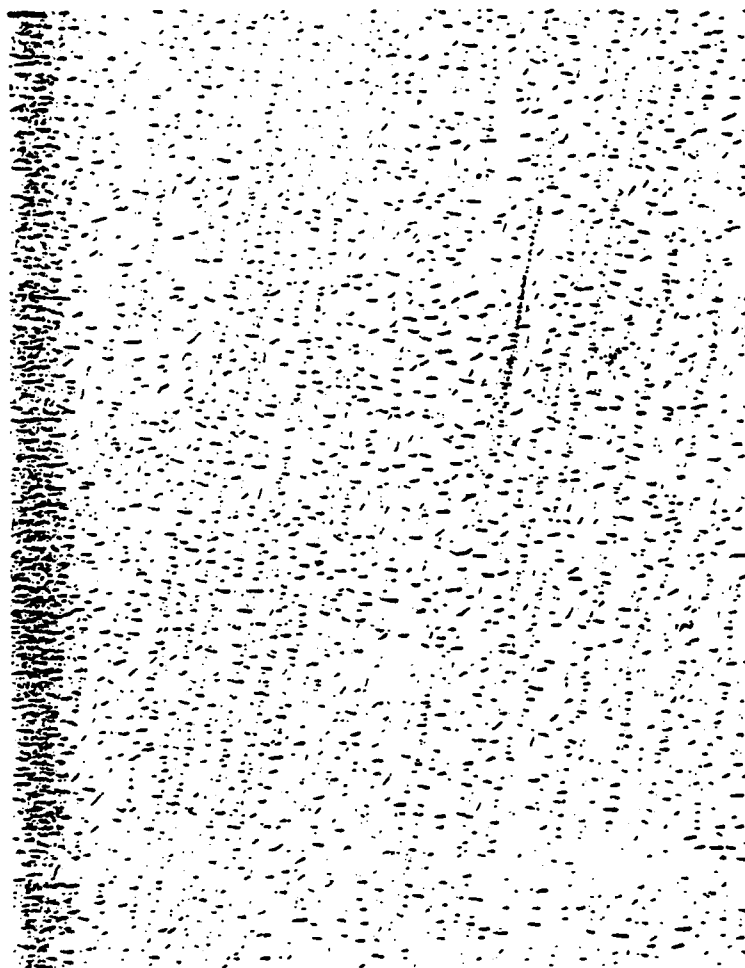


Figure 3. Motamedi *et al.*



Figure 4. Motamedi *et al.*

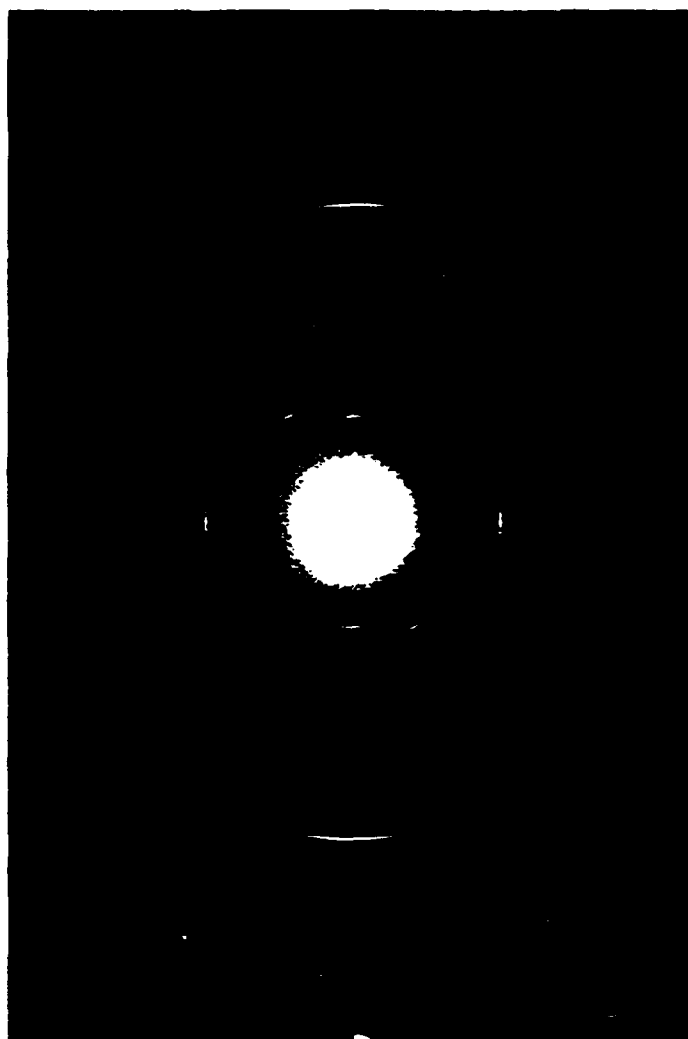


Figure 5. Motamedi *et al.*

# Molecular structure and thickness of highly oriented poly(tetrafluoroethylene) films measured by atomic force microscopy

P. DIETZ, P. K. HANSMA, K. J. IHN\*, F. MOTAMEDI\*, P. SMITH\*

*Department of Physics and \* Materials Department, University of California, Santa Barbara, CA 93106, USA*

Atomic force microscopy (AFM) was used to image thin single-crystal-like layers of poly(tetrafluoroethylene) (PTFE) deposited mechanically on glass. Not only can AFM reveal details of the molecular structure, but it can also provide direct measurement of the absolute thickness and continuity of these films. High-magnification images show individual rod-like molecules with an intermolecular spacing of 0.58 nm. The helix of individual molecules is clearly resolved and fine structures along the polymer chains may indicate individual fluorine atoms. The thickness of the films varies from 7–32 nm depending on deposition temperature and mechanical pressure. The continuity of the films strongly decreases at lower temperatures. The remaining single fibres are not stable and can be modified by the imaging tip.

## 1. Introduction

Recently, a new method for producing highly oriented single-crystal-like films of poly(tetrafluoroethylene) (PTFE) was introduced [1]. The simple technique consists of dragging a bar of the polymer at controlled temperature, pressure and speed against a smooth glass substrate. Electron diffraction studies of the PTFE films reveal that the chains of the PTFE macromolecules are oriented parallel to the glass and along the sliding direction [1]. The significance of these PTFE films derives from the fact that other materials grown on their surface from solution, melt or vapour also show a remarkable degree of alignment. Advantages of highly oriented polymers compared with unoriented materials can include significant increases of stiffness, strength or electrical conductivity; possible applications are materials reinforcement or molecular electronics.

Atomic force microscopy (AFM) was invented in 1986 by Binnig *et al.* [2]. A sharp stylus is mounted on a cantilever with a low spring constant. The sample is raster-scanned beneath the stylus. Forces acting between the sample surface and the stylus will deflect the weak cantilever. Measuring the displacement of the tip gives a real three-dimensional topographic representation of the sample surface. AFM can image the original surface of non-conducting materials with nanometre scale resolution in air and even under liquids [3]. Consequently, the sample need not be exposed to high vacuum, high energy beams or special preparation techniques. In the field of thin polymeric films such as PTFE, AFM has the advantage that it can reveal two different kinds of important information. At high resolution it can image the molecular arrangement with single molecule and even submolecular resolution. Simultaneously, a low-resolution measure-

ment can give the absolute height and homogeneity of the films.

AFM investigations of films and crystals of polymers and polymer-related compounds have been recently reported, including molecular resolution images of polyethylene dendrites [4], cold-extruded polyethylene [5], polypropylene [6], cyclic alkanes [7], PTFE and polycarbonate [8]. A previous AFM study of the structure of highly oriented PTFE films [9] showed that the resolution is sufficient to distinguish individual macromolecules. In this paper we present the first direct observation of the helical structure of individual PTFE molecules and report a method to measure the absolute thickness of highly oriented PTFE films which allows study of the influence of the preparation parameters on the thickness and continuity of the films.

## 2. Experimental procedure

The PTFE layers were imaged with a Nanoscope™ AFM from Digital Instruments [10]. A schematic drawing of the imaging principle is given in Fig. 1. A pyramid silicon nitride microtip is mounted on a V-shaped cantilever with low spring constant. The sample, which is attached to a piezoelectric x-y-z-translator, is raster-scanned beneath the tip. The displacement of the tip is measured by sensing the deflection of a laser beam reflected off the back of the cantilever with a two-segment photodiode. A feedback loop keeps the vertical position of the tip constant by moving the surface up and down with the piezoelectric translator (constant force mode).

Low contact forces are necessary to prevent deformations of the sample surfaces. We achieve forces

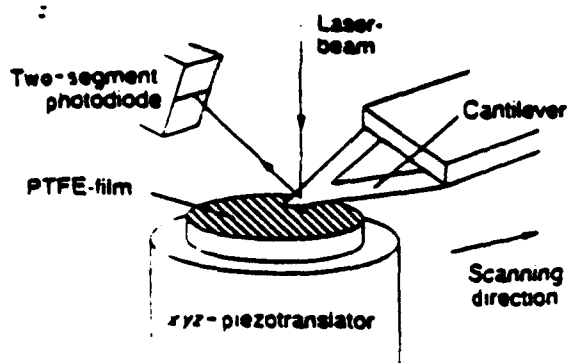


Figure 1. Schematic drawing of the atomic force microscope.

between  $10^{-7}$  and  $10^{-8}$  N by using microfabricated cantilevers with a small spring constant ( $0.027 \text{ Nm}^{-1}$ ) [10] and by minimizing the contact force in the force distance mode of our AFM, as described in detail by Weisenhorn *et al.* [11]. The silicon nitride cantilevers with integrated tips are  $200 \mu\text{m}$  long and  $0.6 \mu\text{m}$  thick. The high-resolution image in Fig. 2 was taken with an "F" scanner, which has a maximum scan range of  $8 \times 8 \mu\text{m}^2$ ; the thickness measurements (Figs 3 and 4) were performed with a  $120 \mu\text{m}$  "J" scanner.

Glass microscope slides cleaned in KOH were used as substrates for the PTFE films. A solid PTFE bar was moved along their surface at a rate of  $1 \text{ mm s}^{-1}$ . In order to study the influence of preparation parameters on thickness and continuity of the films, we varied mechanical pressure and deposition temperature. Films were prepared with pressure between 20 and  $40 \text{ N cm}^{-2}$  and temperature between 100 and  $280^\circ\text{C}$ ; the details are given in Table I. The quality, orientation and continuity of the films were checked in advance by cross-polarized light microscopy. All AFM images were taken in air.

Height measurements of PTFE films could be carried out easily because films prepared at temperatures up to  $280^\circ\text{C}$  do not completely cover the glass substrate. Within scan ranges of  $10 \times 10 \mu\text{m}^2$ , or even smaller, we always found areas where the glass was visible and the height difference between substrate and film could be directly determined from the AFM image. For films with complete coverage, thickness measurements with AFM can still be carried out, e.g. by touching a small soft tool, like a micropipette, to the surface in order to uncover parts of the glass substrate [9]. However, in this case artefacts caused by the damage of the film cannot be ruled out and the height values may be less reliable.

### 3. Results and discussion

#### 3.1. Molecular structure

A high-resolution AFM picture taken on a highly oriented PTFE film is shown in Fig. 2. Individual PTFE macromolecules can be readily distinguished, with intermolecular spacings of  $0.58 \pm 0.06 \text{ nm}$ . The AFM was calibrated in *x*- and *y*-directions by imaging the well-known hexagonal structure of mica, which

TABLE I. Deposition parameters and thickness of the highly oriented PTFE films imaged in this study.

Film	Temperature ( $^\circ\text{C}$ )	Pressure ( $\text{N cm}^{-2}$ )	Thickness (nm)
1	100	20	Single fibres
2	200	20	Single fibres
3	230	20	7.3
4	240	40	11.1
5	250	20	8.5
6	250	40	14.0
7	280	20	26.2
8	280	40	32.0

has a lattice spacing of  $0.52 \text{ nm}$ . Bunn and Howells [12] found from electron diffraction studies that the chain stems of crystalline PTFE molecules are packed on a nearly hexagonal array with distances between single chains of  $0.554 \text{ nm}$ , which is in good agreement with our result.

In addition, twists in individual molecules are clearly visible in these AFM images. The helical structure can be emphasized by entering the image in Fourier space, a procedure that smoothes the fine structure along the single twists, and by using a perspective representation with a view angle of  $60^\circ$  (Fig. 3b). The distance between single twists in this image is about  $0.57 \pm 0.06 \text{ nm}$ . What we imaged here is most likely the top layer of the fluorine helix of individual PTFE molecules. The fine structure along the twists which can be seen in the unfiltered image (Fig. 2a) is presumably produced by individual fluorine chain atoms. Molecule cross-sections indicate that in some areas three or four individual fluorine atoms within one elevation of the molecule can be counted. Earlier AFM observations on  $\text{SrF}_2$  single-crystal surfaces confirm that the AFM is able to resolve individual fluorine atoms [13].

Comparison of our image with a model of the PTFE molecule that was derived for electron diffraction observations [12] (Fig. 2c) shows quantitatively good agreement. In this model, which was based on a PTFE layer prepared below  $20^\circ\text{C}$ , a full  $360^\circ$  twist of the chain occurs in  $3.36 \text{ nm}$ , 13 zigzags or 26 chain atoms, but the actual period is half this, because a zig-zag consists of two lines of atoms, and a half twist brings the fourteenth atom on the second line directly above the first atom on the first line. Taking into account that the elevations of the fluorine helix are observed in our AFM images, we would find four of these elevations within  $3.36 \text{ nm}$  (see model in Fig. 2c) resulting in a periodicity of  $0.84 \text{ nm}$  along the chains. The period measured from Fig. 2 is  $0.57 \pm 0.06 \text{ nm}$ , which is about 30% below the expected value. Because the accuracy of the *x*- and *y*-calibration of the microscope, derived from mica observations, is generally better than  $\pm 10\%$ , we conclude that the special film processing technique which is used here may have produced a different PTFE configuration with an increase of the chain period. Changes in the structure of PTFE at certain transition temperatures, including increase of chain period, have been reported by others [12, 14].

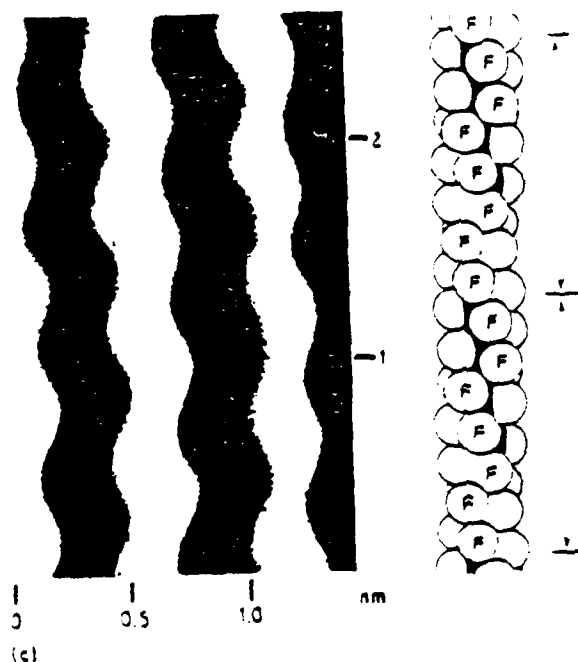
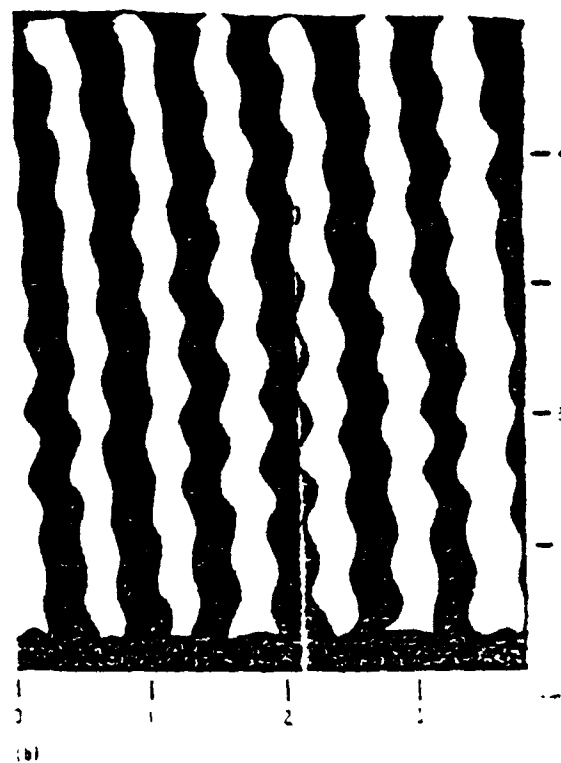
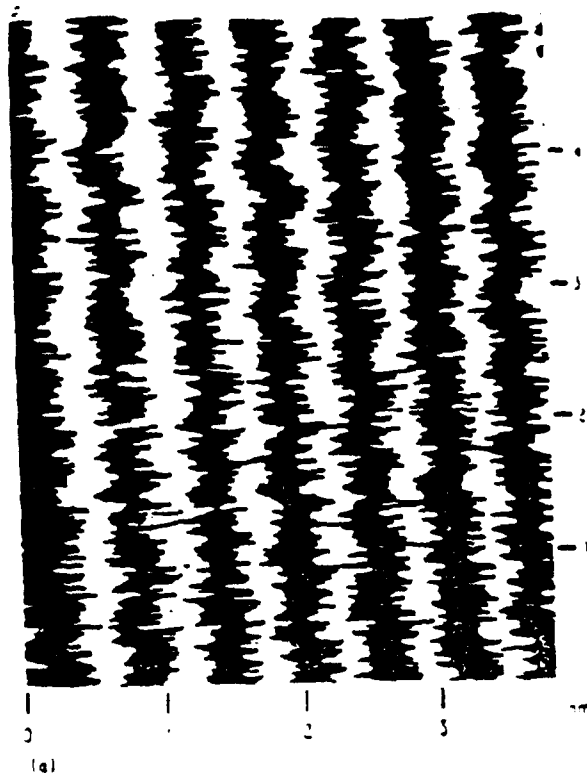


Figure 2. AFM image of individual molecules on a highly oriented polytetrafluoroethylene (PTFE) film. Deposition parameters:  $P = 20 \text{ N cm}^{-2}$ ,  $T = 230 \text{ C}$ . (a) Raw image. Image size is  $15 \times 50 \text{ nm}^2$ ; scanning rate was  $20 \text{ Hz}$ . Note the fine structure along the molecules, which is probably produced by individual fluorine atoms. (b) Same image after Fourier filtering. The perspective representation emphasizes the helical character of the molecules. (c) Comparison between AFM image and a PTFE model derived from electron diffraction studies [12]. The arrows indicate the chain repeat distance. Note how the right molecule in the AFM image resembles the model.

typical examples of films deposited in this temperature range are given in Fig. 3. The cross-sections at the bottom of each picture which were taken perpendicular to the rows, illustrate that the height of the films is not homogeneous but spreads over a wide range up to tens of nanometres. For example, the film in Fig. 3a, which was deposited at  $230 \text{ C}$  and with  $20 \text{ N cm}^{-2}$ , has an average height of only  $8.5 \text{ nm}$  but shows height variations up to  $15 \text{ nm}$ . The uncovered parts of the glass substrate are clearly visible in the picture as well as in the cross-section.

Height distribution curves which can be calculated from the AFM images are excellent both to characterize the homogeneity of the films and to determine the thickness. Generally, two peaks are clearly visible in the distribution curves (see Fig. 3) of our films, one corresponding to the PTFE layer, the other to the glass substrate. The difference between the mean value of the film height distribution and the mean value of the glass height distribution (the glass substrate is not flat on the atomic scale) gives the average thickness of the film. In addition, the width and shape of the height distribution curve contain information on homogeneity and smoothness of the film.

### 3.2. Thickness and continuity

Micrometre-scale AFM images were used to measure smoothness and thickness of eight PTFE films grown under different deposition conditions (Table I). We found that the most influential parameter is the temperature. Films deposited between  $230$  and  $280 \text{ C}$  show typical row-like structures which cover the glass surface almost completely. However,  $5\%$ – $20\%$  of the glass is still visible between these PTFE rows, a fact that can be utilized for the height measurements. Two



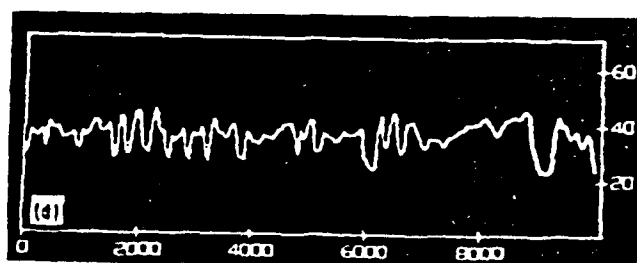
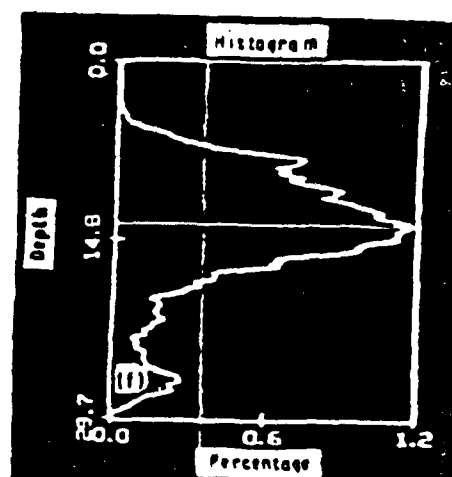
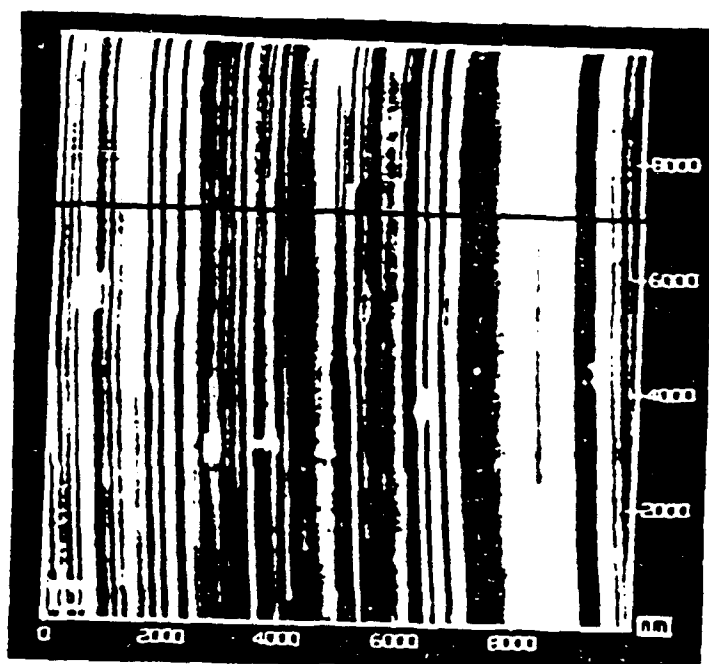
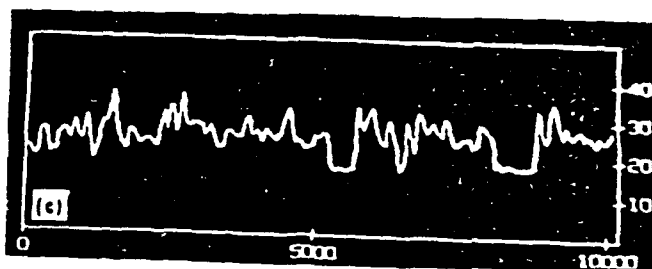
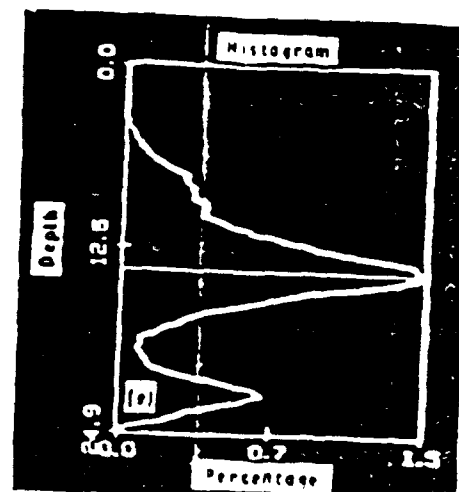
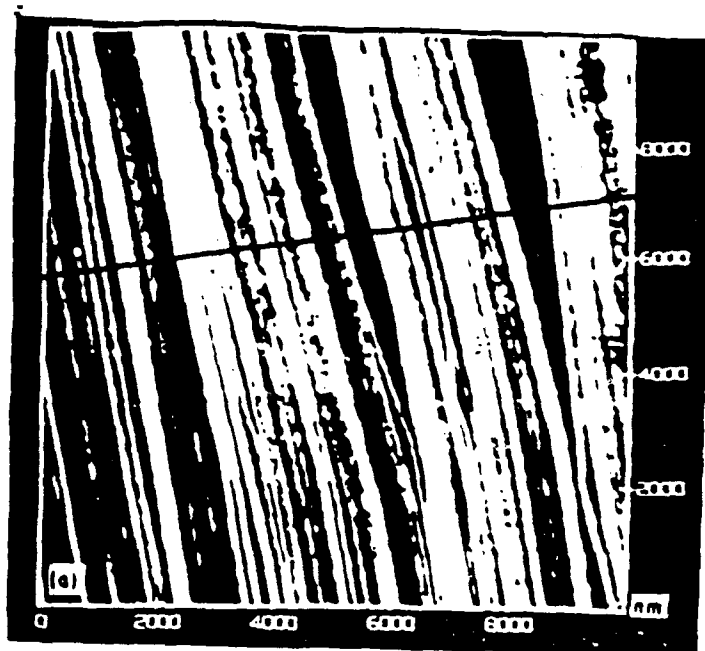


Figure 3. Micrometre-scale AFM images of highly oriented PTFE films deposited under different conditions: (a)  $P = 20$  Ncm<sup>-2</sup>,  $T = 230$  °C; (b)  $P = 40$  Ncm<sup>-2</sup>,  $T = 250$  °C. Image size is  $10 \times 10$   $\mu\text{m}^2$ ; scanning rate was 4.4 Hz. Note the PTFE rows running in the direction in which the polymer was laid down, i.e. (c) Cross-sections perpendicular to the orientation of the films, i.e. (d) Height distribution curves used to determine the average film height.

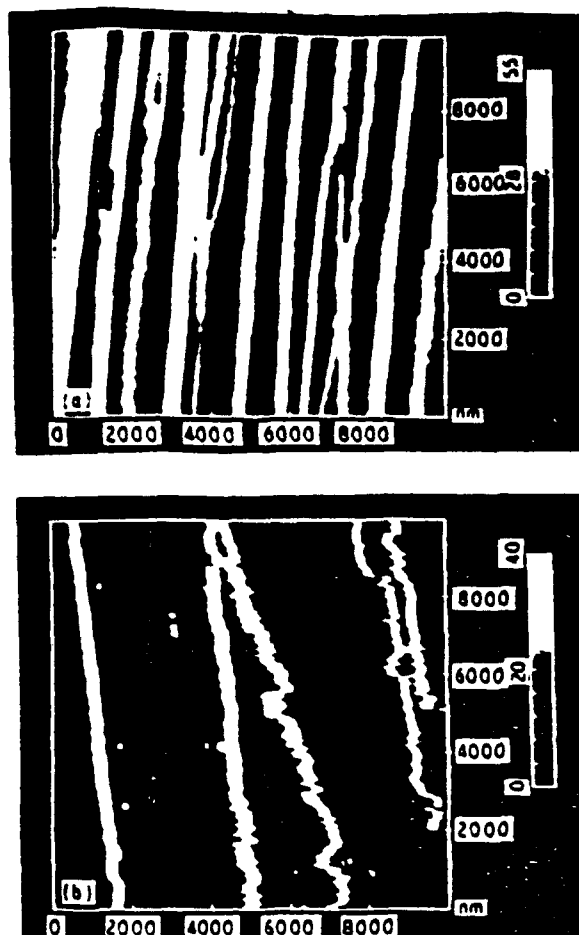


Figure 4 PTFE films grown at lower temperatures. (a) 200 °C, (b) 100 °C. Pressure and scanning parameters as in Fig. 3a. Note the dissection and displacement of single fibres by the AFM tip.

Thickness values for the films in Fig. 3 and for four other films are given in Table I ranging from 7–32 nm. As expected, the thickness increases both with increasing temperature and with increasing mechanical pressure. X-ray data of the films [15] show the same tendency as our results. But in contrast to the AFM, X-ray measurements can only reveal relative values of the film thickness.

At deposition temperatures below 200 °C the quality of the films deteriorates significantly. Less than 50% of the glass surface is covered by a film deposited at 200 °C (Fig. 4a) and less than 10% by a film grown at 100 °C (Fig. 4b). The films disintegrate into single fibres with diameters of about 300 nm. The stability of these fibres is not as high as in the closer packed films, and interactions between the imaging tip and these fibres were frequently observed. Parts of the fibres were dissected and displaced resulting in zigzag structures along the fibres as seen in Fig. 4b.

#### 4. Conclusions

Atomic force microscopy as a new high-resolution technique that provides direct three-dimensional in-

formation of the original unprepared sample surface, has become an invaluable companion to electron microscopy in the field of materials research. We have shown that AFM can be useful for the characterization of highly oriented PTFE films on a scale from tens of micrometres to less than 1 nm. The microscope is able to resolve details of the molecular structure, such as the fluorine helix, with submolecular resolution and at the same time, can provide detailed information on the absolute film thickness and the homogeneity of the films. The latter information will be especially important in developing an understanding of the orienting faculty and in improving the quality of the layers in dependence upon the deposition conditions. Highly oriented PTFE films show a remarkable capability to orient a wide variety of other molecules. Promising AFM applications for the near future might be the characterization of such systems.

#### Acknowledgements

We thank H. Hansma for sharing her AFM experience on PTFE films. This project was supported by the Deutsche Forschungsgemeinschaft fellowship Di 440/1-2 (P.D.), the National Science Foundation Solid State Grant DMR89-17164 (P.K.H.) and the Office of Naval Research (P.K.H.).

#### References

1. J. C. WITTMANN and P. SMITH, *Nature* **352** (1991) 414.
2. G. BINNIG, C. F. QUATE and CH. GERBER, *Phys. Rev. Lett.* **12** (1986) 930.
3. D. RUGAR and P. K. HANSMA, *Phys. Today* **43** October (1990) 23.
4. R. PATIL, S. J. KIM, E. SMITH, D. H. RENKER, and A. L. WEISENHORN, *Polym. Commun.* **31** (1990) 455.
5. S. N. MAGONOV, K. QVARNSTROM, V. ELINGS and H. J. CANTOW, *Polym. Bull.* **25** (1991) 689.
6. B. LOTZ, J. C. WITTMANN, W. STOCKER, S. N. MAGONOV and H. J. CANTOW, *ibid.* **26** (1991) 209.
7. W. STOCKER, G. BAR, M. KUNZ, M. MOLLER, S. N. MAGONOV and H. J. CANTOW, *ibid.* **26** (1991) 215.
8. S. N. MAGONOV, S. KEMPF, M. KIMMIG and H. J. CANTOW, *ibid.* **26** (1991) 715.
9. H. HANSMA, F. MOTAMEDI, J. C. WITTMANN, P. SMITH and P. K. HANSMA, *Polym. Commun.* (1992) 11 (1992) 41.
10. T. R. ALBRECHT and C. F. QUATE, *J. Vac. Sci. Technol. A* **6** (1988) 271.
11. A. L. WEISENHORN, P. K. HANSMA, T. R. ALBRECHT and C. F. QUATE, *Appl. Phys. Lett.* **54** (1989) 2651.
12. C. W. BUNN and E. R. HOWELLS, *Nature* **18** (1954) 549.
13. P. DIETZ, C. A. RAMOS and P. K. HANSMA, *J. Vac. Sci. Technol. B* **10** (1992) 741.
14. J. F. WHITNEY, R. H. PIERCE and W. M. D. BRYANT, Abstracts of the American Chemical Society Meeting (March 1953).
15. P. SMITH, unpublished X-ray results, Materials Department, University of California, Santa Barbara.

Received 17 March  
and accepted 6 July 1992

17 97 111 101

## Elastic Properties of Thin Ultra-Oriented Poly( $\epsilon$ -caprolactone) Films Grown on PTFE Substrates as revealed by Brillouin Spectroscopy.

J. K. Krüger\*, M. Precht†, P. Smith‡, S. Meyer\*\*, J.C. Wittmann\*\*

\*Fachbereich Physik, Universität des Saarlandes, Bau 38, W-6600 Saarbrücken, Germany

†Materials Department and Department of Chemical & Nuclear Engineering, University of Santa Barbara, Santa Barbara, CA 93016 USA

\*\*Institut Charles Sadron (CRM-EAHP), F-67083 Strasbourg

Recently, a simple and unexpectedly versatile method was reported which can be used to orient a wide variety of crystalline and liquid crystalline materials including polymers and oligomers [1]. This method is based on the fact that a highly oriented polytetrafluoroethylene [PTFE] layer, of about 10 nm thickness, mechanically deposited [2] onto a smooth glass surface, induces an outstanding unidirectional texture in thin films grown on such substrate. Preliminary explanations concerning the orientation mechanism were given in reference [1].

The effect of surface induced oriented crystallization onto PTFE of polymers is illustrated in Fig. 1. This figure shows an optical photomicrograph, taken with crossed polarizers, of poly( $\epsilon$ -caprolactone) (PCL) crystallized from the melt onto a glass slide partially covered with a thin layer of oriented PTFE. The left-hand side of the photomicrograph shows the usual spherulitic structure resulting from isotropic crystallization. By contrast, the right hand side of the picture illustrates the strong orientation inducing effect of the PTFE layer. The PCL films are i) uniformly birefringent and ii) homogeneously oriented with the PCL chain axis oriented parallel to the friction direction, i.e. to the PTFE macromolecules [1].

The aim of the present letter is, on the one hand to examine the acoustic and opto-acoustic properties of semi-crystalline polymers oriented by the present method, using PCL as a model system; and, on the other hand, to introduce high-performance Brillouin spectroscopy as an appropriate and useful technique to investigate these properties on films of only a few micrometers thickness.

Highly oriented PCL films were prepared by dissolving the polymer (Cellomer Associates,  $M_w \approx 14,000$ ) at room temperature in  $\text{CHCl}_3$ , spreading the solution onto a PTFE coated glass slide [see ref. 1], and evaporating the solvent; finally, the PCL film was molten and recrystallized. The thickness of the PCL film thus produced was estimated to be  $\sim 5 \mu\text{m}$ , i.e. about 10 times the optical wave length and about sixteen times the acoustical wave length.

The acoustic and opto-acoustic properties were measured with a tandem multi-pass Brillouin spectrometer using the 90A- and 90R- scattering technique [3]. The 90A- scattering technique allows for the determination of the sound velocity polar diagram for wave propagation within the film plane. The 90R- scattering technique permits estimation of the optical birefringence of the sample within the film plane. A detailed discussion of the Brillouin techniques used is given in references [4-6]. Figs. 2a and b give, schematics of the 90A- and 90R- scattering geometries.

Fig. 3 shows the hypersonic frequencies measured at  $T=293 \text{ K}$  and the acoustic wave propagation in different directions relative to the orthogonal coordinate system ( $x=1$ ,  $y=2$ ,  $z=3$ ) of the sample. For convenience, the  $z$ -axis has been chosen to be oriented within the film plane, directed along the preferential axis of the PTFE/PCL molecules. The  $x$ -axis has been chosen to be also within the film plane. Accordingly, the  $y$ -axis is directed orthogonal to the film (Fig. 2).

Angle-resolving Brillouin measurements in connection with the 90A-scattering technique were made (see Fig. 3) to investigate the propagation behavior of quasi-longitudinal (QL) and quasi-transverse (QT) acoustic modes within the plane of the PCL film. From these data, the sound velocity polar diagram (in Fig. 4) could be derived using the corresponding relation for the 90A-scattering geometry [3]:

$$(1) \quad v = f^{90A} \frac{\lambda_0}{\sqrt{2}} = \sqrt{(c_{\text{eff}}/\rho)}$$

where  $f^{90A}$  is the measured phonon frequency,  $c_{\text{eff}}$  is the effective elastic stiffness constant related to  $v$ ,  $\lambda_0 (= 514.5 \text{ nm})$  is the vacuum wave length of the argon ion

laser used and  $\rho$  ( $\approx 1000 \text{ kg/m}^3$ ) is the approximate mass density of PCL. Using the Christoffel equation (cf. [7]) this polar diagram could be fitted with the method of least squares to yield the appropriate elastic stiffness constants:

$$\begin{aligned} c_{11} &= (5.75 \pm .02) \text{ GPa}, c_{13} = (3.16 \pm .04) \text{ GPa}, \\ c_{33} &= (10.62 \pm .03) \text{ GPa and } c_{55} = (0.63 \pm .01) \text{ GPa}. \end{aligned}$$

The birefringence of the sample  $\Delta n = (n_3 - n_1)$  within the film plane can be estimated from the sound frequency data measured with the 90R-scattering geometry, directing the phonon wave vector along the  $y=2$ -coordinate axis and the electric field vectors of the laser light and the scattered light either along the  $z=3$ -axis, yielding  $f_3^{90R}$  (data point [+] in Fig. 3); or along the  $x=1$ -axis, yielding  $f_1^{90R}$  (data point [\*] in Fig. 3). The value of  $\Delta n$  can be estimated from the Brillouin data using the relation

$$(2) \quad \Delta n = n_1 (f_3^{90R} - f_1^{90R}) / f_1^{90R}$$

$n_1$  can be estimated from 90A- and 90R- data, provided that the approximation  $c_{11} = c_{22}$  holds, using the relation [5]:

$$3) \quad n_1 = [0.5(f_1^{90R} / f_{q_{\parallel x}}^{90A})^2 + 1]^{0.5}$$

where  $f_{q_{\parallel x}}^{90A}$  is the hypersonic frequency. The resulting values for the present oriented PCL films are:  $n_1 = 1.502$ ,  $n_3 = 1.554$  and  $\Delta n = 0.052$ . The accuracy of  $\Delta n$  can be further improved by taking into account refined values for the acoustic wave vectors involved.

The reported elastic and optical anisotropy may be discussed in terms of molecular orientation and be compared with optical and acoustical properties of mechanically oriented polymers (cf. [8,9]). In this regard, polyethylene (PE) and polycarbonate (PC) probably belong to the most investigated materials (see e.g. references [6,8,9]). Rather highly oriented PC with an orientation parameter  $P_2 = 0.454$  yields a birefringence of  $\Delta n = 0.049$  and an elastic anisotropy

$$(4) \quad P_2^M = (c_{33} - c_{iso}) / c_{33} = 0.33$$

where  $P_2^M$  is, according to Moseley [10], an estimation of  $P_2$ , on the base of pure elastic data. The index "iso" refers to the isotropic state; the approximation  $c_{iso} = c_{11}$  generally holds true [6]. In case of the present oriented PCL films  $\Delta n$  is comparable to that of highly oriented PC. However, according to eq. 4, Moseley's orientation parameter  $P_2^M = 0.46$  significantly exceeds the value obtained for PC indicating on one hand the high degree of molecular orientation obtained by oriented crystallization onto the PTFE layers and, on the other hand, the role of the internal electric field for the orientation-induced birefringence [11].

It is of interest to compare the present data obtained for oriented PCL with our Brillouin data for ultra-drawn polyethylene (PE) [6]. For the latter material we reported the following elastic constants:

$$c_{33} = 115 \text{ GPa}, c_{11} = 7.34 \text{ GPa}, c_{13} = 3.67 \text{ GPa}, c_{44} = 1.61 \text{ GPa}, \\ c_{66} = 1.83 \text{ GPa} \text{ and } c_{12} = 3.68 \text{ GPa}.$$

From these values an orientation parameter of  $P_2^M = 0.94$  can be calculated for the ultra-drawn PE films, which is significantly larger than that for the present PCL samples. This difference may be caused partly by the large difference between the longitudinal stiffness ( $c_{33}$ ) along the orientation axis  $z$  of PE and PCL. It should be noted, however, that the present oriented PCL films have a distinctly different structure than the ultra-drawn PE specimens. The former are composed of regularly stacked folded chain, lamellar crystals of finite thickness, oriented edge on. By contrast, the PE films are comprised of a continuous, crystalline phase in which the macromolecules adopt a highly extended chain conformation. Therefore, it cannot be excluded that the molecular orientation parameter  $P_2$  of the present PCL films is much larger than reflected by the value of  $P_2^M$ . This would be the case, for example, if the [amorphous] lamellar interfaces of the PCL structure have a rather low longitudinal stiffness for wave propagation along the orientation ( $z$ -) axis. A similar effect has been found responsible for the rather small elastic anisotropies of highly oriented polymer side-chain liquid crystals well above their glass transition [5]. Further investigation of the relations between the molecular structure and the

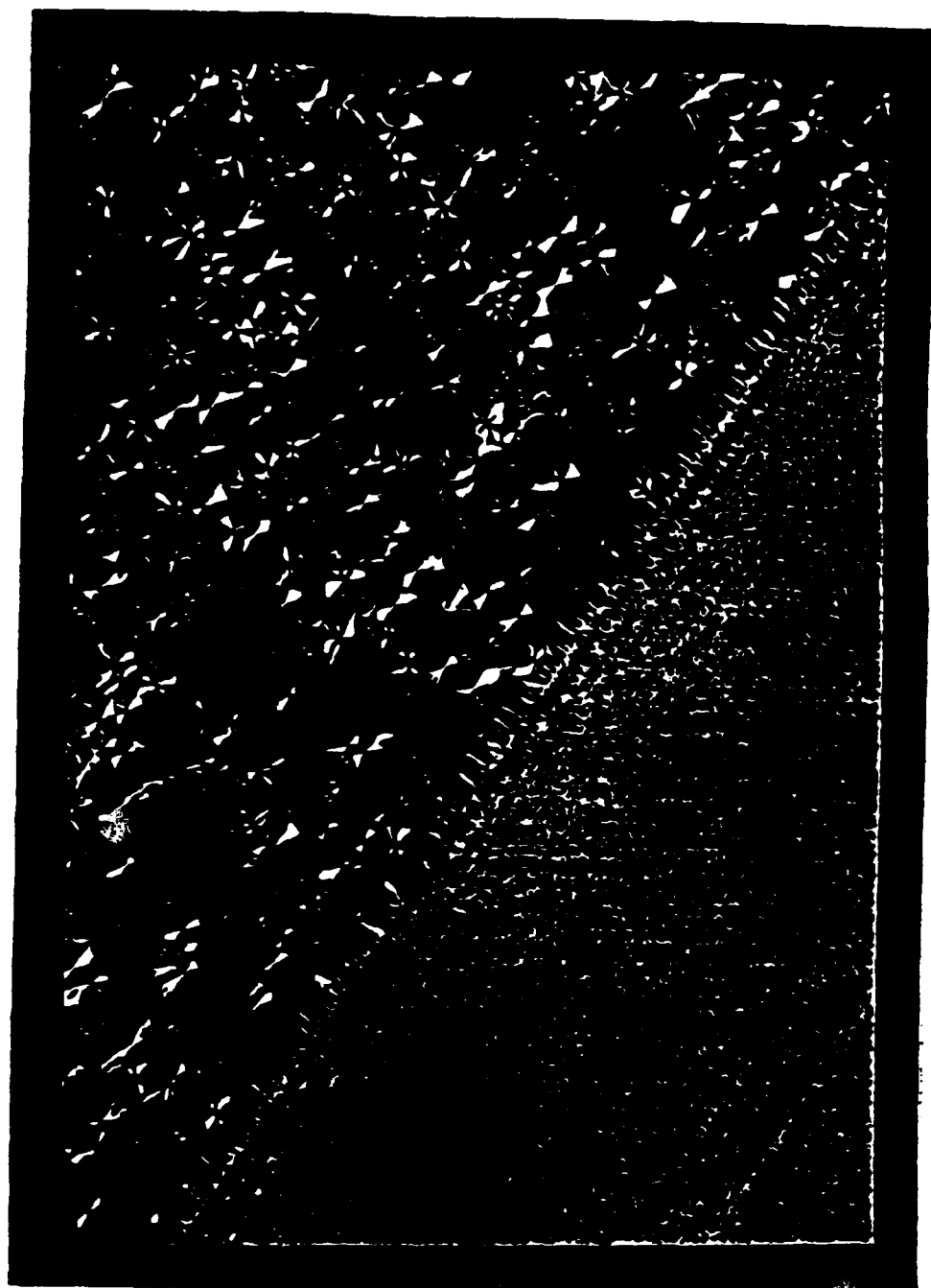
acoustic and opto-acoustic properties of PCL films oriented onto PTFE layers are under way.

## References:

- [1] J.C. Wittmann and P. Smith, *Nature*, 352, 414 (1991)
- [2] C.J. Pooley and D. Tabor, *Proc. R. Soc. Lond.* A329, 251 (1972)
- [3] J.K. Krüger, L. Peetz, W. Wildner, M. Pietralla; *Polymer* 21, 620 (1980)
- [4] J.K. Krüger, A. Marx, L. Peetz, R. Roberts, H.-G. Unruh; *Colloid & Polym. Sci.* 264, 403 (1986)
- [5] J.K. Krüger, L. Peetz, R. Siems, H.-G. Unruh, M. Eich, O. Herrmann-Schönherr, J.H. Wendorff; *Phys. Rev.* A37, 2637 (1988)
- [6] J.K. Krüger in "Optical Techniques to Characterize Polymer Systems", ed. H. Bässler, Elsevier (1989)
- [7] B. Auld, "Acoustic Fields and Waves in Solids", Vol. I, John Wiley & Sons (1973).
- [8] I.M. Ward, (ed.), "Structure and Properties of Oriented Polymers", Appl. Sci. Publ., London (1975) I.M. Ward, (ed.), "Developments in Oriented Polymers-1", Appl. Sci. Publ., London (1982)  
I.M. Ward, "Mechanical Properties of Polymers", Wiley-Interscience (1971)
- [9] H.J. Biangardi, "Bestimmung der Orientierung und molekularen Ordnung in Polymeren", Kunststofftechnik, Berlin (1980)
- [10] W.N. Moseley, *J. Appl. Sci.*, 3, 266 (1960)
- [11] M. Pietralla, H.-P. Grossmann, J.K. Krüger, *J. Polym. Sci., Polym.Phys. Ed.*, 20, 1193 (1982)



Top



Section

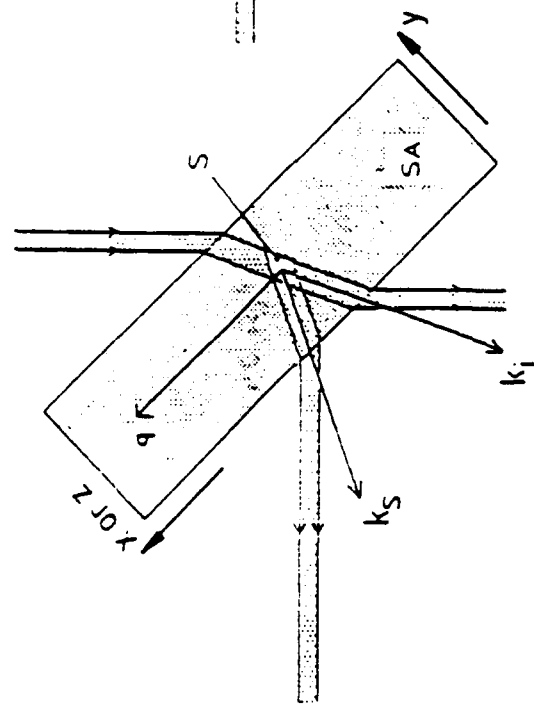
Figure captions:

Figure 1: Optical photomicrograph, taken with crossed polarizers, of poly( $\epsilon$ -caprolactone) crystallized from the melt onto a glass slide partially covered with a thin layer of oriented PTFE. It should be noted that the latter, very thin ( $\sim 10$  nm) layer itself is virtually invisible in the polarizing optical microscope. Magnification 100X.

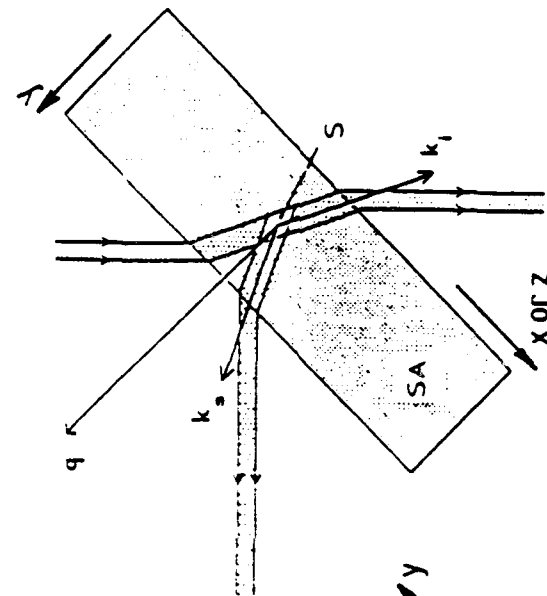
Figure 2: Schematic representation of the 90A (a) and 90R (b) scattering geometries. SA: sample; S: scattering volume;  $k_i, k_s$ : wave vectors of the incident and scattered laser light.

Figure 3: Sound frequencies of quasi-longitudinal (QL, o) and quasi-transverse (QT, •) acoustic modes, measured using the 90A scattering geometry, as a function of the sample rotation angle  $\Phi$ . The ( $y=2$ )-axis is the rotation axis. Data points (–) and (x) have been measured using the 90R scattering geometry (further explanations in the text).

Figure 4: Polar diagram of the measured quasi-longitudinal (o) and quasi-transverse (•) sound velocities. The full lines are fit curves (for explanation see text).

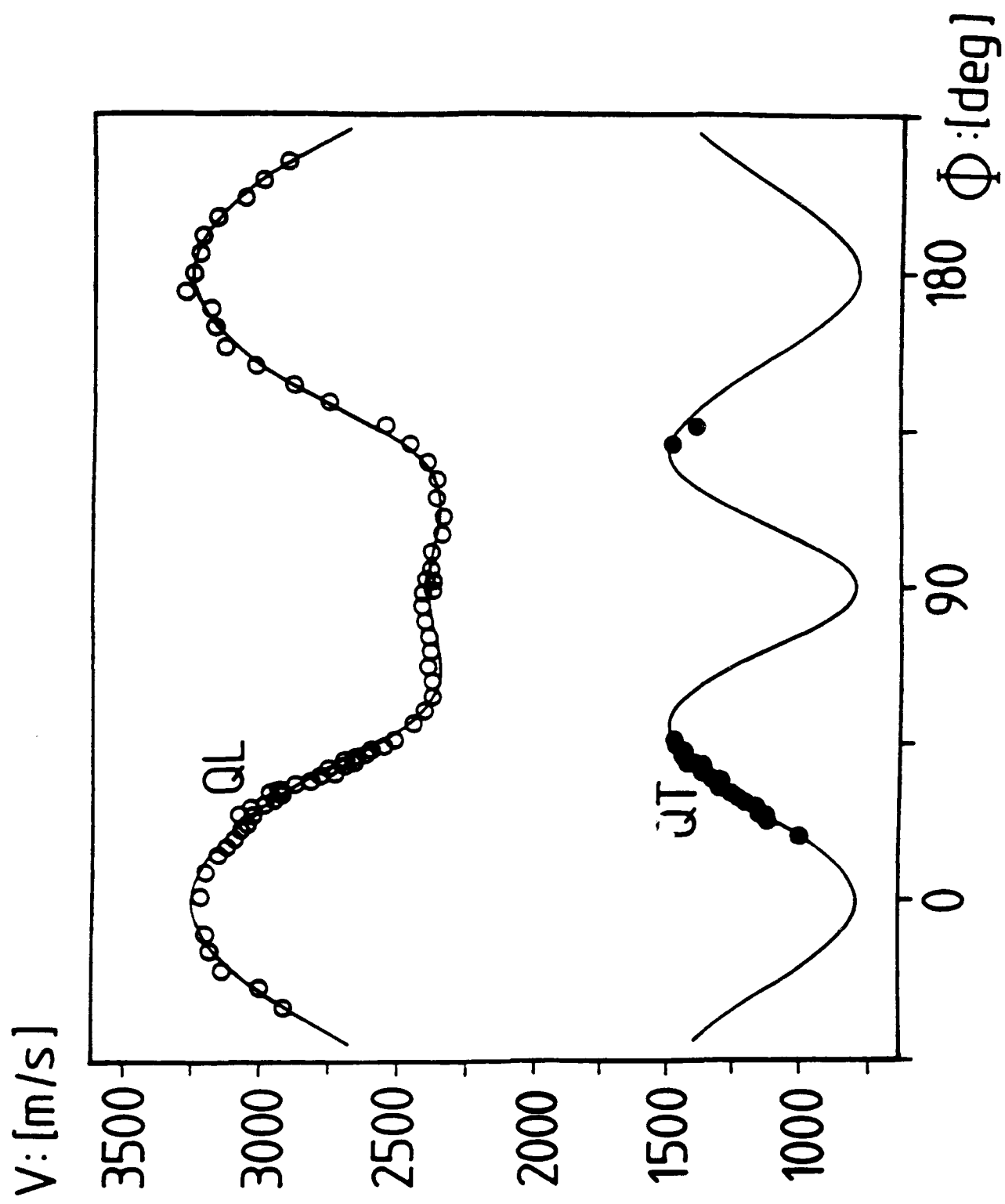


90A-scattering geometry



90R-scattering geometry

Fig. 1. a)  $\Phi = 0^\circ$ ; b)  $\Phi = 180^\circ$



# polymer communications

Molecular resolution of thin, highly oriented poly(tetrafluoroethylene) films with the atomic force microscope

Helen Hansma, Farshad Motamedi\*, Paul Smith\*† and Paul Hansma

Department of Physics, \*Materials Department and †Chemical & Nuclear Engineering Department, University of California at Santa Barbara, CA 93106, USA

and Jean Claude Wittman

Institut Charles Sadron (CRM-EAHP), Strasbourg, France

(Received 18 July 1991)

Thin, highly oriented layers of poly(tetrafluoroethylene) (PTFE, Teflon®) were produced with a simple mechanical deposition technique. Previously, it was shown that these films are exceptionally efficient substrates for oriented growth of a variety of materials. In this communication we report on the structure of the PTFE layers, as revealed with the atomic force microscope (AFM), at a resolution sufficient to distinguish the individual macromolecules. AFM images showed the surface roughness from scan sizes of a few nanometres up to 40  $\mu\text{m}$ . Analysis of damaged films allowed an estimation of the film thickness, which ranges from  $\sim 15$  to 40 nm thick.

(Keywords: poly(tetrafluoroethylene); orienting substrates; atomic force microscope)

## Introduction

Recently, a new, versatile method for orienting materials has been developed<sup>1</sup>. The technique consists of mechanically depositing a thin, oriented layer of poly(tetrafluoroethylene) (PTFE) onto a smooth counterface such as glass, by dragging the polymer at controlled temperature, pressure and speed against the substrate. Subsequently, the species of interest are deposited onto these PTFE films from the melt or vapour phase or from solution to yield surprisingly well-oriented materials. Electron diffraction of the orientation-inducing films revealed that the macromolecules were oriented parallel along the dragging direction<sup>1</sup>. It was postulated that the PTFE layers were not molecularly smooth, and that their orienting faculty derived, in part, from the multitude of ridges in the film, which presumably provided effective nucleation sites that induced the oriented growth of a great number of materials<sup>2</sup> deposited onto the PTFE films. However, no direct evidence was available with regard to the structure and topology of the PTFE layer to directly substantiate the proposed mechanism.

This paper reports on the characterization of the thin PTFE films with the atomic force microscope (AFM). The AFM was invented in 1985 by Binnig, Quate and Gerber<sup>2,3</sup>. It images surfaces by raster-scanning a sharp tip over the surface at a constant very low force. Under optimum conditions, the resolution of the AFM may be as low as a few angstroms, sufficient to resolve atoms, molecules and polymers<sup>4-9</sup>. Magonov *et al.*<sup>10</sup> have observed oriented polyethylene (PE) at submolecular resolution with the AFM and have detected overlapping fibrils in an extruded PE rod. Patil *et al.*<sup>11</sup> have shown that the AFM is useful for measuring lamellar thicknesses in dendritic crystals of PE.

## Methods

**Preparation of PTFE orienting substrates<sup>1</sup>.** Glass microscope slides used as substrates for PTFE films were cleaned overnight in ethanolic KOH. A solid PTFE (commercial grade Teflon®) bar was moved along the surface of the cleaned glass slide at a rate of  $1 \text{ mm s}^{-1}$  and a pressure on the order of  $1 \text{ kg cm}^{-2}$ . The temperature of both the PTFE rod and the glass surface was  $300^\circ\text{C}$ . The PTFE layers when imaged by cross-polarized light microscopy were barely visible; nevertheless very fine parallel, birefringent rows were detected, which were relatively free of defects.

**AFM imaging.** The PTFE layers were imaged with a NanoScope II from Digital Instruments (Santa Barbara, CA, USA). The image in *Figure 1* was taken using an AFM with a  $60 \mu\text{m}$  'F' scanner. The image in *Figure 2* was taken with a custom AFM built into a light microscope. This AFM had a  $0.6 \mu\text{m}$  scan range. All imaging was done in air. The silicon nitride cantilevers with integrated tips<sup>12</sup> were  $100 \mu\text{m}$  long with narrow arms.

## Results

The AFM image of the PTFE layers in *Figure 1* reveals parallel ridges running in the direction in which the Teflon® bar was moved over the microscope slide. Also, a kink band can be seen, about half way across the field and running in a horizontal direction. Defects of this type were uncommon and were probably caused by an abnormal vibration during deposition of the layer.

Heights and spacings of the PTFE ridges were estimated from many AFM images. Measured spacings between ridges ranged from  $< 25 \text{ nm}$  to  $> 1 \mu\text{m}$ . Heights of individual ridges typically ranged from 1 to  $\sim 30 \text{ nm}$ ; ridges as high as 60–70 nm were occasionally seen. The measured heights of individual ridges agreed well with the measurements of overall surface roughness on a

<sup>1</sup> In this work we also observed that the present PTFE films effectively induced the ordered growth of a low molecular weight DNA, i.e. a fluorescein-labelled 25-mer

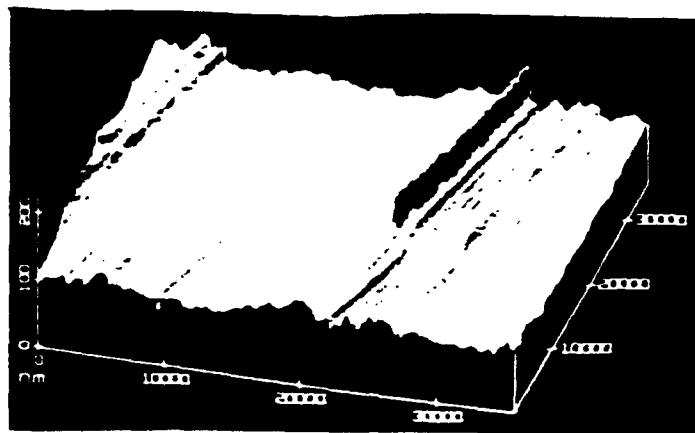


Figure 1. AFM image of a thin PTFE film. Image area is  $36 \times 36 \mu\text{m}$ . Height scale of 200 nm greatly magnifies the surface roughness. Surface would appear flat if height were plotted on the same scale as length and width. The image has no highpass or lowpass filtering. Note finely spaced PTFE rows running in the direction in which the polymer was laid down; also, a kink band is seen.

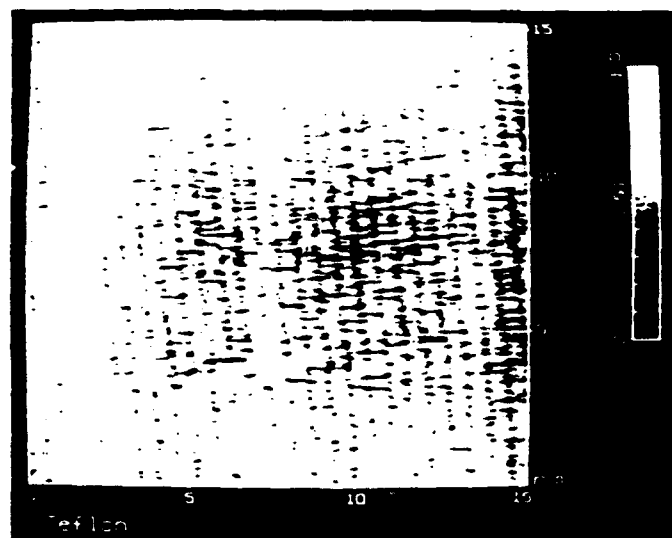


Figure 2. AFM image of a thin PTFE film showing rows of  $\sim 0.5 \text{ nm}$  spacing. Image area is  $15 \times 15 \text{ nm}$ . The image was taken with NanoScope II AFM settings of lowpass filter = 1, highpass filter = 4 and was not filtered further. Unfiltered images of the PTFE rows have a similar appearance and identical spacing; the estimated height of PTFE rows in unfiltered images is  $0.15 \text{ nm}$ .

number of samples. The AFM image in Figure 1, for example, was of a height of 42 nm, or less, over 96% of the surface; the height of the remaining 4% of the surface reached values as high as 95 nm. It should be noted that the AFM may underestimate the heights of closely spaced peaks, because the AFM tip is pyramidal, with a radius of curvature estimated<sup>12</sup> at 20–40 nm.

A higher magnification AFM image of the PTFE surface unveiled individual molecules (Figure 2). The characteristic intermolecular spacing<sup>13</sup> of the PTFE crystal lattice is 0.49 nm, which is not significantly different from the row spacing seen in AFM images of PTFE films. The AFM typically is calibrated by imaging mica, which has a lattice spacing of 0.52 nm. When PTFE and mica were imaged sequentially under the same conditions in the AFM, the spacing of the rows on PTFE was virtually indistinguishable from the spacing in the mica lattice. The molecular weight of the PTFE used was

$\sim 10^5 \text{ kg/kmol}$ , which corresponds to a molecular length of  $\sim 30 \mu\text{m}$ . Thus it is not surprising that no evidence of molecular ends in AFM images of molecular resolution were seen, since such high resolution could only be observed in scans of 40 nm or less. Occasionally, AFM images showed traces of structure along the PTFE rows with the approximate spacing expected for  $-\text{CF}_2$  groups. Such structure was seen more often when the scan direction was rotated by  $90^\circ$ .

A damaged PTFE film was imaged in the AFM to estimate the thickness of the layer on the glass microscope slide. The average thickness of the PTFE layer deposited under the present conditions varied from 15 to 40 nm on different regions of the film. Interestingly, the PTFE films, unlike many surfaces, could not be damaged with the AFM, even by deliberately increasing the force. The AFM, operating in air, typically scans surfaces with forces<sup>14</sup> of  $\sim 10^{-11} \text{ N}$ . The PTFE layers could, however,

be easily damaged by such actions as touching a plastic pipette tip to the surface.

### Conclusions

Highly oriented PTFE layers show an unusual ability to orient a wide variety of molecules and have the potential for many practical applications<sup>1</sup>. The AFM was successfully employed to characterize the complex surfaces of PTFE layers on a scale from tens of micrometres to less than a nanometre, thus revealing both molecular features and gross surface topology. The latter information will be of critical importance in developing an understanding of the orienting faculty of the PTFE layers and once more identifies the AFM as an exceptionally powerful tool in materials research.

### Acknowledgements

We thank Matt Wilson for building the custom AFM, Robert Sinsheimer, Albrecht Weisenhorn, Craig Prater, Srin Manne and Jason Cleveland for their helpful discussions and technical advice, and Gregory Kelderman for expert technical assistance.

This work was supported by NSF grants DIR-9018846 and DM89-17164 (HGH, PKH), the Office of Naval

Molecular resolution of PTFE films: H. Hansma et al.

Research (PKH, HGH), and AFOSR grant AF90-0283 (FM, JCW and PS).

### References

- 1 Wittmann, J. C. and Smith, P. *Nature* 1991, 352, 414
- 2 Binnig, G., Quate, C. F. and Gerber, Ch. *Phys. Rev. Lett.* 1986, 56, 57
- 3 Rugar, D. and Hansma, P. *Physics Today* 1990, 43, 23
- 4 Binnig, G., Gerber, Ch., Stoll, E., Albrecht, T. R. and Quate, C. F. *Europhys. Lett.* 1987, 3, 1281
- 5 Albrecht, T. R. and Quate, C. F. *J. Vac. Sci. Technol.* 1988, 16, 271
- 6 Manne, S., Butt, H.-J., Gould, S. A. C. and Hansma, P. K. *Appl. Phys. Lett.* 1990, 56, 1758
- 7 Meyer, G. and Amer, N. M. *Appl. Phys. Lett.* 1990, 56, 2100
- 8 Meyer, E., Heinzelmann, H., Rudin, H. and Güntherodt, H.-J. *Z. Phys. B Cond. Matter* 1990, 79, 3
- 9 Weisenhorn, A. L., MacDougall, J. E., Gould, S. A. C., Cox, S. D., Wise, W. S., Manne, J., Maivald, P., Elings, V. B., Stucky, G. D. and Hansma, P. K. *Science* 1990, 247, 1330
- 10 Magosov, S. N., Qvarnstrom, K., Elings, V. and Cantow, H. J. *Polym. Bull.* 1991, 25, 689
- 11 Patil, R., Kim, S.-J., Smith, E., Reneker, D. H. and Weisenhorn, A. L. *Polym. Commun.* 1990, 31, 455
- 12 Akamine, S., Barrett, R. C. and Quate, C. F. *Appl. Phys. Lett.* 1990, 57, 316
- 13 Bunn, C. W. and Howells, E. R. *Nature* 1954, 18, 549
- 14 Weisenhorn, A. L., Hansma, P. K., Albrecht, T. R. and Quate, C. F. *Appl. Phys. Lett.* 1989, 54, 2651

molecular  
that no  
molecular  
ion could  
asionally.  
the PTFE  
for -CF<sub>2</sub>  
when the

AFM to  
icroscope  
deposited  
40 nm on  
FE films.  
with the  
orce. The  
aces with  
however.

# Highly ordered conjugated polymers in polyethylene: orientation by mesoepitaxy

T. W. Hagler, K. Pakbaz, J. Moulton, F. Wudl, P. Smith and A. J. Heeger\*

*Institute for Polymers and Organic Solids, University of California at Santa Barbara,*

*Santa Barbara, CA 93106, USA*

*(Received 1 February 1991)*

We report the anisotropic absorption,  $\alpha(\omega)$ , and photoluminescence,  $L(\omega)$ , spectra from films obtained by using gel processing for orienting a conjugated polymer guest blended into ultra-high molecular weight polyethylene (UHMW-PE). Both  $\alpha(\omega)$  and  $L(\omega)$  are anisotropic; for example, the polarization dependence of  $L(\omega)$  indicates an anisotropy  $> 60:1$  with preferred direction parallel to the draw axis. We conclude that gel processing results in orientation and a reduction in disorder through mesoepitaxy; epitaxial orientation of the conjugated polymer on the internal surfaces of the gel-processed PE.

(Keywords: conjugated polymers; polyethylene; mesoepitaxy)

Interest in conjugated polymers as materials with potentially useful linear and non-linear optical properties originates primarily from the relatively broad energy bands and the strong  $\pi$ - $\pi^*$  interband transition which are characteristic of these semiconducting polymers<sup>1</sup>. The implied delocalization of the  $\pi$ -electrons provides a mechanism for relatively high carrier mobilities upon doping or photoexcitation.

Delocalization of the electronic wavefunctions in conjugated polymers is also expected to lead to a large third-order non-linear optical susceptibility,  $\chi^{(3)}$ . Calculations<sup>2</sup> predict a dramatic increase in non-linear response with chain length;  $\chi^{(3)}$  is proportional to  $N^2$  where  $N$  is the polymerization index and  $\nu \approx 4$ -5. Although  $\chi^{(3)}$  must saturate in the thermodynamic (long chain) limit, the calculations imply that saturation does not occur until  $N$  reaches values of order  $10^2$ . However, because of the tendency for localization of the electronic wavefunctions in quasi-one-dimensional systems, the localization length may be much less than the chain length, thus limiting  $\chi^{(3)}$ . The same disorder-induced localization limits the electrical conductivities in all but the most highly ordered samples of doped conducting polymers<sup>3,4</sup>. There is, therefore, a clear scientific and technological need for quality thin films of aligned and ordered conjugated polymers.

We report the polarized absorption and emission spectra from a conjugated polymer blended into ultra-high molecular weight polyethylene (UHMW-PE) and oriented by gel processing. By varying the draw ratio and the concentration of conjugated polymer in the blend, the optical dichroism and the optical density can be independently controlled, thus providing the opportunity to obtain anisotropic  $\pi$ - $\pi^*$  absorption spectra and anisotropic emission spectra for highly aligned samples of poly(2-methoxy, 5-(2'-ethyl-hexyloxy)-*p*-phenylene vinylene)<sup>5</sup>, MEH-PPV, and other soluble conjugated polymers. The results indicate that gel processing causes a reduction in disorder through mesoepitaxy<sup>6</sup>; an epitaxial orientation of the MEH-PPV on the internal surfaces of the gel-processed PE.

The simplest method of achieving chain extension and chain orientation of a polymer is by tensile drawing. Unfortunately, the relatively high density of entanglements present in most polymers limits the available draw ratios ( $\lambda$ ) to modest values. A principal advantage of gel processing is that because of the dilution of the polymer in the gel (e.g. UHMW-PE forms gels at volume fractions even below 1%), the density of entanglements is far lower than in polymers prepared from the melt, etc.<sup>7</sup>. Moreover, the low entanglement density remains even after removing the solvent. Thus such gels (or gel-processed films and fibres) can be tensile drawn to remarkable draw ratios ( $\lambda > 200$ ) during which the macromolecules are chain extended and aligned.

Can this high degree of structural order achieved through gel processing be transferred to a conjugated polymer in a UHMW-PE blend? On first thought this would seem unlikely for the two-component polymers are typically immiscible (since the entropy of mixing is essentially zero for macromolecules). However, there is evidence of a strong interfacial interaction when conjugated polymers are added to an UHMW-PE gel; the frequency dependent conductivity results<sup>8</sup> suggest that the conjugated polymer adsorbs onto the PE and decorates the complex surface of the gel network, thereby forming connected (conducting) pathways at volume fractions nearly three orders of magnitude below the threshold for three-dimensional percolation<sup>8</sup>. The implied strong interfacial interaction suggests that gel processing of conjugated polymers in PE may lead to orientation of the conjugated polymer component.

PE/MEH-PPV blends were prepared<sup>7-9</sup> by mixing 7.5 mg of MEH-PPV ( $M_w \approx 250\,000$ ) in xylene with 0.75 g of UHMW-PE (Hostalen GUR 415;  $M_w \approx 4 \times 10^6$ ) in xylene such that the PE:solvent ratio was 0.75 wt%. This solution was thoroughly mixed and allowed to equilibrate in a hot oil bath at 126°C for 1 h. The solution was then poured into a glass container to cool, forming a gel which was allowed to dry (into a film) for several days. Films were then cut into strips and tensile drawn over a hot pin at 110-120°C. The resulting films are extremely durable due to a combination of the stability of MEH-PPV and the self-encapsulation advantage of

\*To whom correspondence should be addressed



polymer blends: repeated thermal cycling and constant exposure to air caused no observable degradation.

The spectra were measured with a 0.3 m single grating monochromator, and a mechanically chopped tungsten-halogen light source; light was detected by a photomultiplier tube (Hamamatsu R372) and the output was sent to a lock-in amplifier. The samples were mounted on sapphire substrates which were fitted into a copper sample holder and mounted on the cold finger of a vacuum cryostat. To study the polarization dependence of  $\alpha(\omega)$ , a dichroic sheet polarizer (MG 03 FPG 005) was inserted on a rotational stage just before the sample. Because of the dilution (1% conjugated polymer) of the gel-processed films, the index is dominated by that of PE so that the reflection losses were limited to a few per cent even for relatively thick samples with moderate optical density. Thus, the absorption coefficients,  $\alpha_{\parallel}$  and  $\alpha_{\perp}$ , were accurately determined after correcting for the background with a blank substrate. For the photoluminescence (PL), the sample was excited by a polarized, mechanically chopped (400 Hz) Ar<sup>+</sup> ion laser (Coherent model 70) tuned to 457.9 nm. To determine the polarization dependence of  $L(\omega)$ , the polarizer was placed on a rotation stage at the entrance slit of the monochromator. All PL spectra were corrected by replacing the sample with an NIST referenced lamp. Absorption spectra were monitored before and after luminescence runs to insure against optical damage.

The absorption spectra for an oriented free-standing film ( $\lambda \sim 50$ ) of PE/MEH-PPV are shown in Figure 1 for polarization both parallel to ( $\parallel$ ) and perpendicular to ( $\perp$ ) the draw axis and for a spin-cast film of pure

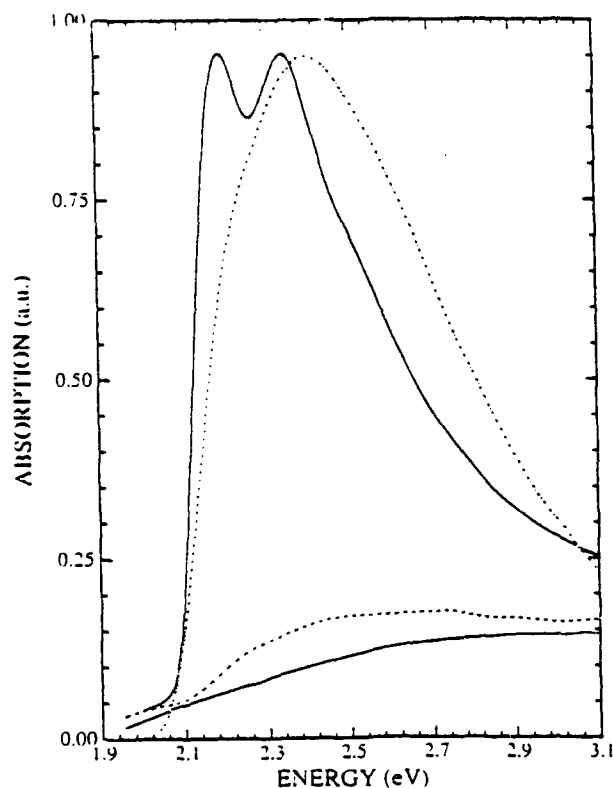


Figure 1 Anisotropic absorption for an oriented film ( $\lambda \sim 50$ ) of PE/MEH-PPV for polarization both parallel to (—) and perpendicular to (---) the draw axis and for a spin-cast film of pure MEH-PPV (· · ·), all at 80 K. The scattering loss from a UHMW-PE film of comparable thickness and draw ratio is shown (- · -) for comparison

MEH-PPV (both at 80 K). These spectra were scaled to that of  $\alpha_{\parallel}(\omega)$  which has a maximum value of  $2.2 \times 10^3 \text{ cm}^{-1}$  at 2.2 eV (1% MEH-PPV in PE). A high degree of macroscopic orientation of the conjugated polymer has been achieved by tensile drawing the gel-processed blend. Moreover,  $\alpha_{\parallel}(\omega)$  shows a distinct red shift, a sharper absorption onset, and a reduced total width compared to  $\alpha(\omega)$  for the spin-cast film. These features, together with the appearance of resolved vibronic structure, indicate a significant improvement in the structural order of the conjugated polymer in the oriented blend.

The transverse 'absorption' (Figure 1) is dominated by scattering from microstructure in the PE as demonstrated by comparing  $\alpha_{\perp}(\omega)$  with the artificial 'absorption', due to residual scattering, obtained from an undecorated UHMW-PE film of comparable thickness and draw ratio. The initial slope is the same and the overall spectral shape is similar. To circumvent the problem of residual scattering, the dichroism of selected infra-red (i.r.)-active modes associated with MEH-PPV has been studied as a function of the draw ratio; the dichroic ratio<sup>10</sup> continues to improve monotonically with  $\lambda$  to  $\alpha_{\parallel}/\alpha_{\perp} > 100$ .

The PE scattering was investigated by passing a He-Ne laser (632.8 nm) through the various samples and examining the speckel pattern. For oriented samples (both decorated and nondecorated), the pattern consisted of a sharp line in the equatorial plane superimposed on a diffuse isotropic background. By treating the samples with mineral oil, the diffuse background (from surface scattering) was eliminated, leaving only the sharp equatorial line. The scattering cross section of the equatorial line was found to be independent of the radial angle  $\phi$ , thus implying a scattering centre with dimensions  $L$  such that  $L_{\perp} \ll \lambda_{\text{He-Ne}} \ll L_{\parallel}$ . The residual equatorial scattering is therefore attributed to elongated microstructure in the PE<sup>11</sup>. Efforts are underway to modify the gel processing to reduce the scattering by the oriented films.

Figure 2 compares  $\alpha(\omega)$  of a non-oriented free-standing film of PE/MEH-PPV,  $\alpha_{\parallel}(\omega)$  of the oriented film of PE/MEH-PPV and  $\alpha(\omega)$  of the spin-cast film (all at 80 K). The spectrum obtained from the non-oriented blend is intermediate between that of the spin-cast film and the oriented blend; it shows the red shift, the sharper absorption onset, the reduced total bandwidth and the emergence of vibronic structure. Thus, even in the non-oriented blend, the MEH-PPV spectra are in every way consistent with a significant enhancement of microscopic order. Comparison of  $\alpha_{\parallel}(\omega)$  of the oriented film of PE/MEH-PPV with  $\alpha(\omega)$  of the non-oriented film of PE/MEH-PPV shows that there is a sharpening of all spectral features and a clear redistribution of spectral weight into the zero-phonon line (i.e. the direct photoproduction of a polaron-exciton in its vibrational ground state)<sup>11</sup>. The data thus indicate a further enhancement of structural order by tensile drawing.

The inset to Figure 2 compares  $\alpha_{\parallel}(\omega)$  of an oriented film of PE/MEH-PPV at 80 K with that at 300 K. As the temperature is raised the peak shifts, the onset of absorption broadens and there is both loss of resolution and redistribution of spectral weight out of the lowest energy vibronic feature. The changes in  $\alpha_{\parallel}(\omega)$  at 300 K are indicative of increased disorder, similar to the changes caused by the structural disorder of the spin-cast films.

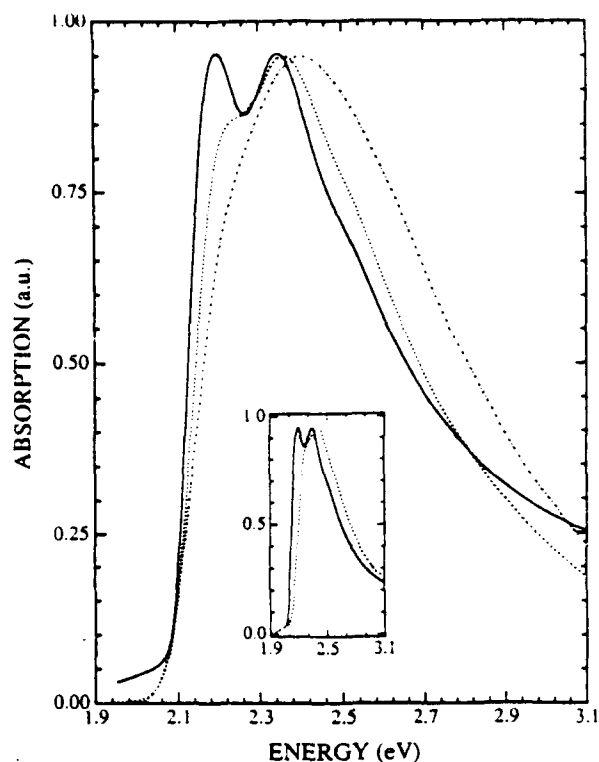


Figure 2 Anisotropic absorption,  $\alpha(\omega)$ , of a non-oriented free-standing film of PE/MEH-PPV (---),  $\alpha_{\parallel}(\omega)$  of the oriented film of PE/MEH-PPV (—) and  $\alpha(\omega)$  of the spin-cast film (···), all at 80 K. The inset compares  $\alpha_{\parallel}(\omega)$  of the oriented film at 80 K (—) and at 300 K (---)

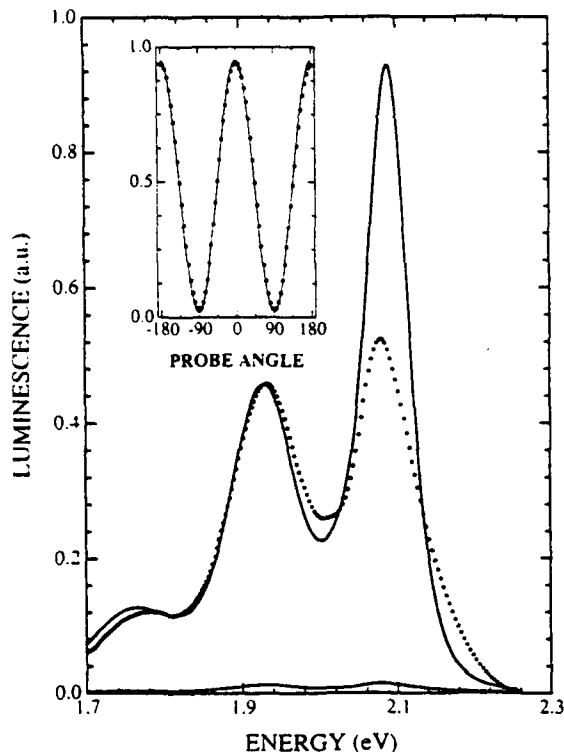


Figure 3 Anisotropy in the 80 K PL spectrum,  $L(\omega)$ , from an oriented film of PE/MEH-PPV for parallel pumping; the upper solid curve is  $L_{\parallel}(\omega)$ ; the lower solid curve is  $L_{\perp}(\omega)$ ; the dotted curve is  $L_{\perp}(\omega)$  scaled ( $\times 40$ ) for clarity. The inset shows the dependence of  $L(\omega)$  on the polarization angle relative to the chain axis (the solid curve is a fit to  $\cos^2 \theta$ )

Figure 3 demonstrates the anisotropy in the 80 K emission spectrum,  $L(\omega)$  of an oriented free-standing film of PE/MEH-PPV for parallel pumping. The inset displays the polarization dependence of  $L(\omega)$  measured at the zero-phonon line<sup>11</sup> (2.091 eV). The residual scattering sets a lower limit on this anisotropy of  $L_{\parallel}/L_{\perp} > 60$  with the preferred direction parallel to the draw axis. In addition to being much weaker,  $L_{\perp}(\omega)$  shows relatively less spectral weight in the zero-phonon line<sup>11</sup>, consistent with a higher degree of disorder in the residual non-oriented material. For perpendicular pumping, the anisotropy ( $\sim 30:1$ ) and spectral features were similar, but with the intensity of the parallel emission reduced by a factor of  $\sim 4$ . To our knowledge, this is the first observation of truly anisotropic emission (magnitude and lineshape) in a conjugated polymer system.

The polarized nature of  $L(\omega)$  implies that the emission is from neutral bipolaron excitons (formed from positive and negative polarons) localized on MEH-PPV chains. This is particularly significant since the energy of the pump (457.9 nm) is sufficient for charge separation and polaron formation. Even with a perpendicularly polarized pump,  $L(\omega)$  is polarized along the chain direction, implying that polarons on separate chains migrate until an oppositely charged polaron is encountered on the same chain. The relatively large confinement energy of PPV may be responsible for efficient formation of such neutral bipolaron excitons<sup>12,13</sup>.

We conclude that the MEH-PPV is chain extended and ordered by the gel-processed PE, with macroscopic chain alignment and improved order induced by tensile drawing. Since there is evidence from the earlier studies of such gels that the conjugated polymer adsorbs onto the PE and decorates the complex surface of the self-assembled PE network<sup>8,14</sup>, we suggest that the conjugated polymer is oriented (and ordered) by a mesoscale epitaxy on the internal PE surfaces, i.e. mesoepitaxy<sup>6</sup>. There are two observations which imply alignment by mesoepitaxy. First, there is spectroscopic evidence of improved order in the PE/MEH-PPV blends even prior to tensile drawing (Figure 2). This is consistent with mesoepitaxial adsorption of the conjugated macromolecules onto the lamellar PE crystallites within the gel. Second, when MEH-PPV is cast onto a film of pure UHMW-PE which has been stretched to a moderate draw ratio (e.g.  $\lambda > 20$ ), the MEH-PPV orients spontaneously along the draw direction. This characteristic feature of mesoepitaxy was first observed for polyaniline when brought out of solution (from sulphuric acid) onto a surface coated with a thin ( $< 100$  Å) oriented poly(tetrafluoroethylene) film<sup>6</sup>.

During the tensile drawing of gel-processed PE fibres and films, there are several stages of evolution of the microstructure<sup>15</sup>. Initially, the lamellar PE crystals are simply aligned without a significant change in the amorphous fraction. At higher draw ratios, the lamellar crystals are pulled apart and chain extended; simultaneously, the amorphous interconnecting regions are chain extended and chain aligned leading to an overall degree of chain extension, chain alignment and interchain coherence that approaches the order in a single crystal. Figures 1 and 2 demonstrate that throughout this process, the conjugated chains (in the blend) are ordering and aligning on the evolving internal surfaces of the PE.

The fact that the alkyl side chains on the MEH-PPV

are ethylene-like may serve to enhance the interfacial interaction. There is evidence that adsorption of the MEH-PPV onto the PE surface is energetically favoured over dissolution in the solvent; the small amount of solvent which is expelled during processing is only very lightly coloured. We note, in this context, that we have been able to achieve similar results with poly(3-octylthiophene) through gel processing with PE.

In summary, we have demonstrated a novel method for obtaining highly aligned and structurally ordered conjugated polymers by mesoscale epitaxy using gel processing in blends with PE and subsequent tensile drawing. By controlling the concentration of conjugated polymer in the blend, we have obtained highly aligned, durable samples with controlled optical density. This allows the direct observation of the spectral changes that occur as a result of the improved structural order induced by mesoepitaxial alignment of the conjugated macromolecules. The details of the spectral changes (sharper absorption edge and enhancement of the zero-phonon vibronic transition) imply a significant increase of the localization length. The PL spectrum is polarized ( $>60:1$ ) indicative of emission from bipolaron excitons on the ordered and aligned chains. Experiments are in progress to determine the effect of the improved order and the implied delocalization (which profoundly affect the linear optical properties) on the non-linear optical properties.

#### Acknowledgements

This research was supported by the Air Force Office of Scientific Research (AFOSR 90-0283). We thank

Z. Ni and G. Srdanov for synthesis of the MEH-PPV, K. Voss and J. Van Smoot for communicating their i.r. dichroism results, and K. Voss, D. McBranch, A. Hays and C. Halvorson for important comments and discussions.

#### References

- 1 Patil, A. O., Heeger, A. J. and Wudl, F. *Chem. Rev.* 1988, **88**, 183
- 2 Silbey, R. in 'Conjugated Polymeric Materials: Opportunities in Electronics, Optoelectronics and Molecular Electronics' (Eds J. L. Bredas and R. R. Chance), NATO ASI Series, Series E: Applied Sciences, Vol. 182, 1990
- 3 Andreatta, A., Tokito, S., Smith, P. and Heeger, A. J. *Mol. Cryst. Liq. Cryst.* 1990, **189**, 169
- 4 Kivelson, S. and Heeger, A. J. *Synth. Met.* 1988, **22**, 371
- 5 Wudl, F. and Srdanov, G. to be published
- 6 Smith, P. and Wittman, J. *US Pat.* (filed)
- 7 Smith, P. and Lemstra, P. J. *J. Mater. Sci.* 1980, **15**, 505
- 8 Fizazi, A., Moulton, J., Pakbaz, K., Rughooopath, S. D. D., Smith, P. and Heeger, A. J. *Phys. Rev. Lett.* 1990, **64**, 2180
- 9 Smith, P., Lemstra, P. J., Pijpers, J. P. L. and Kiel, A. M. *Colloid Polym. Sci.* 1981, **259**, 1070
- 10 Van Smoot, J. and Voss, K. private communication
- 11 Hagler, T. W., Pakbaz, K., Voss, K. F. and Heeger, A. J. *Phys. Rev. B* submitted for publication
- 12 Lauchlan, L. S., Etemad, S., Chung, T.-C., Heeger, A. J. and MacDiarmid, A. G. *Phys. Rev.* 1983, **B27**, 2301
- 13 Voss, K., Foster, C. M., Smilowitz, L., Mihailovic, D., Askari, S., Srdanov, G., Ni, Z., Shi, S., Heeger, A. J. and Wudl, F. *Phys. Rev.* 1991, **B43**, 5109
- 14 Suzuki, Y., Pincus, P. and Heeger, A. J. *Macromolecules* 1990, **23**, 4730
- 15 Peterlin, A. in 'Ultrahigh Modulus Polymers' (Eds A. Ciferri and I. M. Ward), Ch. 10, Applied Science Publishers, London, 1979

## Enhanced order and electronic delocalization in conjugated polymers oriented by gel processing in polyethylene

T. W. Hagler, K. Pakbaz, K. F. Voss, and A. J. Heeger

*Department of Physics and Institute for Polymers and Organic Solids University of California, Santa Barbara, Santa Barbara, California 93106*

(Received 26 February 1991)

We report the polarized absorption  $\alpha_e(\hbar\omega)$  and photoluminescence  $L_e(\hbar\omega)$  spectra of gel-processed blends of poly(2-methoxy,5-(2'-ethyl-hexoxy)-*p*-phenylenevinylene), MEHPPV, in ultrahigh-molecular-weight polyethylene. Both  $\alpha_e(\hbar\omega)$  and  $L_e(\hbar\omega)$  are highly anisotropic, with preferred direction polarized parallel to the draw axis, demonstrating that gel processing and subsequent tensile drawing results in the orientation of the conjugated polymer guest. In contrast to cast films of the pure conjugated polymer (MEHPPV), the oriented blends display a sharpening of the vibronic structure and a redistribution of spectral weight into the zero-phonon line in both absorption and emission for light polarized parallel to the draw axis. In the most highly oriented MEHPPV-polyethylene blends, the induced order is sufficient to enable the determination of the intrinsic line shape of the absorption: we find the band-edge square-root singularity characteristic of a one-dimensional semiconductor. The changes in the spectral features resulting from materials processing are quantified using a Franck-Condon analysis and interpreted in terms of a modification of the ground- and excited-state configurational manifolds. We conclude that processing the blends via the gel intermediate state and subsequently orienting by tensile drawing yields a system with significantly reduced disorder.

### I. INTRODUCTION

#### A. Vibrational relaxation and electronic localization in one-dimensional $\pi$ -electron systems

In conjugated polymers, the coupling of the  $\pi$  electrons to the polymer backbone via the electron-phonon interaction causes structural relaxation in the excited state and the formation of self-localized nonlinear excitations: solitons, in the case of a degenerate ground state, or confined soliton pairs (polarons or bipolarons) in the case of a nondegenerate ground state. Both the structural relaxation in the bond alternation pattern and the associated (transient) localized electronic states in the gap have been studied in detail using the techniques of photoinduced absorption as excitation spectroscopy.<sup>1</sup>

In addition to this intrinsic self-localization, quasi-one-dimensional systems are especially sensitive to localization induced by disorder.<sup>1</sup> In one-dimensional systems, all electronic states are localized by disorder.<sup>2</sup> The localization length (i.e., the spatial extent of the electronic wave function) is determined by the degree of disorder and by the energy of the state. For states near the band edges, the localization length is smallest, increasing to maximum values near the band centers. Although the interchain transfer interactions which lead to three-dimensional band structures tend toward electronic delocalization, we expect that, because of the high degree of intrinsic anisotropy in conjugated polymers, disorder-induced localization will be of major importance in all but the most well-ordered systems.

Independent of its origin, localization of the electronic

wave functions has far reaching ramifications for such diverse phenomena as the nonlinear optical response of the pure semiconducting state and the electronic transport in the doped conducting state. Disorder-induced localization is known to convert doped conducting polymers from true metals, with large mean free paths and coherent transport, into poor conductors in which the transport is limited by phonon-assisted hopping.<sup>3</sup> Delocalization of the electronic wave functions in conjugated polymers is also expected to lead to a large third-order nonlinear optical susceptibility  $\chi^{(3)}$ . Since calculations<sup>4</sup> predict a dramatic increase in the nonlinear optical response with increasing conjugation length, electronic localization can be expected to seriously limit the magnitude of  $\chi^{(3)}$ .

In order to optimize the broad range of electrical and mechanical properties of conjugated polymers, a variety of processing techniques have been developed<sup>5</sup> which focus on chain extension and chain alignment with the goal of improving the structural order to the point that the intrinsic properties of the macromolecular chains can be achieved in real materials. Post-synthesis tensile drawing (stretch orientation) techniques have demonstrated significant improvements in the electrical conductivity,<sup>6</sup> the electro-optic effect,<sup>7</sup> and third harmonic generation<sup>8,9</sup> in *trans*-polyacetylene. Similar improvements in the electrical and mechanical properties of poly(phenylenevinylene) and its derivatives,<sup>10</sup> poly(thienylene vinylene),<sup>11</sup> and the poly(3-alkylthiophenes) (Ref. 12) have shown that the correlated improvements of the electrical and mechanical properties which result from chain extension, chain alignment, and structural order are general phenomena.<sup>5</sup>

However, further improvement in material quality is necessary to enable the exploration of the intrinsic electronic properties of conjugated polymers.

### B. Polymer blends: Conjugated polymers in polyethylene

Our interest in blends containing conjugated polymers as guests in polyethylene (PE) originated in the opportunity to utilize the high degree of chain extension, chain alignment, and structural order attained by gel-processing polyethylene<sup>13</sup> to induce similar order on the guest conjugated macromolecules incorporated in the blend, and from the desire to combine the attractive mechanical properties of ultrahigh-molecular-weight (UHMW) polyethylene with the electronic properties (electrical conductivity, anisotropic linear and nonlinear optical properties etc.) of the conjugated polymer.

The advantage of utilizing the thermoreversible gelation of polyethylene for processing is that because of the dilution of the polymer in the gel (UHMWPE forms gels at volume fractions even below 1%), the density of entanglements is far lower than for polymers prepared from the melt or cast from concentrated solution.<sup>13</sup> Moreover, the low entanglement density which characterizes the gel remains even after removing the solvent.<sup>13</sup> Thus, such gels (or gel-processed films and fibers) can be tensile drawn to remarkable draw ratios (greater than 200) during which the macromolecules are chain extended and aligned to a degree of structural order that approaches that of a single crystal.<sup>14</sup>

In the initial publication on this subject,<sup>15</sup> we reported the anisotropic absorption and photoluminescence spectra obtained from such oriented blends. The results demonstrated the ability to transfer the high degree of orientation and order known for polyethylene to the conjugated polymer guest in such blends with polyethylene. The 80-K absorption spectra for an *oriented* (draw ratio:  $\times 50$ ) MEHPPV-PE film are reproduced in Fig. 1 for optical polarization both parallel and perpendicular to the draw axis (The anisotropic photoluminescence is described in detail below).

In addition to this axial alignment, a number of important observations were made concerning the effects of gel processing (followed by tensile drawing) of MEHPPV-PE on the line shape of the interband transition. We observed a sharpening of the vibronic structure and a redistribution of spectral weight into the zero-phonon line in both absorption and emission for light polarized parallel to the draw axis. Based on these results, it was concluded that gel processing causes orientation and a reduction in disorder through mesoepitaxy: a mesoscale epitaxial orientation of the conjugated polymer on the internal surfaces of the PE host.<sup>15</sup>

### C. Focus of the paper

In this paper, we present the results of a comprehensive study of the polarized absorption  $\alpha(\hbar\omega)$  and photoluminescence  $L(\hbar\omega)$  spectra of poly(2-methoxy,5-(2'-ethyl-

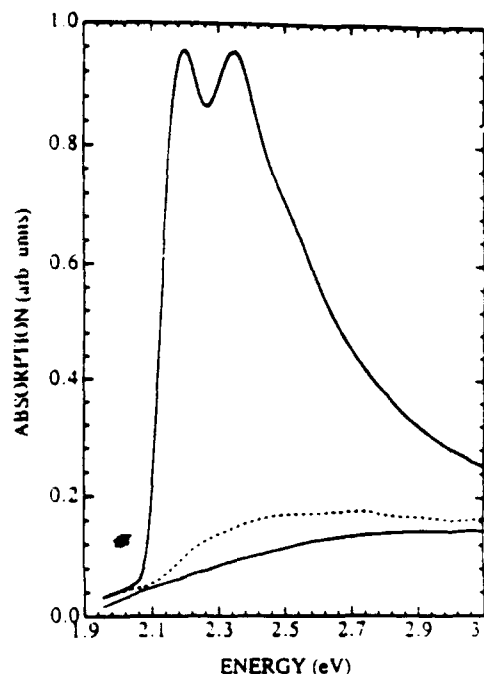


FIG. 1. The polarized absorption spectra  $\alpha(\hbar\omega)$  for an oriented ( $\times 50$ ) free-standing film of MEHPPV-PE for optical polarization both parallel (solid) and perpendicular (dashed) to the draw axis. The scattering loss from an undecorated UHMWPE film of comparable thickness and draw ratio is shown (dotted) for comparison.

hexoxy)-*p*-phenylenevinylene), MEHPPV, as the guest in ultrahigh-molecular-weight polyethylene. In Sec. II we describe the processing techniques and the apparatus used in obtaining the absorption and emission spectra. The results of the measurements are presented in Sec. III. In Sec. IV we examine the effects of localization on the interband transition; specifically addressing the conditions under which vibronic structure is to be expected in a conjugated polymer system. In Sec. V, we summarize the results of a Franck-Condon analysis of the absorption and emission spectra which indicate a modification of the ground- and excited-state configurational manifolds as a consequence of materials processing. Finally, in Sec. VI, we address the implications of these results.

## II. EXPERIMENT

### A. Sample preparation

MEHPPV-PE blends are prepared by mixing 10 mg of poly(2-methoxy,5-(2'-ethyl-hexoxy)-*p*-phenylenevinylene) in xylenes with 1.0-g ultrahigh-molecular-weight polyethylene in xylenes such that the total solute to solvent ratio is 0.7% by weight. This solution is thoroughly mixed and allowed to equilibrate in a hot oil bath kept at 126°C. The solution is then poured into a glass container, where it forms a gel upon cooling, and is allowed to dry for several days. The small amount of sol-

vent that is purged from the gel in the early stage of this procedure is essentially colorless, implying an attractive interfacial interaction between the two polymers.

To fabricate the oriented samples, the resulting MEHPPV-PE films (made via gelation) are subsequently tensile drawn over a hot pin at 110–120°C. Although such films can be stretched (and oriented) to moderate draw ratios even at room temperature, our best results were obtained at elevated temperatures. Once processed in this manner, the films are extremely durable: repeated thermal cycling (80–300 K) and constant exposure to air (over several months) caused no observable degradation. Typical thickness of the oriented samples is several micrometers.

### B. Absorption spectroscopy

The apparatus used to investigate the absorption spectra consists of a 0.3-m single-grating monochromator outfitted with a 500-nm blaze grating ruled 1200 lines/mm and a mechanically chopped tungsten-halogen light source. The optical resolution at the exit slits was chosen to be 1.0 nm. To facilitate the study of polarization dependent effects, a UV-VIS dichroic sheet polarizer (MG 003FPG 005) is inserted just before the sample on a rotational stage. The samples are mounted on zero orientation, one-inch-diameter sapphire substrates which fit into a copper sample holder mounted onto the cold finger of a cryostat. Typical pressures are on the order of  $10^{-5}$  torr. The transmitted light is detected by a photomultiplier tube (Hamamatsu R372); the output is sent via a lock-in amplifier (Stanford Research SR-530) to a computer. Absorption spectra are determined using Lambert-Beer's law by taking background spectra with a blank substrate for all optical configurations considered.

### C. Steady-state luminescence spectroscopy

For the steady-state photoluminescence measurements, the tungsten-halogen light source is replaced by the photomultiplier tube, and the sample is excited by a polarized, mechanically chopped (400 Hz) cw argon ion laser (Coherent model 70) tuned to 457.9 nm. A long-wavelength pass filter (MG 03 FCG 067) is inserted to prevent scattered laser light from reaching the photomultiplier tube. To determine the polarization dependence of the photoluminescence, a polaroid is placed on a rotation stage before the entrance slit of the monochromator. All spectra are corrected by replacing the sample with an NBS referenced lamp. Absorption spectra are obtained before and after luminescence runs to ensure that no permanent optical damage has occurred.

## III. ANALYSIS OF THE EXPERIMENTAL RESULTS

### A. Absorption

The 80-K absorption spectra for an oriented ( $\times 50$ ) free-standing film of MEHPPV-PE are shown in Fig. 1 for

optical polarization both parallel and perpendicular to the draw axis. As demonstrated by the scattering loss of an undecorated UHMWPE film of comparable thickness and draw ratio (dotted), the transverse "absorption" in the oriented blend is dominated by scattering from residual microstructure in the PE. To circumvent the problem of residual scattering, the dichroism of selected ir-active modes associated with MEHPPV have been studied as a function of draw ratio; the dichroic ratio improves monotonically with draw ratio to  $\alpha_{\parallel}/\alpha_{\perp} > 100$ .<sup>16</sup>

The PE scattering was investigated by passing a He-Ne laser beam (632.8 nm) through the various samples and examining the speckle pattern. For oriented samples (both decorated and nondecorated), the pattern consisted of a sharp line in the equatorial plane superimposed on a diffuse isotropic background. By treating the samples with mineral oil, the diffuse background (from surface scattering) was eliminated, leaving only the sharp equatorial line. The scattering cross section of the equatorial line was found to be independent of the radial angle  $\phi$ , thus implying a scattering center with dimensions  $L$  such that  $L_{\perp} \ll \lambda_{\text{He-Ne}} \ll L_{\parallel}$ .<sup>17</sup> The residual equatorial scattering is therefore attributed to elongated microstructure in the PE.<sup>13</sup> Efforts are underway to modify the gel processing to reduce the scattering by the oriented films.

For the oriented ( $\times 50$ ) blend,  $\alpha_{\parallel}(\hbar\omega)$  is found to have a maximum value of  $2.2 \times 10^3 \text{ cm}^{-1}$  at 2.2 eV for 1.0% MEHPPV in PE. Errors due to reflection from the front and back surfaces are of order a few percent, since the index of refraction of the dilute blend is approximately that of PE.

Figure 2 displays the 80-K absorption spectra of a

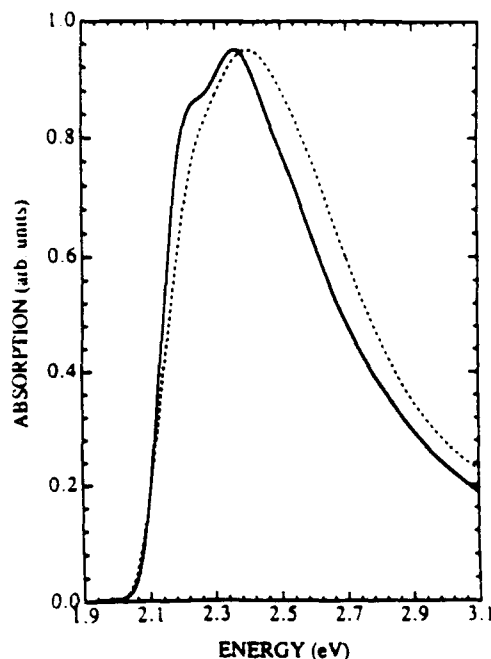


FIG. 2. 80-K absorption spectra of a nonoriented free-standing film of MEHPPV-PE (solid) and a cast film (dashed) of MEHPPV.

nonoriented free-standing film of MEHPPV-PE and a cast film of MEHPPV. It is evident that a considerable fraction of the oscillator strength is redistributed toward lower energy in the MEHPPV-PE blend in comparison to the cast film. In addition, the spectrum of MEHPPV in PE shows a sharper absorption onset and a narrower absorption band than that of the cast MEHPPV film. Finally, we note the emergence of a well defined shoulder on the leading edge of the nonoriented MEHPPV-PE spectrum that is not resolved in the spectrum of the cast film.

Figure 3 compares the 80-K absorption spectra of oriented ( $\times 50$ ) and nonoriented free-standing films of MEHPPV-PE. The data in Figs. 1-3 show that tensile drawing the blend leads to absorption anisotropy, to a further sharpening of the absorption edge, to a continued redistribution of spectral weight to lower energy, and to improved resolution of the vibronic features. The lowest energy feature, clearly distinguishable in the oriented blend, is attributed to a purely electronic transition between the ground and excited states, and is henceforth referred to as the zero-phonon absorption line.

In order to examine the effects of temperature, we compare the 80-K and 300-K absorption spectra for an oriented ( $\times 50$ ) free-standing film of MEHPPV-PE in Fig. 4. Temperature is seen to have a large effect on both the position and spectral density of the absorption line shape. In the 300-K spectrum, a considerable amount of spectral weight has been redistributed out of the zero-phonon line and into the higher energy vibronic features. In addition, the 300-K spectrum is blue-shifted by approxi-

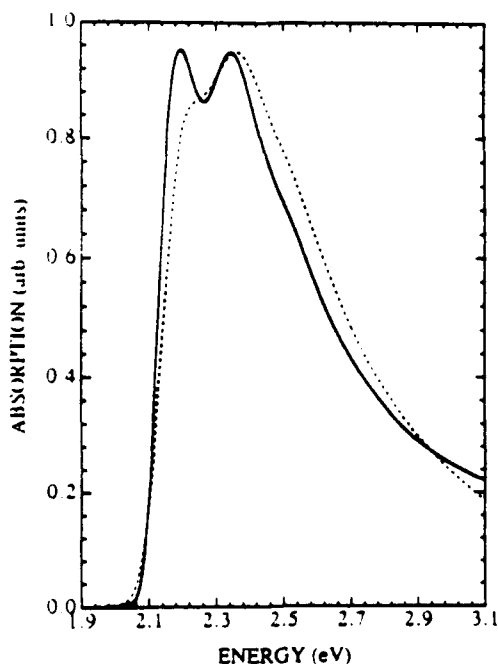


FIG. 3. 80-K absorption spectra of an oriented ( $\times 50$ ) free-standing film of MEHPPV-PE (solid) and a nonoriented (dashed) free-standing film of MEHPPV-PE.

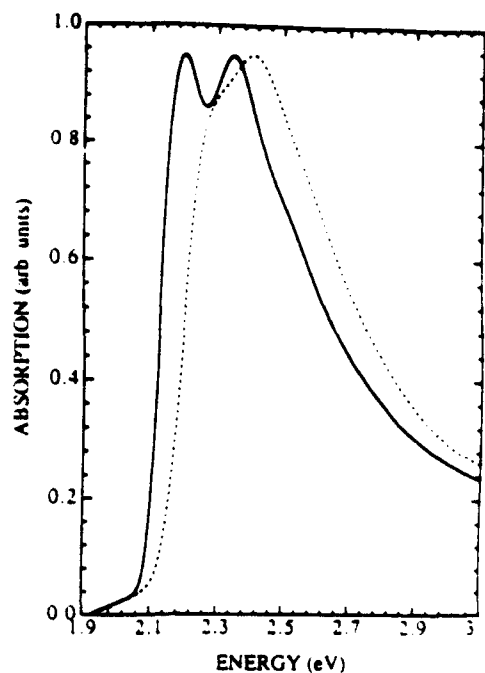


FIG. 4. 80-K (solid) and 300-K (dashed) absorption spectra of an oriented ( $\times 50$ ) free standing film of MEHPPV-PE for optical polarization parallel to the drawing axis.

mately 85 meV relative to the 80-K spectrum.

The similarity between the 300-K spectrum of the oriented blend and that of the nonoriented blend at 80 K is particularly interesting, implying that the structural disorder in the nonoriented blend at 80 K is comparable to the thermally induced disorder in the oriented blends at 300-K.

The qualitative features of Figs. 2-4 are consistent with a significant reduction of disorder in the MEHPPV-PE films relative to pure MEHPPV cast directly from solution; tensile drawing orients the conjugated guest polymer and causes a further reduction of disorder. These qualitative observations are consistent with the quantitative conclusions obtained from the fits presented in Sec. V.

### B. Emission

Figure 5 shows the 80-K absorption and emission spectra for a cast film of MEHPPV. The photoluminescence spectrum consists of a series of well-defined vibronic bands with very distinct Lorentzian line shape and with an energy spacing of approximately 180 meV. The largest feature, at 2.01 eV, which we assign as the zero-phonon emission line, has a full width at half maximum (FWHM) of 105 meV. Also shown in Fig. 5 is the negative numerical derivative of the absorption spectrum (NNSD spectrum).

By comparing to results of electroabsorption experiments on polyacetylene, it was shown<sup>7,18</sup> that the sharp features in the second derivative of the polymer absorption spectra are indicative of underlying vibronic structure. From the second derivative spectrum, the energy

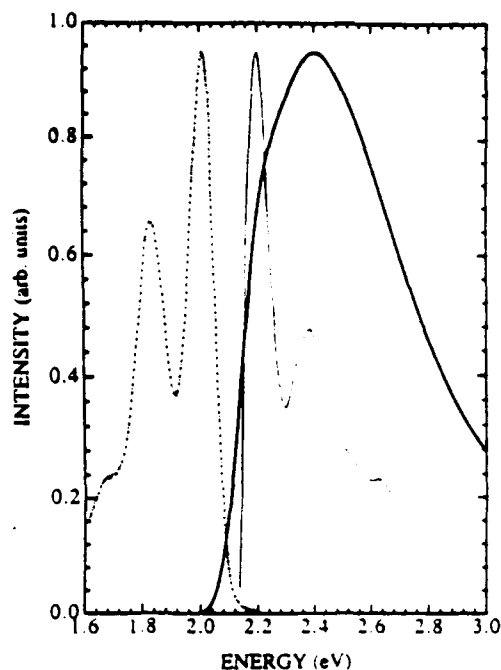


FIG. 5. 80-K absorption (solid) and emission spectra (dot-dashed) and the negative numerical second derivative of the absorption spectrum (NNSD spectrum) (dotted) for a cast film of MEHPPV.

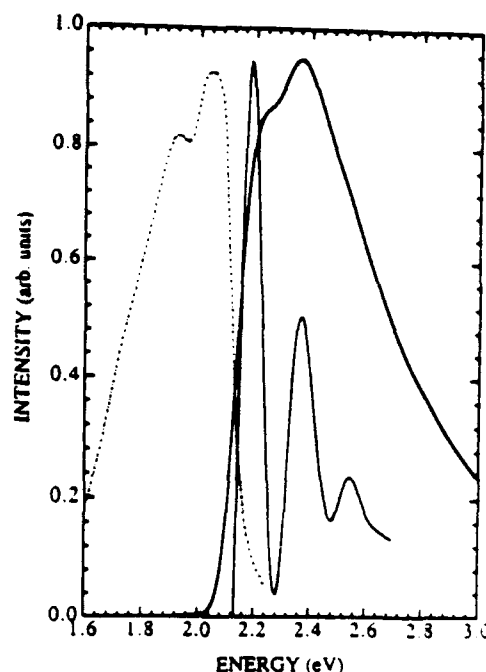


FIG. 6. 80-K absorption (solid) and emission spectra (dot-dashed) and the NNSD spectrum (dotted) for nonoriented free-standing film of MEHPPV-PE.

gap  $2\Delta_0$  and the vibronic splitting  $\hbar\omega_{ph}$  are obtained; the values are summarized in Table I. We assign the peak in the second derivative spectrum at 2.20 eV to be the zero-phonon absorption line, and from this we estimate the Stokes shift (i.e., the energy difference between the zero-phonon line in absorption and the zero-phonon line in emission) in the cast film to be 189 meV.

Figure 6 presents the combined 80-K absorption and emission spectra and the NNSD spectrum for a nonoriented free-standing film of MEHPPV-PE. Significant differences are evident in the vibronic character of the absorption and emission spectra for the nonoriented blend. From the NNSD spectrum, the absorption profile is composed of a well-defined and quite harmonic Franck-Condon progression, while the emission spectrum displays broader features, implying a higher degree of disorder. This asymmetry in the absorption and emission line shapes might result from a competitive nonradiative decay channel that is suppressed in the more well-ordered

material obtained at high draw ratios (shown below), as nonradiative recombination is known to be catalyzed by defects and imperfections.

Figure 7 displays the 80-K absorption and emission spectra and the NNSD spectrum for an oriented ( $\times 50$ ) free-standing film of MEHPPV-PE for light polarized parallel to the draw axis. The photoluminescence spectrum of the oriented blend consists of a series of well-defined vibronic bands, but with reduced energy spacing (162 meV) relative to that of the cast film (189 meV). In addition, the zero-phonon emission line, now at 2.09 eV, has a FWHM of only 66 meV, which is smaller by nearly a factor of 2 than in the cast film. In the oriented blend absorption spectrum, the zero-phonon line is centered at 2.16 eV, implying a Stokes shift of 72 meV; less than half the value found in the cast film.

Figure 8 demonstrates the anisotropy in the 80-K emission spectra of an oriented ( $\times 50$ ) free-standing film of MEHPPV-PE for parallel pumping. The inset displays

TABLE I. Second-derivative analysis: absorption.

Sample	Temp. (K)	$2\Delta_0$	$\hbar\omega_{ph}$
OB	80	2.160	0.186
OB	300	2.244	0.174
NB	80	2.182	0.180
NB	300	2.250	0.172
Cast	80	2.198	0.186



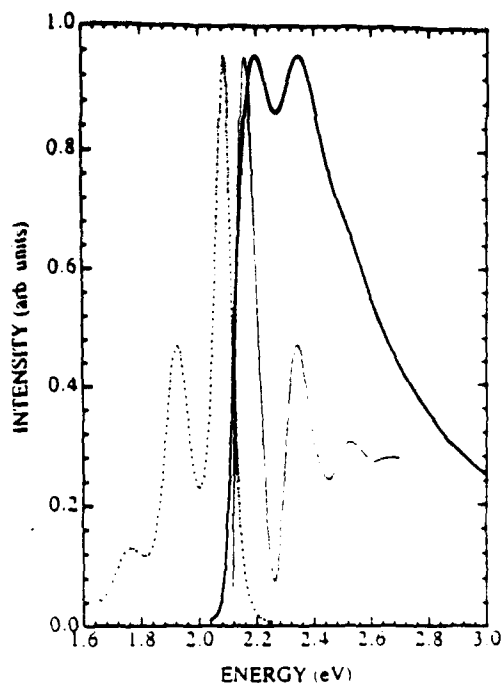


FIG. 7. 80-K absorption (solid) and emission spectra (dot-dashed) and the NNSD spectrum (dotted) for an oriented ( $\times 50$ ) free-standing film of MEHPPV-PE for optical polarized (pump and probe) parallel to the draw axis.

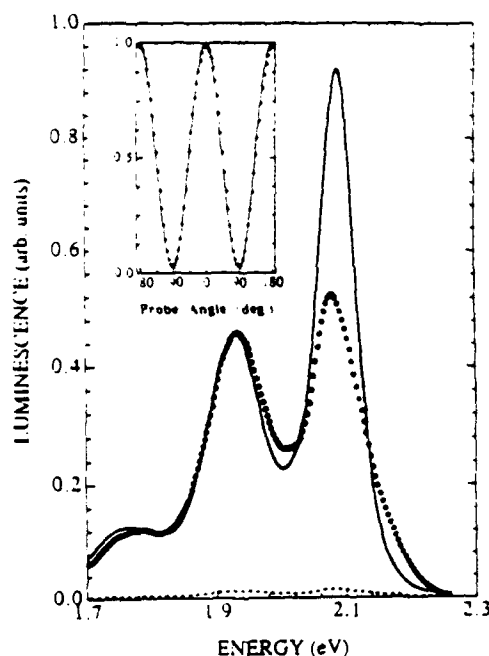


FIG. 8. 80-K (pump parallel) photoluminescence spectra  $L_{\theta}(\hbar\omega)$  of an oriented ( $\times 50$ ) free-standing film of MEHPPV-PE for emission polarization both parallel and perpendicular to the draw axis. The dotted curve is  $L_{\perp}(\hbar\omega)$  scaled (times 40) for clarity. The inset shows the dependence of  $L_{\theta}(\hbar\omega)$  on the emission polarization angle relative to the draw axis for parallel pumping [the solid curve is a fit to  $\cos^2(\theta)$ ].

the polarization dependence of the emission measured at the zero-phonon line (2.09 eV). Residual scattering of the pump sets a lower limit on this anisotropy of 60:1 with the preferred direction parallel to the draw axis.

The perpendicular component of the emission (parallel pumped), scaled times 40 for clarity, is also shown in Fig. 8. In contrast to the parallel emission spectrum (and in addition to being much weaker), the perpendicular emission spectrum shows broader lines and considerably more spectral weight in the higher-order phonon lines. To our knowledge, this is the first observation of truly anisotropic emission (both magnitude and line shape) in a conjugated polymer system. The spectral density of  $L_{\perp}(\hbar\omega)$  is similar to that observed in the cast films (Fig. 5), suggesting that the perpendicular component of the luminescence originates from residual disordered, and possibly amorphous, MEHPPV in the blend.

The polarization dependence of the photoluminescence was also investigated for perpendicular pumping, again showing that the preferred polarization of the emission is parallel to the draw axis with an observed anisotropy of at least 30:1 at 2.09 eV. The spectral densities for both parallel and perpendicular emission were found to be independent of the pump polarization and scaled with the anisotropic absorption.

#### IV. EFFECTS OF LOCALIZATION ON THE INTERBAND TRANSITION

Although the vibronic structure observed in emission is qualitatively understood in terms of the localized nature of the relaxed configuration of the excited state, the question arises as to why one should see vibronic structure in the absorption spectra of a conjugated polymer. For an undistorted lattice, the normal mode vibrational wave functions  $\chi(\nu_i)$ , by definition, form an orthonormal set

$$\langle \chi(\nu_i) | \chi(\nu_j) \rangle = \delta_{i,j} \delta_{\nu,\nu'} \quad (1)$$

and therefore transitions between the various vibrational states are forbidden. This strict orthogonality is removed by a difference in the linear term in the electron-phonon interaction between the ground and excited states,<sup>19</sup> which results in a change in the equilibrium positions of the lattice ions in the excited state relative to that of the ground state. It is convenient to model this structural relaxation by a set of orthonormal configurational coordinates  $Q_i$  (e.g., in studies on finite polyenes: carbon-carbon single and double bond-stretch modes<sup>20,21</sup>), and to work within the harmonic approximation.<sup>19</sup> In this picture, the excited-state vibronic potential surface is displaced along the vector  $\vec{Q}$  with respect to that of the ground state. The magnitude of this displacement (i.e., the change in bond lengths upon excitation) is found to be proportional to the difference in the electron-phonon coupling constant  $\lambda$  between the ground and excited states. It is common<sup>19</sup> to characterize the magnitude of this displacement by the dimensionless Huang-Rhys parameters,  $S_i$

$$S_i = \frac{1}{2} \frac{M_i \omega_i^2}{\hbar \omega_i} (\Delta Q_i)^2 \quad (2)$$

where  $\hbar \omega_i$  is the vibronic level spacing,  $\Delta Q_i$  is the normal coordinate displacement, and  $M_i$  is the reduced ionic mass for the mode  $Q_i$ . In terms of  $S_i$ , the zero-temperature Franck-Condon factors (which determine the relative amplitudes of the phonon sidebands) are defined as<sup>19</sup>

$$|\langle \chi(\nu_i) | \chi(0) \rangle|^2 = \frac{e^{-S_i} S_i^{\nu_i}}{\nu_i!} \quad (3)$$

where  $\nu_i$  is the number of phonons in the excited state vibronic potential. It is clear from Eqs. (2) and (3) that the appearance of vibronic structure requires a finite normal coordinate displacement, and therefore a finite Huang-Rhys parameter.

For a small molecule, the promotion of an electron from the highest occupied molecular orbital (bonding) to the lowest unoccupied molecular orbital (antibonding) has a large effect on the local bond order and thus on the lattice elasticity coefficient  $K$ . Hence, we expect to see the largest normal coordinate displacements (and therefore the largest Huang-Rhys parameters) on the smallest molecules. Granville, Kohler, and Snow<sup>22</sup> demonstrated this trend by performing a Franck-Condon analysis on the absorption spectra of a system of linear polyenes with two to six double bonds. Their results indicate that the magnitude of the change for both the double and single bond lengths decreases as the length of the polyene increases.

In a completely ordered one-dimensional semiconductor, where the electronic wavefunctions are delocalized over the entire lattice, the change in bond order due to an electronic excitation would be of order  $1/N$ . Hence, the change in the linear electron-phonon interaction (i.e., the Huang-Rhys parameter) should be infinitesimal and a Franck-Condon vibronic structure should be strictly forbidden.

Recent calculations by Salkola and Kivelson<sup>23</sup> show that, even in a perfectly ordered system, the Holstein phonon emission process leads to the appearance of phonon sidebands in the absorption spectrum. They find that the relative amplitudes of the multiphonon lines decrease monotonically as  $\lambda(\hbar \omega_{ph}/2\Delta_0)$ . For realistic values of the electron-phonon coupling constant<sup>1</sup> (i.e.,  $\lambda < 1$ ), the relative amplitude of successive phonon sidebands should be weighted by a factor  $\sim 0.05$ : an order of magnitude smaller than experimental observations (e.g., see Fig. 1).

Moses *et al.*<sup>24</sup> suggested that localization (to yield a finite Huang-Rhys factor) in concurrence with a sharp feature in the electronic joint density of states (such as the band-edge square-root singularity) would lead to the appearance of vibronic structure in the absorption spectrum; the more localized the electronic states, the more pronounced the vibronic structure. In the analysis that follows, we shall assume that the dominant mechanism responsible for the vibronic structure observed in the absorption spectra is disorder-induced localization.

Qualitatively, the disordered  $\pi$ -electron system might

be thought of as equivalent to a distribution of finite oligomers whose effective length is the mean localization length. Although not strictly correct, since the localization length is strongly dependent on the energy of the state within the  $\pi$  and  $\pi^*$  bands and since the centers of the various localized states are randomly distributed, localization tends to qualitatively mimic some aspects of short chain behavior.

Localization also has implications for the joint density of electronic states, and therefore the absorption line shape. Disorder-induced localization removes the strict momentum conservation (i.e., the electronic wave vector  $k$  is no longer a good quantum number), which in turn suppresses the square-root singularity in the joint density of electronic states,<sup>25</sup> causing the observed line shape to appear more symmetric.

## V. FRANCK-CONDON ANALYSIS

### A. The models

#### 1. Absorption model

In order to facilitate a deeper understanding of the changes impressed on the coupled electron-phonon system by the reduction of disorder and the enhanced localization in the MEHPPV-PE blends at high draw ratios, we utilize a variation of the model proposed by Moses *et al.*,<sup>24</sup> and assume that the total absorption line shape is a Franck-Condon progression of a zeroth-order purely electronic line shape,  $\alpha_o(\hbar \omega)$ :

$$\alpha(\hbar \omega) = \sum_{\{\nu_i\}} \alpha_o \left( \hbar \omega - \sum \nu_i \hbar \omega_i \right) \prod_i |\langle \chi(\nu_i) | \chi(0) \rangle|^2 \quad (4)$$

where the  $\hbar \omega_i$ 's are the relevant phonon energies of the lattice vibrational wave functions  $\chi(\nu_i)$ . The zeroth-order line shape is assumed to be that derived for a one-dimensional semiconductor in the context of the Su-Schrieffer-Heeger (SSH) theory,<sup>1</sup> but assuming a Gaussian distribution of the energy gap (to account for disorder) centered about the mean value,  $2\Delta_0$ .

$$\alpha_o(\hbar \omega) = \frac{1}{(\hbar \omega)^2} \int d\Delta \frac{e^{-(\Delta - \Delta_0)^2/\tau^2}}{\sqrt{(\hbar \omega)^2 - (2\Delta)^2}} \quad (5)$$

The inclusion of disorder through a Gaussian distribution of energy gaps was inspired by the work of Vardeny *et al.*,<sup>26</sup> where dispersion effects observed in the resonant Raman scattering of *trans*-polyacetylene were attributed to a distribution in values of the electron-phonon coupling constant  $\lambda$ . The distribution in  $\lambda$  arises from finite localization lengths, which in turn are due to disorder. Other parameters being fixed,  $\lambda$  uniquely determines the energy gap.

#### 2. Emission model

To model the photoluminescence spectrum, we consider a Franck-Condon progression of Lorentzians (to ac-

TABLE II. Franck-Condon analysis: absorption.

Sample	Temp. (K)	$2\Delta_0$	$\hbar\omega_{ph}$	$\gamma$	$S$
OB	80	2.136	0.172	0.040	0.41
OB	300	2.214	0.162	0.060	0.46
NB	80	2.156	0.168	0.054	0.51
Cast	80	2.176	0.182	0.070	0.62

count for the localized nature of the gap states<sup>27</sup>) and parameterize their height and linewidth according to

$$I(\hbar\omega) = \sum_{\{\nu_j\}} \frac{(\Gamma_{\nu_j}/2)^2}{(\hbar\omega - \hbar(2\omega_0) + \sum \nu_j \hbar\omega_j)^2 + (\Gamma_{\nu_j}/2)^2} \times \prod_j |\langle \chi(\nu_j) | \chi(0) \rangle|^2 \quad (6)$$

where  $\Gamma_{\nu_j}$  is the linewidth broadening parameter for the  $j$ th mode with occupation  $\nu_j$ , and  $2\omega_0$  is the energy separation of the two self-localized gap states.

### 3. Franck-Condon factors

Because of the relatively simple harmonic progressions observed for both absorption (via second derivative analysis) and emission, we will consider electronic coupling to a single Raman-active vibrational mode (although a number of Raman-active modes appear in the 1200–1600  $\text{cm}^{-1}$  range,<sup>28</sup> the experimental resolution observed in Figs. 1–8 does not justify considering more than one mode), and assume that the Franck-Condon factors can be written as Eq. (3).

### B. Fitting procedure

The absorption spectra are fit by a two-step process where the zeroth-order line shape, calculated from Eq. (5), is fit to the first feature in the NNSD spectrum of the experimental absorption until a best fit (via  $\chi^2$ ) is obtained. Once  $\Delta_0$  and  $\gamma$  are fixed, Eq. (4) is fit (again via  $\chi^2$ ) to the entire experimental absorption line shape to determine the vibronic spacing  $\hbar\omega_{ph}$  and the Huang-Rhys parameter  $S$ . Since the experimental resolution is limited to 1 nm (4 meV at 600 nm) the resolution of the three energy parameters ( $\Delta_0$ ,  $\gamma$  and  $\hbar\omega_{ph}$ ) is chosen to be 2 meV.

For the emission analysis, Eq. (6) is fit to the data with all six parameters ( $\omega_0$ ,  $\omega_{ph}$ ,  $S$ , and the  $\Gamma_{\nu_j}$ 's) varying. Although the best fits require allowing the individ-

ual Lorentzian linewidths to vary,  $\omega_0$ ,  $\omega_{ph}$ , and  $S$  are found to be rather insensitive to  $\Gamma_1$  and  $\Gamma_2$ . The fits are weighted by the luminescence profile itself, thus ensuring a proper fit of the largest features (i.e., the zero and one-phonon lines). Rapid convergence is found for all fits; the parameters obtained from the Franck-Condon analysis are summarized in Tables II and III for absorption and emission, respectively.

### C. Results of the Franck-Condon analysis

The best-fit zeroth-order line shape [Eq. (5)] for the oriented ( $\times 50$ ) MEHPPV-PE blend is shown as the solid curve in Fig. 9. The energy gap  $2\Delta_0$  and the Gaussian broadening parameter  $\gamma$  are found to be 2.136 eV and 40 meV, respectively. Also shown in the figure (dashed line) is the square-root singularity characteristic of the intrinsic line shape for an ideal one-dimensional semiconductor (i.e.,  $\gamma=0$ ). It is clear from Fig. 9 that the zeroth-order line shape of MEHPPV in the oriented blend is approaching that of the ideal one-dimensional semiconductor.

Figures 10 and 11 present the results of the Franck-Condon analysis for the 80-K absorption and emission spectra of an oriented ( $\times 50$ ) thin film of MEHPPV-PE for optical polarization parallel to the drawing axis. For the oriented blend (OB), the model fits both the absorption and emission spectra quite well. Small deviations in the photoluminescence fit are attributed to anharmonic effects on the low-energy side of the spectrum and reabsorption on the high-energy side (see Fig. 7). We find a best-fit Huang-Rhys parameter of 0.41 for the absorption spectrum and 0.47 for the emission spectrum. The observed increase in  $S$  upon emission is consistent with structural relaxation due to bipolaron-exciton self-localization.<sup>27</sup>

By differentiating Eq. (5) it is found that, due to the asymmetric nature of the zeroth-order line shape, the peak in the second derivative spectrum is always greater than  $2\Delta_0$ , and hence the NNSD spectra (see Table I)

TABLE III. Franck-Condon analysis: emission.

Sample	Temp. (K)	$\hbar(2\omega_0)$	$\hbar\omega_{ph}$	$\Gamma_0$	$S$
OB	80	2.088	0.162	0.066	0.47
OB $\perp$	80	2.084	0.154	0.098	0.85
Cast	80	2.011	0.180	0.105	0.63

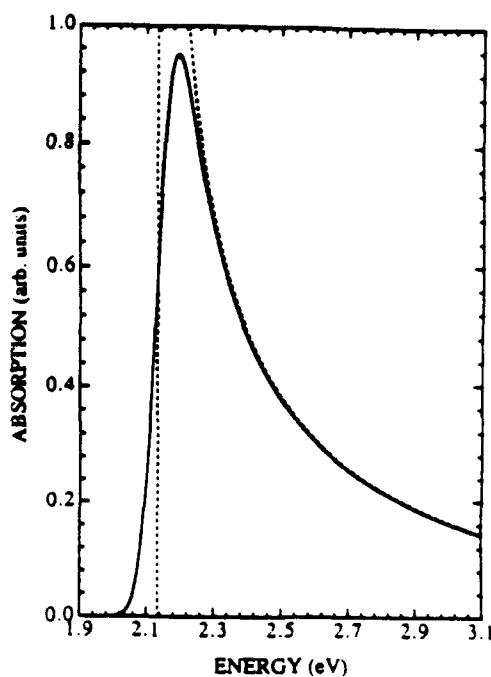


FIG. 9. The solid line is the zeroth-order line shape as calculated from Eq. (5) for the parameters listed in Table II, row 1. Also included in the figure is the SSH line shape (dashed) calculated for a perfectly dimerized one-dimensional chain with no disorder (i.e.,  $\gamma=0$ ).

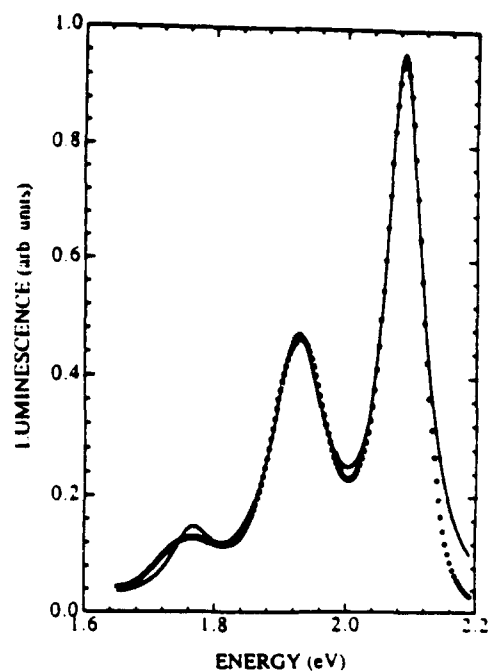


FIG. 11. Results of the Franck-Condon photoluminescence analysis for an oriented ( $\times 50$ ) thin film of MEHPPV-PE at 80 K for emission polarization parallel to the drawing axis.

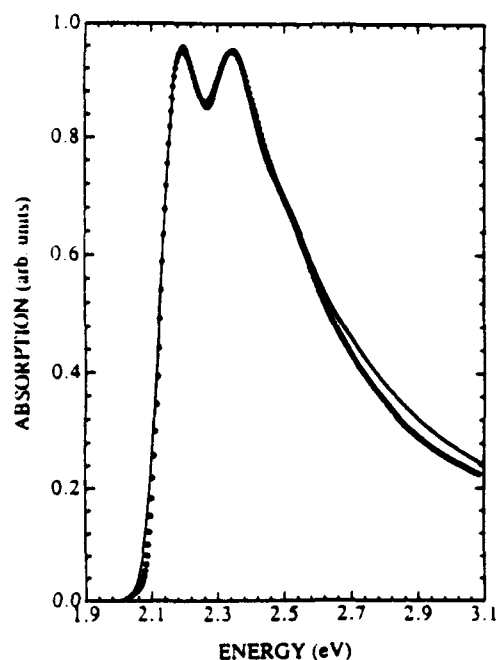


FIG. 10. Results of the Franck-Condon absorption analysis for an oriented ( $\times 50$ ) free-standing film of MEHPPV-PE at 80 K for optical polarization parallel to the drawing axis. As in all subsequent plots, the fit is the solid line and the data appears as dots.

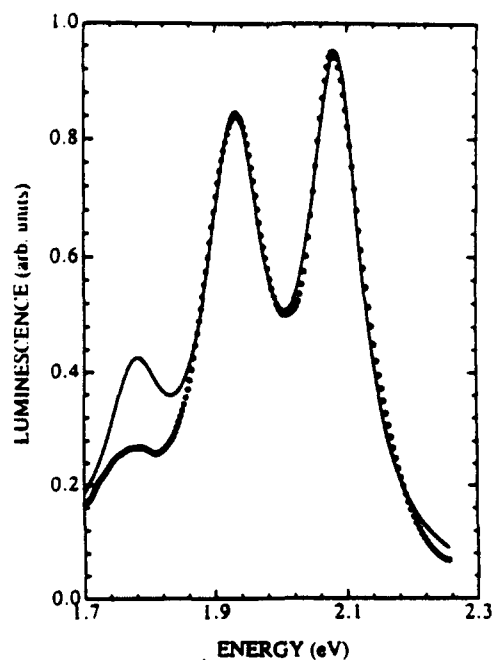


FIG. 12. Results of the Franck-Condon photoluminescence analysis for an oriented ( $\times 50$ ) thin film of MEHPPV-PE at 80 K for emission polarization perpendicular to the drawing axis.

always overestimate the energy of the zero-phonon line. Using the results of the Franck-Condon analysis ( $2\Delta_0 = 2.136$  eV and  $2\omega_0 = 2.088$  eV), we find that chain orientation and improved structural order in the drawn ( $\times 50$ ) films has reduced the Stokes shift to a mere 48 meV.

In Figure 12 we present the results of the Franck-Condon analysis for the parallel pumped 80-K photoluminescence spectrum of an *oriented* ( $\times 50$ ) thin film of MEHPPV-PE for emission polarization perpendicular to the drawing axis. The large increase in the Huang-Rhys parameter for perpendicular emission ( $S_{\perp} = 0.85$  vs  $S_{\parallel} = 0.47$ ) is consistent with a significantly higher degree of disorder-induced localization in the residual nonorientable fraction of MEHPPV in the blend.

The differences in vibronic character for emission parallel and perpendicular to the draw axis are of particular interest since they provide information about the local environment of the recombination centers. Although the position of the zero-phonon line is insensitive to the state of polarization, the vibronic spacing  $\hbar\omega_{ph}$  decreases from 162 meV to 154 meV, and the zero-phonon linewidth  $\Gamma_0$  increases from 66 meV to 98 meV for the perpendicular component relative to the parallel component. These observations are again consistent with a higher degree of disorder in the residual nonorientable fraction of MEHPPV in the blend.

Figure 13 presents the results of the Franck-Condon analysis for the 300-K absorption spectrum of an *oriented* ( $\times 50$ ) thin film of MEHPPV-PE for optical polarization parallel to the draw axis. Because of the lack of vibronic information present in the emission spectrum, a

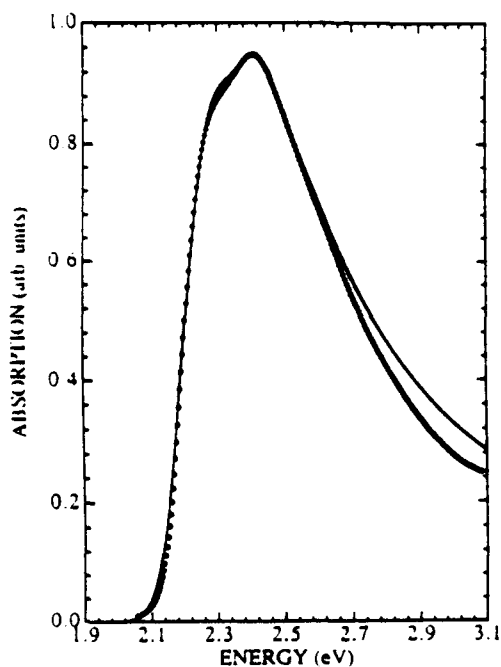


FIG. 13. Results of the Franck-Condon analysis for an *oriented* ( $\times 50$ ) thin film of MEHPPV-PE at 300 K for optical polarization parallel to the drawing axis.

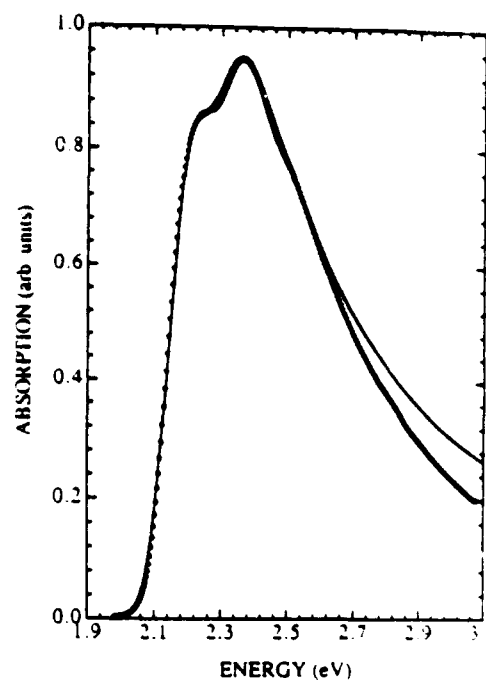


FIG. 14. Results of the Frank-Condon analysis for a *nonoriented* free-standing film of MEHPPV-PE at 80 K.

fit is not justified. At 300 K, the position of the zero-phonon line (2.214 eV), the Gaussian broadening parameter (60 meV), and the magnitude of the Huang-Rhys parameter (0.46) have all increased relative to the 80-K spectrum. The deviations between the fit and the measured absorption line shape at high energy (absent at 80

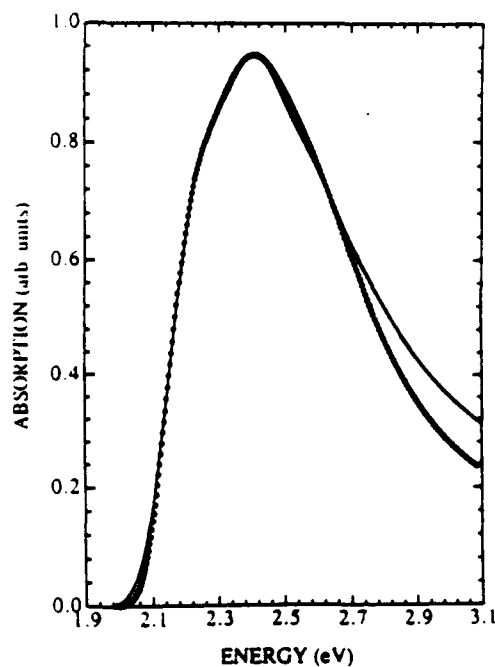


FIG. 15. Results of the Franck-Condon absorption analysis for a cast film of pure MEHPPV at 80 K.

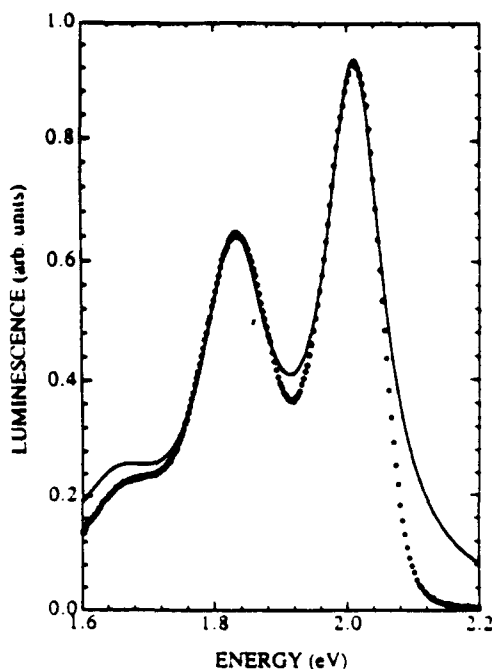


FIG. 16. Results of the Franck-Condon emission analysis for a cast film of pure MEHPPV at 80 K.

K) imply that increased temperature causes the zeroth-order line shape of the *oriented* blend to become more symmetric.

Figure 14 shows the results of the Franck-Condon analysis for the 80-K absorption spectrum of a *nonoriented* thin film of MEHPPV-PE. Because of the lack of vi-

bronic information present in the emission spectrum, a fit is again not justified. For the absorption spectrum, we find a quite reasonable fit for a Huang-Rhys parameter of 0.51. The deviations between the fit and experiment again imply a more symmetric line shape. From Table II we see that the parameters found for the *nonoriented* blend (NB) at 80 K (aside from the gap energy) are similar to those found for the *oriented* blend at 300 K, in agreement with the qualitative observations reported in Fig. 4.

In Figures 15 and 16 we show the results of the Franck-Condon analysis for a cast film of pure MEHPPV. The results yield  $2\Delta_0 = 2.176$  eV and  $2\omega_0 = 2.011$  eV, implying a Stokes shift of 165 meV. The best-fit Huang-Rhys parameter was determined to be 0.62 for absorption, and 0.63 for emission.

To better demonstrate the mirror symmetry that exists between the vibronic progressions of absorption and emission, Figures 17(a) and 17(b) summarize the results of the Franck-Condon analysis for the *oriented* blend and the cast film at 80 K. Note that the relative heights of the progressions in absorption and emission come from the Franck-Condon analysis; the normalization of the zero-phonon amplitude in absorption and emission is arbitrary and is not intended to imply unit quantum efficiency. Figure 17 is a graphic depiction of the degree to which the ground- and excited-state configurational manifolds have been modified as a result of gel processing and subsequent tensile drawing. The observed mirror symmetry and finite Stokes shift imply that the relaxation pathway that yields the Stokes shift and that yielding the harmonic progression are nearly orthogonal.

## VI. DISCUSSION

The results of polarization spectroscopy and the Franck-Condon analysis show that gel processing and subsequent tensile drawing result in the following: (1) Reductions in the linewidth broadening parameters for both absorption and emission; (2) quasi-one-dimensionality; (3) decrease in the Huang-Rhys parameter; (4) changes in the phonon frequencies; (5) decrease in the Stokes shift; (6) macroscopic orientation and microscopic order; (7) changes in vibronic structure.

### A. Linewidth broadening parameters

The observed decrease in the linewidth broadening parameters (see Tables II and III) and the implied increase in the localization length in the *oriented* MEHPPV-PE blend are consistent with a reduction in disorder.

The large temperature dependence observed in the *oriented* blend Gaussian broadening parameter ( $\gamma_{80\text{ K}} = 40$  meV and  $\gamma_{300\text{ K}} = 60$  meV) suggests that a portion of this broadening may be due to low-frequency librations (i.e., internal torsional modes).<sup>20</sup> We point out, however, that further cooling samples to 10 K yielded no additional decrease in the Gaussian broadening parameter.

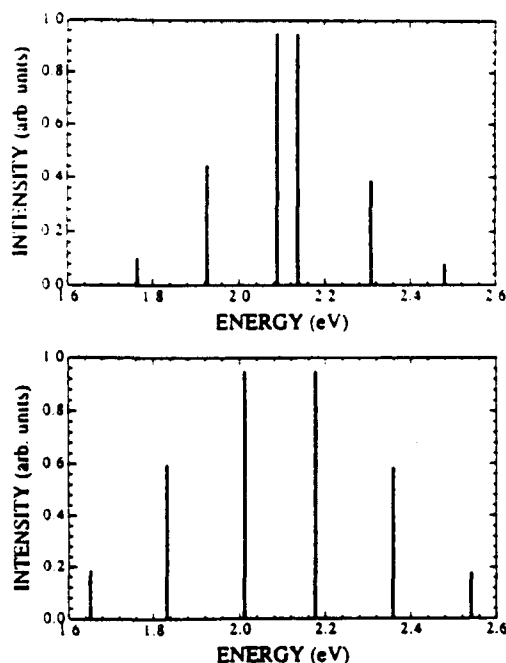


FIG. 17. Summary of the Franck-Condon overlap intensities for (a) an *oriented* ( $\times 50$ ) thin film of MEHPPV-PE at 80 K for optical polarization parallel to the drawing axis, and (b) for a cast film of pure MEHPPV at 80 K.

### B. Quasi-one-dimensional band structure

The polarization dependence of the absorption and photoluminescence spectra in the oriented blend (Figs. 1 and 8) are indicative of a highly anisotropic electronic system. This, in conjunction with the zeroth-order line shape (Fig. 9), suggests that the conjugated polymer system MEHPPV-PE can be accurately described in the context of the SSH tight-binding formalism.

The best-fit 80-K Gaussian broadening parameter in the oriented blend (40 meV) sets an upper limit on the interchain (3d) bandwidth,  $W_{\perp} = 2zt_{\perp}$ , where  $t_{\perp}$  is the interchain transfer integral and  $z$  is the number of nearest-neighbor MEHPPV chains. This remarkably small value is particularly important, for it implies a quasi-one-dimensional band structure.

This weak interchain coupling might be the result of relatively large interchain spacing in MEHPPV. Because of the asymmetric side chains, the macromolecules cannot pack as closely, for example, as the poly(phenylenevinylene) parent polymer. On the other hand, gel processing in PE may effectively reduce the number of MEHPPV nearest neighbors. Frequency-dependent conductivity results<sup>29</sup> suggest that the conjugated polymer adsorbs onto the PE and decorates the complex surface of the gel network,<sup>30</sup> thereby forming connected (conducting) pathways at volume fractions nearly three orders of magnitude below the threshold for three-dimensional percolation. In this case, at low guest concentration, the conjugated polymer forms essentially a monolayer on PE and  $z$  is reduced accordingly. Finally, although the two component polymers are expected to be immiscible (since the entropy of mixing is essentially zero for macromolecules), the extended side chains of MEHPPV might be sufficiently "polyethylenelike" to cause a true molecular solution of MEHPPV in PE, thereby reducing  $z$  to zero.

The relative magnitudes of the interchain (three-dimensional) bandwidth and the polaron binding energy have interesting implications on the nature of the nonlinear excitations, for if the strength of the interchain coupling exceeds the magnitude of the polaron binding energy (i.e., the Stokes shift  $E_S$ ), the one-dimensional self-localized polaron (or bipolaron) will not be stable.<sup>31</sup> Since in the oriented blend the bipolaron-exciton binding energy ( $E_S = 48$  meV) is of the same order as the upper limit for the transverse bandwidth, it is not clear whether or not this stability criterion is satisfied.

Recently, Rausche *et al.*<sup>32</sup> questioned the validity of the band picture in describing the absorption and photoluminescence spectra in poly-(*p*-phenylenevinylene), PPV. Their argument is based upon a dispersion effect where the spectral dependence of the photoluminescence is seen to be dependent on the excitation energy near the excitation onset. From the results presented here, it is clear that disorder induced localization plays a significant role in determining both the position and spectral profile of the interband transition, as demonstrated in Fig. 8, where the emission of the oriented and ordered system is found to have a polarization-dependent spectral profile. In addition, we find that the position of the zero-

phonon line (for both absorption and emission) changes as the system becomes more ordered (see Fig. 17). It is not surprising to find excitation-dependent (site selective) emission in severely disordered materials. Further, the appearance of an excitation threshold, above which the emission is independent of excitation energy, is consistent with the concept of a mobility edge, above which the electronic states are delocalized. We conclude that the band picture provides a valid description of the  $\pi$ - $\pi^*$  transition at least in MEHPPV-PE, and that deviations from this theory are primarily a consequence of disorder.

### C. Localization and the Huang-Rhys parameter

As summarized in Tables II and III, both gel processing MEHPPV in UHMWPE and subsequent chain alignment by tensile drawing cause a decrease in the Huang-Rhys parameter. We interpret this result as a reduction in  $\Delta\lambda$ , the difference in the electron-phonon interaction between the initial and final state, by enhanced electronic delocalization—the  $1/N$  effect.

By comparing the results of the 80-K and 300-K analysis of the oriented blend, it is clear that the Huang-Rhys parameter, and thus  $\Delta\lambda$ , is an increasing function of temperature. Since it is well known that thermal disorder decreases the localization length of the electronic states, the results of the Franck-Condon analysis demonstrate a reduction of disorder and an enhancement of electronic delocalization in the oriented MEHPPV-PE films.

### D. Phonon energies

The observed decrease in the phonon energies of the emission progression, relative to that of the absorption progression, (Tables II and III) is consistent with a significantly higher degree of electronic localization (self-localization) in the split-off gap states. It is emphasized that neither the vibronic structure observed in absorption nor that observed in emission is that of the true ground state. Absorption spectroscopy probes the vibrational manifold of the excited-state prior to self-localization effects, while photoluminescence probes the restricted manifold of the self-localized gap states  $\pm\omega_0$ . The increased localization yields a larger change in the local bond order in the gap state, causing a softening of the gap-state vibrational manifold with respect to that of the initial (i.e., before self-localization) excited state. Hence, one would expect to find softer phonons and a higher degree of anharmonicity in the luminescence spectra, consistent with experimental observations. This explanation is substantiated by examining the effects of increasing temperature, well known to decrease the localization length, on these phonon energies. Tables I and II show a decrease (with increasing temperature) in the spacing of the vibronic features observed in absorption. Qualitatively, the conclusion is once again clear: the structural disorder in the *nonoriented* films and the thermal disorder in the *oriented* films have comparable effects and therefore lead to comparable changes in the electronic localization lengths.

### E. Stokes shift and confinement

Perhaps the most intriguing effect of gel processing and subsequent stretch orientation on the electronic structure of the conjugated polymer guest is the reduction of the Stokes shift. Using the values obtained from the Franck-Condon analysis (Tables II and III) we find a Stokes shift of 165 meV for the cast film and 48 meV for the oriented blend, a reduction by more than a factor of 3. Based on this result, it is not unreasonable to expect that in a perfectly ordered system the Stokes shift would be even smaller (perhaps zero). Certainly, if one can neglect guest-host caging effects (e.g., the Stokes pressure effect<sup>33</sup>), the 48-meV value sets an upper limit on the intrinsic Stokes shift arising from self-localization to form a neutral bipolaron-exciton in the perfectly ordered polymer.

Using the analysis of Brazovskii and Kirova,<sup>34</sup> the polaron-exciton confinement parameter, as defined by the Stokes shift,  $E_S = 2(\Delta_o - \omega_o)$ , is given by

$$\gamma_{BE} = \left( \frac{\omega_o}{\Delta_o} \right) \frac{\sin^{-1} \left( \frac{\omega_o}{\Delta_o} \right)}{\sqrt{1 - \left( \frac{\omega_o}{\Delta_o} \right)^2}} \quad (7)$$

As seen from Tables II and III the bipolaron-exciton confinement parameter increases by more than a factor of 2 when going from the cast film ( $\gamma_{BE} \approx 2.85$ ) to the oriented blend ( $\gamma_{BE} \approx 6.30$ ). These values should be compared to those obtained by photoinduced absorption. For charged bipolarons, Voss *et al.*<sup>35</sup> find a photoinduced confinement parameter of 0.23 for MEHPPV. It is known, however,<sup>27</sup> that the confinement parameter, as defined by the gap states of the neutral bipolaron-excitons (via luminescence spectroscopy), is found to be an order of magnitude larger than that inferred from the spectroscopy of charged bipolarons (generated either by doping or by photoexcitation). This discrepancy has been attributed to the neglect of the Coulomb interaction between the two charges comprising the defect.<sup>27</sup>

The Brazovskii and Kirova<sup>34</sup> analysis also allows one to define the spatial extent of the bipolaron exciton

$$L_{BE} = 2(x_o + \xi), \quad (8)$$

where the kink pair separation  $2x_o$ , and kink coherence length  $\xi$  are given by

$$2x_o = \xi_o \alpha \coth(\alpha) \quad (9)$$

$$\xi = \xi_o \coth(\alpha) \quad (10)$$

and Brazovskii and Kirova's parameter  $\alpha$  is related to the confinement parameter  $\gamma_{BE}$  [Eq. (7)] by

$$\gamma_{BE} = \text{csch}(\alpha) \sin^{-1}[\text{sech}(\alpha)] \quad (11)$$

If we use the confinement parameter obtained from the Stokes shift, the spatial extent of the bipolaron exciton is calculated to be 38 Å in the cast film and 63 Å in the oriented blend.

### F. Aligned versus ordered

The polarized absorption and photoluminescence of stretch oriented poly(phenylenevinylene) (PPV) has been studied in great detail by Friend, Brodiey, and Townsend.<sup>27</sup> Their results indicate a dichroic ratio of 10:1 for absorption and an emission anisotropy of only 3:1. In addition, the spectral dependence of the emission profile was found to be independent of polarization (pump and probe). They attributed these observations to the localized nature of the bipolaron exciton.

In MEHPPV oriented by gel processing in UHMWPE, we observe anisotropic photoluminescence (both in magnitude and spectral density) and an exceedingly small Stokes shift. These results imply that the bipolaron exciton is delocalized over many unit cells [e.g., Eq. (8)]. To accommodate this relatively high degree of electronic delocalization, the conjugated polymer must not only be macroscopically aligned, but microscopically ordered as well.

### G. Interpretation of vibronic structure

#### 1. System free of disorder

The extrapolation of the results of the Franck-Condon analysis to the ideal conjugated macromolecule, free of disorder, suggests that there will be neither vibronic structure nor a Stokes shift (i.e., an absence of structural relaxation in the excited state). The latter is quite surprising in light of the work of Schuttler and Holstein,<sup>31</sup> where the quasi-one-dimensional polaron stability criterion is found to set rather liberal constraints on the transverse bandwidth. The observed anisotropy in both the interband transition and the recombination luminescence in oriented MEHPPV-PE implies a quasi-one-dimensional electronic structure, seemingly in contradiction with the observed trend in the Stokes shift.

#### 2. System with disorder

While it is clear that the structure observed in the emission spectrum results from vibronic transitions between localized levels, the assignment of the corresponding features seen in absorption is the subject of debate. Moses *et al.*<sup>24</sup> attributed the vibronic structure observed in *cis*-polyacetylene to a specifically nonlocalized phonon-assisted interband transition. If this were indeed the case, one would not expect to see a correlation between the relative magnitudes of the Franck-Condon overlap factors for emission (transition between localized levels) and the interband transition. As demonstrated above, there exists not only a correlation, but near perfect mirror symmetry (see Fig. 17). Furthermore, the effects of gel processing and subsequent tensile drawing on these Franck-Condon progressions are virtually identical.

Hence, it seems clear that the vibronic structure observed in absorption in real samples (with imperfect structural order) is indicative of the direct photoproduction of an excited-state relaxed configuration whose zero-point motion overlaps that of the ground state (i.e., quan-



tum lattice effects). With improved order, the higher-order features in the vibronic progression decrease in amplitude and the absorption approaches that of the interband transition in the ideal quasi-one-dimensional semiconductor.

The observed Stokes shift between the zero-phonon lines of absorption and emission indicates that prior to emission, the bipolaron-exciton undergoes a secondary dynamical relaxation (i.e., photoexcitation occurs to a configurational saddle point which subsequently relaxes to a localized state before emission can occur). The fact that the subsequent dynamical relaxation does not destroy the Franck-Condon mirror symmetry suggests that the dynamical configurational coordinate which yields the Stokes shift is essentially orthogonal to the coordinate responsible for the observed vibronic structure.

## VII. CONCLUSION

We have demonstrated a method for obtaining aligned and structurally ordered conjugated polymers by mesoscopic-scale epitaxy using gel processing in blends with PE and subsequent tensile drawing. By controlling the concentration of conjugated polymer in the blend, durable samples with desired optical density and anisotropy have been obtained. Using these materials, we have identified the spectral changes that occur as a result of the improved structural order induced by alignment of the conjugated macromolecules. The principal conclusions of these studies are as follows.

(1) The electronic structure of MEHPPV in PE is quasi-one-dimensional with weak interchain coupling,  $W_{\perp} \leq 40$  meV.

(2) For MEHPPV in PE, the structural order is sufficient to enable the determination of the intrinsic line shape of the interband absorption; we find the band-edge square-root singularity characteristic of a one-dimensional semiconductor.

(3) The polarized photoluminescence ( $L_{\parallel}/L_{\perp} \geq 60:1$ ) implies that the dominant source of emission is from delocalized bipolaron-excitons extended along the MEHPPV chains. Even with a perpendicularly polarized pump,  $L_{\theta}(\hbar\omega)$  is strongly polarized along the chain direction, implying that photoinjected polarons on separate chains migrate until an oppositely charged polaron is encountered on the same chain.

(4) The details of the spectral changes (sharper absorption edge and enhancement of the zero-phonon vi-

bronic transition) that are induced by the improvements in structural order imply a significant increase of the localization length. The Franck-Condon analysis of the vibronic sidebands shows a reduction in  $\Delta\lambda$ , the difference in the electron-phonon interaction between the initial and final state, by enhanced electronic delocalization—the  $1/N$  effect.

The principal trends observed with chain alignment and improved order are in agreement with intuitive expectations. However, the remarkably small Stokes shift in the most highly aligned and ordered material is difficult to understand. The observed anisotropy in both the interband transition and the recombination luminescence in oriented MEHPPV-PE implies a quasi-one-dimensional electronic structure, seemingly in contradiction with the observed trend in the Stokes shift. Although the interchain coupling is weak,  $W_{\perp} \leq 40$  meV, it might nevertheless be sufficient to prevent polaron self-localization. Only if this is the case and if, in addition, the attractive Coulomb interaction between the electron and the hole is sufficiently well screened to prevent the formation of a bound exciton, would the Stokes shift actually go to zero.

Thus, through gel processing of a conjugated polymer in ultrahigh-molecular-weight polyethylene, we have succeeded in achieving sufficiently ordered material that we are able to begin to study the intrinsic anisotropic optical properties (both in absorption and emission) of the conjugated polymer, MEHPPV. By comparing the data from samples with different degrees of disorder, we have been able to separate those features which arise explicitly from disorder. The remarkable anisotropy (e.g., greater than 60:1 in the polarized luminescence) emphasizes once again the unique features and the special opportunities which result from the quasi-one-dimensional electronic structure of conjugated polymer semiconductors.

## ACKNOWLEDGMENTS

This research was supported by the Air Force Office of Scientific Research (AFOSR 90-0283). We thank Z. Ni, G. Srdanov, and Professor F. Wudl for synthesis of the MEHPPV and N. Colaneri, C. M. Foster, S. Kivelson, D. McBranch, D. Mihailović, D. Moses, J. Moulton, S. D. Phillips, and P. Smith for important comments and discussions.

<sup>1</sup>A. J. Heeger, Rev. Mod. Phys. **60**, 781 (1989).

<sup>2</sup>N. F. Mott and E. A. Davis, *Electronic Processes in Non-Crystalline Materials* (Clarendon, Oxford, 1979), Chap. 2.

<sup>3</sup>S. Kivelson and A. J. Heeger Synth. Met. **22**, 371 (1988).

<sup>4</sup>R. Silbey, in *Conjugated Polymeric Materials: Opportunities in Electronics, Optoelectronics and Molecular Electronics*, Vol. 182 of NATO Advanced Study Institute Series, Series E: Applied Sciences edited by J. L. Bredas and R. R. Chance (Kluwer Academic, Dordrecht, 1990), and references therein. The results indicate that  $\chi^{(3)}$  is propor-

tional to  $N^{\nu}$  where  $N$  is the polymerization index, and  $\nu$  is in the range 4–5, the precise value being sensitive to the detailed approximations in the method used.

<sup>5</sup>A. Andreatta, S. Tokito, P. Smith, and A. J. Heeger, Mol. Cryst. Liq. Cryst. **189**, 169 (1990).

<sup>6</sup>Y. Cao, P. Smith and A. J. Heeger, Polymer **32**, 1210 (1991).

<sup>7</sup>S. D. Phillips, R. Worland, G. Yu, T. W. Hagler, R. Freedman, Y. Cao, V. Yoon, J. Chiang, W. C. Walker, and A. J. Heeger, Phys. Rev. B **40**, 9751 (1989).

- <sup>8</sup>M. Sinclair, D. Moses, K. Akagi, and A. J. Heeger, *Phys. Rev. B* **38**, 10724 (1987).
- <sup>9</sup>E. Wintner, F. Krauss, and G. Leising, *Phys. Rev. B* **39**, 3701 (1989).
- <sup>10</sup>S. Tokito, P. Smith, and A. J. Heeger, *Polymer* (to be published).
- <sup>11</sup>S. Tokito, P. Smith, and A. J. Heeger, *Synth. Met.* **36**, 183 (1990).
- <sup>12</sup>J. Moulton and P. Smith, *Synth. Met.* (to be published).
- <sup>13</sup>P. Smith and P. Lemstra, *J. Mater. Sci.* **15**, 505 (1980).
- <sup>14</sup>P. Smith, P. Lemstra, J. P. L. Pijpers, and A. M. Kiel, *Coll. Polym. Sci.* **259**, 1070 (1981).
- <sup>15</sup>T. W. Hagler, K. Pakbaz, J. Moulton, F. Wudl, P. Smith, and A. J. Heeger, *Polym. Commun.* (to be published).
- <sup>16</sup>J. Van Schoot and K. F. Voss (private communication).
- <sup>17</sup>J. J. Bowman, T. B. A. Senior, and P. L. E. Uslenghi, *Electromagnetic and Acoustic Scattering by Simple Shapes* (Hemisphere, New York, 1987), p. 99.
- <sup>18</sup>J. Orenstein, G. L. Baker, and Z. Vardeny, *J. Phys. (Paris) Colloq.* **3**, C3-407 (1983).
- <sup>19</sup>B. Henderson and G. F. Imbusch, *Optical Spectroscopy of Inorganic Solids* (Clarendon, Oxford, 1969).
- <sup>20</sup>A. R. Mantini, M. P. Marzocchi, and G. Smulevich, *J. Chem. Phys.* **91**, 85, (1989).
- <sup>21</sup>W. Siebrand and M. Z. Zgierski, *J. Chem. Phys.* **79**, 3561, (1979).
- <sup>22</sup>M. F. Granville, B. E. Kohler, and J. B. Snow, *J. Chem. Phys.* **75**, 3765, (1981).
- <sup>23</sup>M. Salkola and S. Kivelson (unpublished).
- <sup>24</sup>D. Moses, A. Feldblum, E. Ehrenfreund, A. J. Heeger, T.-C. Chung, and A. G. MacDiarmid, *Phys. Rev. B* **26**, 3361 (1982).
- <sup>25</sup>N. Suzuki, M. Ozaki, S. Etemad, A. J. Heeger, and A. G. MacDiarmid, *Phys. Rev. Lett.* **45**, 1209 (1980).
- <sup>26</sup>Z. Vardeny, E. Ehrenfreund, O. Brafman, and B. Horovitz, *Phys. Rev. Lett.* **51**, 2326 (1983).
- <sup>27</sup>R. H. Friend, D. D. C. Bradley, and P. D. Townsend, *J. Phys. D* **20**, 1367 (1987).
- <sup>28</sup>D. Lederman (private communication).
- <sup>29</sup>A. Fizazi, J. Moulton, K. Pakbaz, S. D. D. Rughooputh, P. Smith, and A. J. Heeger, *Phys. Rev. Lett.* **64**, 2180 (1990).
- <sup>30</sup>Y. Y. Suzuki, A. J. Heeger, and P. Pincus, *Macromolecules* **23**, 4730 (1990).
- <sup>31</sup>H. B. Schuttler and T. Holstein, *J. Phys.* **166**, 93 (1986).
- <sup>32</sup>U. Rauscher, H. Bassler, D. D. C. Bradley, and M. Hennecke, *Phys. Rev. B* **42**, 9830 (1990).
- <sup>33</sup>R. M. Macnab and K. Sauer, *J. Chem. Phys.* **53**, 2805 (1970).
- <sup>34</sup>S. A. Brazovskii and N. N. Kirova, *Pis'ma Zh. Eksp. Teor. Fiz.* **33**, 6 (1981) [*JETP Lett.* **33**, 4 (1981)].
- <sup>35</sup>K. F. Voss, C. M. Foster, L. Smilowitz, D. Mihailovic, S. Askari, G. Srdanov, Z. Ni, S. Shi, A. J. Heeger, and F. Wudl, *Phys. Rev. B* **43**, 5109 (1991).

---

## Highly oriented thin films of poly(tetrafluoroethylene) as a substrate for oriented growth of materials

Jean Claude Wittmann\* & Paul Smith†

Materials Department and †Department of Chemical and Nuclear Engineering, University of California at Santa Barbara, Santa Barbara, California 93106, USA

THE formation of highly oriented structures such as single crystals, single-domain liquid crystals and systems comprising uniaxially oriented crystallites is important in many applications of thin films and interfaces, ranging from materials reinforcement to molecular electronics. Of the methods that exist for forming such oriented structures, however, few have sufficient generality to make them applicable to materials of differing chemical composition or physical properties. Here we present a simple and surprisingly versatile method<sup>1</sup> for orienting a wide variety of crystalline and liquid-crystalline materials, including polymers, mesomers and small organic and inorganic molecules. In our technique, a thin, single-crystal-like film of poly(tetrafluoroethylene) (PTFE) is deposited mechanically on a smooth substrate such as glass. Materials grown on this coated surface from solution, melt or vapour phases show a remarkable degree of alignment.

The commercial significance of oriented systems derives from the fact that the properties of the oriented materials may exceed those of the isotropic species by orders of magnitude. For example, increases of more than a factor of 100 have been reported for the stiffness and strength of highly oriented crystalline polymers<sup>2-4</sup> and for the electrical conductivity of doped and aligned conjugated macromolecules<sup>5-7</sup> compared with un-oriented materials. Amongst many other examples of improved

---

\* Permanent address: Institut Charles Sadron (CRM-EAHP), 6 rue Bouscangaut, 67083 Strasbourg, France

performance of oriented materials are enhanced thermal conductivity<sup>8</sup>, piezoelectric properties<sup>9</sup> and optical transparency.

A wide variety of techniques has been developed to promote oriented growth. For example, metals, polymers and small molecules not prone to form large single crystals have been processed into oriented structures through epitaxial crystallization on single-crystal substrates<sup>10,11</sup> or on moderately oriented polymers<sup>12-14</sup>. In isolated cases, graphoepitaxy<sup>15</sup>, which is oriented growth on substrates of supramolecular, microscopic gratings (of typical spacing  $\sim 0.3 \mu\text{m}$ ), has been reported to be successful. Small-molecule liquid crystalline compounds, which are important in display technology, are oriented into domains by deposition on 'rubbed' surfaces of certain polymers<sup>16,17</sup> and/or in magnetic or electric fields. Oriented structures of macromolecules, such as films and fibres, are generally made by mechanical deformation in the solid, gel or liquid crystalline state<sup>2-4</sup>, or by epitaxial crystallization (see, for example, reviews in refs 18 and 19). Virtually all of the above techniques either produce only a limited degree of order, or are restricted to a limited range of materials. The method that we present here, however, is highly versatile, enabling oriented growth of a wide variety of materials.

The deposition of the thin, orientation-inducing layers of PTFE is relatively straightforward, and derives from detailed observations made by workers in the field of polymer wear<sup>20,21</sup>. The method is schematically depicted in Fig. 1a. Electron-diffraction studies of the PTFE layers (Fig. 1b) showed, in accordance with previous observations<sup>20</sup>, that the chain axis of the PTFE macromolecules was oriented parallel to the glass surface (in other words in the plane of the layer) and along the sliding direction. The observed alignment and crystalline perfection of deposited layers were very high and compared favourably with those found in extended chain whiskers of PTFE directly

formed during synthesis<sup>22</sup> or in high-performance, gel-processed ultra-high molecular weight polyethylene<sup>23</sup>. A transmission electron micrograph of a platinum/carbon replica of the PTFE layer is presented in Fig. 1c. This micrograph shows that the surface was not molecularly smooth, but consisted of many steps of various heights, which extended along the path of deposition.

These PTFE-coated glass slides subsequently were used as substrates for the deposition of a variety of materials. The species of interest were grown on the substrates from the melt, solution or gas phase, at temperatures below the melting point of PTFE ( $\sim 340^\circ\text{C}$ ).

A first example is given in Fig. 2a, which shows an optical micrograph of poly( $\epsilon$ -caprolactone), PCL, crystallized from the melt onto the oriented PTFE layer, and on the adjacent bare glass surface as a reference. The left-hand side of the figure reveals the typical isotropic, spherulitic growth habit of poly( $\epsilon$ -caprolactone) crystallized on the uncoated glass. The right-hand side, by contrast, shows the striking, homogeneously oriented morphology of the polymer grown on the PTFE layer. The optical properties of the film unambiguously demonstrated that the poly( $\epsilon$ -caprolactone) macromolecules are oriented parallel to the PTFE chains.

Interestingly, precipitation on PTFE-coated substrates from solutions of various species in many cases also yielded oriented films. Illustrative examples are poly-paratphenyleneterephthalamide, which is the constituent of the high-performance aramid fibres Kevlar<sup>®</sup> and Twaron<sup>®</sup>, and the electrically conducting polymer polyaniline, both of which were precipitated from concentrated (96%) sulphuric acid by exposure to moist air<sup>24</sup>. An optical micrograph of the latter polymer is shown in Fig. 2b. Again, this micrograph illustrates the conspicuous structural differences between the polyaniline precipitated on the

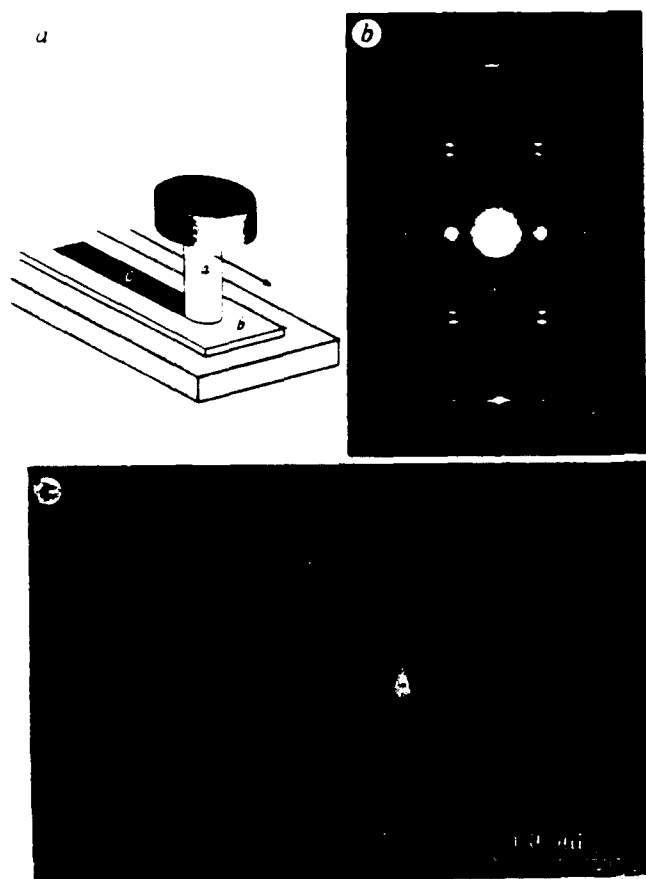


FIG. 1 a. Schematic diagram of mechanical deposition of thin layer of poly(tetrafluoroethylene) (PTFE). A bar of solid PTFE (A) is moved against a smooth counterface, for example glass (B), at controlled rate and temperature, while applying a pressure. This simple procedure leaves on the glass surface a thin layer of highly oriented PTFE (C). Typically, the temperature of the glass surface was  $130^\circ\text{C}$ , the sliding rate  $1 \text{ mm s}^{-1}$  and the pressure  $\sim 1 \text{ kg cm}^{-2}$ . Depending on the pressure, temperature and sliding rate the thickness of the deposited layer can be varied from  $\sim 2$ – $100 \text{ nm}$ . b. Electron diffraction pattern of the PTFE layer. The chain axes of the macromolecules are oriented along the sliding direction, which was vertical. This pattern shows the extraordinary degree of orientation and crystalline perfection of the PTFE layer. c. Transmission electron micrograph of the mechanically deposited PTFE film. The film was shadowed with platinum and carbon and backed with a carbon support layer (arrow indicates sliding direction).

FIG. 2 a Optical micrograph, taken with crossed polarizers, of poly( $\epsilon$ -caprolactone) crystallized on a glass slide partially covered with a thin layer of oriented PTFE. The poly( $\epsilon$ -caprolactone) was precipitated from a  $\text{CHCl}_3$  solution by evaporation of the solvent. Subsequently the polymer was melted and recrystallized from the melt. The left-hand side of the photograph shows the typical isotropic spherulites observed for isotropically crystallized poly( $\epsilon$ -caprolactone). By contrast, the right-hand side of the picture displays a highly birefringent, homogeneously oriented poly( $\epsilon$ -caprolactone) structure, which resulted from growth on the PTFE layer. It should be noted that the latter, very thin ( $\sim 10$  nm) layer itself is virtually invisible in the polarizing optical microscope. Note also the presence of a marked transcrystalline zone at the boundary of the PTFE layer. b Optical micrograph, taken with crossed polarizers, of polyaniline crystallized onto a thin layer of oriented PTFE. The polyaniline was precipitated from 96% sulphuric acid by absorption of moisture from the air. The left-side of the photograph shows the typical isotropic spherulites observed for polyaniline. By contrast, the right-hand side shows a highly birefringent, homogeneous polyaniline structure resulting from growth on the PTFE layer. The scale bar represents 1 mm on both micrographs. c Electron diffraction pattern of a highly oriented poly(*p*-xylylene) (PPX) film in its  $\beta$  crystal form. The polymer film was directly synthesized from the gaseous monomer *p*-xylylene by deposition under vacuum on a glass slide coated with oriented PTFE (J.C.W., S. Graff, S. Meyer and P.S., manuscript in preparation, and ref. 26). The as-polymerized PPX film was subsequently annealed at  $\sim 300^\circ\text{C}$ . PPX chain axis is vertical.

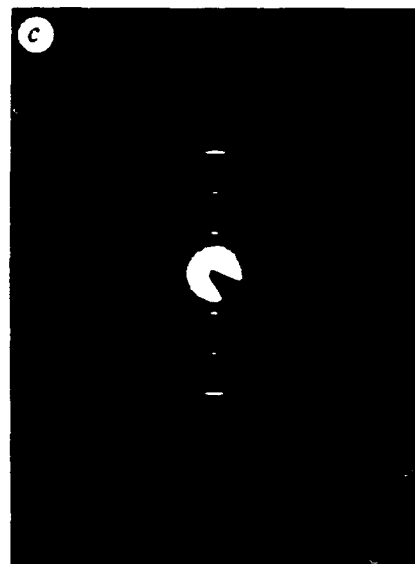
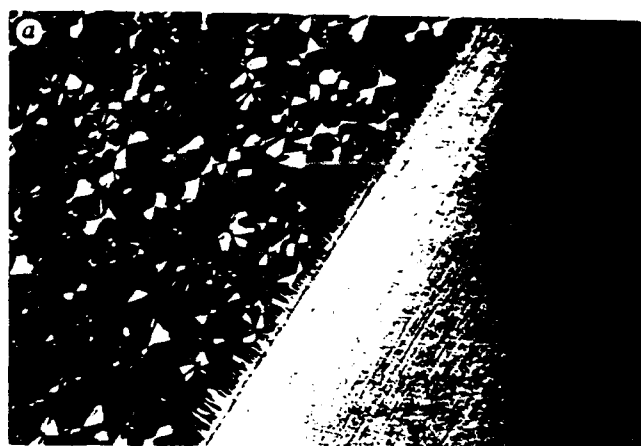


FIG. 3 Optical micrograph, taken with crossed polarizers, of the small-molecule liquid crystalline compound 4-cyano-4'-*n*-hexylbiphenyl (K 18, BDH Ltd) grown on a glass substrate that was coated with a thin layer of PTFE in a helical pattern. In this case a continuous, nonlinear structure was produced by moving a pencil-shaped PTFE rod in a spiralling path across the glass substrate. The liquid crystalline compound was then applied to the decorated substrate. This optical micrograph shows that the liquid crystalline material formed domains with a continuously changing director following the orientation of the underlying PTFE layer. Scale bar represents 1 mm.

TABLE 1 Examples of materials grown in highly oriented form on mechanically deposited thin films of PTFE

Species	Conditions*
<b>Small organic</b>	
adipic acid	vapour
anthraquinone	melt, 200 °C
chloranil (tetrachloro- <i>p</i> -benzoquinone)	vapour
alkanes	melt, 100 °C
perfluoroalkanes	melt, 180 °C
2-methyl 4-nitroaniline	vapour
<b>Inorganic</b>	
thallium chloride	vapour
<b>Liquid crystalline</b>	
mixtures of 4-cyano-4'- <i>n</i> -alkylbiphenyls	melt, 80 °C
4- <i>n</i> -propyl-cyclohexyl-4'-ethoxybenzene	melt, 100 °C
poly-[4-cyanophenyl 4-(6 acryloyloxy-hexyloxy) benzoate]	melt, 150 °C
<b>Monomer</b>	
para-xylylene, polymerized into poly(p-xylylene)	†
<b>Polymer</b>	
poly(tetrafluoroethylene) oligomers	melt, 200 °C
poly(ethylene terephthalate)	melt, 270 °C
poly(butylene terephthalate)	melt, 260 °C
polyethylene	melt, 160 °C
nylon 6	melt, 280 °C
nylon 11	melt, 200 °C
poly(1-butene)	melt, 150 °C
poly-ε(caprolactone)	melt, 100 °C
polyaniline	5 wt% solution in H <sub>2</sub> SO <sub>4</sub> , 25 °C
poly-para-(phenylene terephthalamide)	2 wt% solution in H <sub>2</sub> SO <sub>4</sub> , 25 °C

\* Conditions refer to the method of deposition.

† J.C.W., S. Graff, S. Meyer and P.S., manuscript in preparation; see also ref 26

orienting PTFE layer and on the uncoated glass surface. These examples illustrate an important advantage of the present PTFE orienting layers, which is their excellent resistance against most known chemicals, including highly aggressive acids.

Oriented polymer structures were obtained not only by crystallization but also by direct polymerization of a monomer on the PTFE orienting layers, as is exemplified by poly-*p*-xylylene (PPX) (J.C.W., S. Graff, S. Meyer and P. S., manuscript in preparation). An electron diffraction pattern showing the outstanding uniaxial orientation of the polymerized PPX macromolecules is shown in Fig. 2c.

Figure 3 illustrates the use of the orientation-inducing PTFE layers to form ordered structures of small-molecule liquid crystalline compounds. Featureless mono-domains of certain liquid crystals were observed when deposited on uniaxially oriented PTFE layers. The micrograph of Fig. 3 shows a structure manufactured by depositing PTFE in a continuous, nonlinear pattern, and subsequently applying the liquid crystalline compound 4-cyano-4'-*n*-hexylbiphenyl. This optical micrograph shows that the latter compound formed domains with a continuously changing director (principal axis of orientation), following and, in fact, 'developing' the underlying PTFE orientation layer.

Table 1, finally, gives a sample of the variety of species that were found to form highly oriented films on the PTFE layers.

It is useful to contrast the present orientation technique with previously reported methods that use polymeric substrates. As mentioned above, workers have attempted to induce epitaxial growth of various materials on polymer films oriented by tensile

drawing<sup>12-14</sup>. Note, however, that conventional tensile deformation often yields relatively thick films of only modest, often inhomogeneous orientation, typically with an average angle of mismatch between the draw direction and molecular axis of ~15° or more. Crystalline species grown on these modestly oriented films therefore have only moderate order over limited distances. By contrast, the present ultra-thin PTFE films, and the materials grown on them, display an outstanding degree of orientation, as is shown by Figs 2-4. In addition, unlike our results (see Table 1), relatively few materials have generally been reported to grow in an oriented fashion on films produced by tensile drawing.

In a different, commonly used process, small-molecule liquid crystals are oriented on rubbed or buffed polymer coatings<sup>16,17</sup>. Presumably the rubbing technique, which involves several steps, induces some orientation of the chains and/or the formation of grooves on the macromolecular substrate surface, which may be responsible for its ability to orient the crystals<sup>16,17,25</sup>. The present PTFE-deposition technique is much simpler, involving only one step, yields very thin films of outstanding orientation and seems more versatile.

The origin of this remarkable orienting capacity of the PTFE layers is as yet unclear. Nevertheless, the high degree of orientation of the present layers is likely to improve oriented growth of the few species that have previously been reported to show 'epitaxial' interactions with moderately oriented PTFE, such as poly(ε-caprolactone), polyethylene and polyamides<sup>14</sup>. But as is evident from Table 1, many more species can be oriented on the present PTFE layers. Their improved orienting capacity and versatility originate in a specific surface topography combined with a favourable crystal structure. The surface, which resembles a nanometre-scale artificial grating, may induce preferential oriented nucleation of the multitude of steps running along the deposition direction, and allow for crystal lattice matching normal to it. In this regard, we note that above 19 °C (where most of the depositions are carried out), the orienting PTFE layers have an unusual crystal structure, with a regular periodicity perpendicular to the chains of ~5 Å, which is a fairly common characteristic dimension in solids; and the structure largely lacks order along the chains, which might have restricted oriented growth.

Received 6 May; accepted 11 June 1991.

- Wittmann, J. C. & Smith, P. *US Patent Applic. No. 361, 129* (1989).
- Ultra-High Modulus Polymers* (eds Ciferri, A. & Ward, I. M.) (Applied Science, London, 1979).
- Blades, H. *US Patents No. 3,787,757; 3,869,429; and 3,869,430* (to Du Pont).
- Smith, P. & Lemstra, P. J. *J. Mater. Sci.* **18**, 505-514 (1980).
- Oh, S. Y., Akagi, K. & Shirakawa, H. *Synth. Met.* **32**, 245-252 (1989).
- Gagnon, D. R., Karsaz, F. E., Thomas, E. L. & Lentz, R. W. *Synth. Met.* **28**, 85-95 (1987).
- Andreazza, A., Tokito, S., Smith, P. & Heeger, A. J. *Molec. Cryst. Liq. Cryst.* **180**, 169-182 (1990).
- Capaccio, G., Gibson, A. G. & Ward, I. M. in *Ultra-High Modulus Polymers* (eds Ciferri, A. & Ward, I. M.) 70 (Applied Science, London, 1979).
- Lovinger, A. J. *Science* **220**, 1115-1121 (1983).
- Dorset, D. L. *J. Electron Microsc. Techn.* **7**, 35-46 (1987).
- Pashley, D. W. *Adv. Phys.* **14**, 327-352 (1985).
- Parish, D. & Phillips, P. J. *J. chem. Phys.* **63**, 1948-1951 (1985).
- Petermann, J. & Broza, G. *J. Mater. Sci.* **22**, 1108-1112 (1987).
- Takahashi, T., Terakura, F. & Tsujimoto, I. *J. macromolec. Sci.-Phys.* **B12**, 303-315 (1976).
- Smith, H. I., Gels, M. W., Thompson, C. V. & Atwater, H. A. *J. Crystal Growth* **63**, 527-546 (1983).
- Cognerd, J. *Molec. Cryst. Liq. Cryst.* **83**, 1-74 (1982).
- Geary, J. M., Goodby, J. W., Kmetz, A. R. & Patel, J. S. *J. appl. Phys.* **62**, 4100-4108 (1987).
- Swei, G. S., Lando, J. B., Rickert, S. A. & Mauntz, K. A. in *Encyclopedia of Polymer Science and Engineering* vol. 6, 209-224 (Wiley, New York, 1988).
- Wittmann, J. C. & Lotz, B. *Prog. Polym. Sci.* **15**, 908-948 (1990).
- Poolley, C. M. & Tabor, D. *Proc. R. Soc. Lond. A* **328**, 251-274 (1972).
- Briscoe, B. *J. Am. Chem. Soc. Symp. Ser.* **287** (ed. Lee, L.-H.) 151-170 (1985).
- Ford, T., Hoffmann, H., Chanzy, H. D. & Smith, P. *Nature* **333**, 55-56 (1988).
- Smith, P., Lemstra, P. J., Pijpers, J. P. L. & Kiel, A. M. *Colloid Polym. Sci.* **268**, 1070-1080 (1990).
- Andreazza, A., Cao, Y., Chiang, J. C., Heeger, A. J. & Smith, P. *Synth. Met.* **28**, 383-389 (1988).
- Peter, J. S., Lee, S.-D., Baker, G. L. & Shulburt, J. A. *Appl. Phys. Lett.* **66**, 131-133 (1990).
- Isoda, S. *Polymer* **28**, 615-624 (1984).

ACKNOWLEDGEMENTS. We thank A. Andreazza (UNIAx Corporation), F. Motamedi and D. Bothman (UCSB) and J.-P. Gabel, S. Graff, S. Meyer and C. Strauss (ICS) for their help in this work, and P. Petroni (UCSB) for his guidance. This work was supported in part by a grant from AFOSR.